Manipulation of Droplets and Plugs using Surface Acoustic Waves

by

Muhsincan Sesen

Master of Science in Mechatronics Engineering

Thesis submitted in fulfilment

of the requirements for the degree of

Doctor of Philosophy

Supervisor: Assoc. Prof. Adrian Neild

Supervisor: Dr. Tuncay Alan

Laboratory for Micro Systems (LMS)

Department of Mechanical and Aerospace Engineering

Faculty of Engineering

Monash University

Australia

August 2016

Manipulation of Droplets and Plugs using Surface Acoustic Waves

Copyright Notices

Muhsincan Sesen
5th August 2016

Acknowledgements

I am filled with joy in writing this section of my thesis because I saved it for last. This has been a fantastic journey for me; I have gained extensive knowledge about my research topic alongside many others via collaboration, learned valuable lessons in the art of publishing and bureaucracy. Just as importantly, I forged beautiful friendships and experienced living in a foreign country. For this reason, I would like to exhibit my sincere gratitude to the people and organisations that made this journey possible.

Foremost, I would like to express my deepest appreciation to my supervisors, Adrian and Tuncay. You have always supported me in my own decisions while providing valuable insight into the matter in hand. Your unparalleled knowledge, creativity and project management skills quickly became a major inspiration for me. I consider myself very lucky to have two of the very best supervisors in the world, thanks for everything.

I would also like convey my warmest regards to my family for being there every step of the way; supporting, loving and caring. I can't thank you enough; you have done an amazing job, you should be proud, love you!

This amazing journey wouldn't have been as sweet and smooth if it wasn't for my wife. For that matter, I would like to utter my profound gratitude for your endless love, support and understanding.

I would like to thank all my friends and colleagues for their help and support during this journey as well. The fruitful, sometimes crazy, discussions and ideas we had will always be remembered. To Bulut; thanks for giving me a call on my most desperate day encouraging me to apply to this Ph.D position as well as your support and friendship along the way.

I would also like to thank Department of Mechanical and Aerospace Engineering, Faculty of Engineering, Monash Institute of Graduate Research and Melbourne Centre for Nanofabrication for their facilities as well as technical and administrative support provided throughout my candidature.

LABORATORY FOR MICROSYSTEMS

Muhsincan Sesen
Laboratory for Micro Systems
Monash University
August 2016

Contents

List of Figures

List of Tables

Abstract

Microfluidics, the study of fluid flow at the sub-millimetre scale, is an enabling technology that offers scaling down of common laboratory procedures into what is called lab-on-a-chip (LOC) devices. Such devices exhibit significantly reduced fluid consumption, faster reaction times and higher sensitivity. Droplet microfluidics, where nanoliter to femtoliter volume droplets are dispersed in an immiscible carrier medium, offers physical and chemical isolation of droplets so that they could be used as micro-reactors to study reactions. However, it's quite challenging to manipulate droplets in closed microfluidic channels. Researchers have designed passive as well as active manipulation techniques to accomplish tasks such as merging, sorting or mixing of droplets. Elegant and efficient as they may be, such systems fail to demonstrate cross-compatibility due to fabrication differences and imposed flow conditions. This thesis presents three novel droplet microfluidic devices capable of performing highest demand droplet manipulation techniques, starting with sensing and sorting to merging and splitting, in an integrable manner offering exceptional on-demand control using surface acoustic waves (SAWs). SAWs are nm-scale amplitude, MHz frequency waves that are generated by electrodes deposited on piezoelectric substrates. Microfluidic devices utilising SAWs are easy to fabricate and operate; they are portable, energy efficient and safe to biological samples. Droplet trapping and coalescence, steering at Y-junctions and splitting at T-junctions using SAWs were realised and thoroughly characterised in the presented thesis. They were designed in such a way that they could be mixed and matched in order to perform a specific study. Moreover, it was shown that a combinatorial library could be formed using an automated LOC device presented here that can sense, split, merge and mix droplets. These systems could easily be coupled with existing LOC devices or modified to carry out required workflows in an efficient manner.

Monash University

Declaration for thesis based or partially based on conjointly published or unpublished work

General Declaration

In accordance with Monash University Doctorate Regulation 17.2 Doctor of Philosophy and Research Master's regulations the following declarations are made:

I hereby declare that this thesis contains no material which has been accepted for the award of any other degree or diploma at any university or equivalent institution and that, to the best of my knowledge and belief, this thesis contains no material previously published or written by another person, except where due reference is made in the text of the thesis.

This thesis includes 2 original papers published in peer reviewed journals and 1 unpublished publication, currently under preparation. The core theme of the thesis is manipulation of droplets and plugs using surface acoustic waves. The ideas, development and writing up of all the papers in the thesis were the principal responsibility of myself, the candidate, working within the Laboratory for Micro Systems (LMS), Department of Mechanical and Aerospace Engineering, Faculty of Engineering, under the supervision of Assoc. Prof. Adrian Neild and Dr. Tuncay Alan.

The inclusion of co-authors reflects the fact that the work came from active collaboration between researchers and acknowledges input into team-based research.

In the case of Chapters 4-6 my contribution to the work involved the following:

Thesis chapter	**Publication title**	**Publication status**	**Nature and extent of candidate's contribution**
4	Microfluidic on-demand droplet merging using surface acoustic waves	Published	Design and fabrication of devices, experimentation, development, result analysis, interpretation and writing.
5	Microfluidic plug steering using surface acoustic waves	Published	Design and fabrication of devices, experimentation, development, result analysis, interpretation and writing.
6	Towards an ordered library of droplets: Plug sensing, splitting and merging using surface acoustic waves	In preparation	Design and fabrication of devices, experimentation, development, result analysis, interpretation and writing.

I have not renumbered sections of submitted or published papers in order to generate a consistent presentation within the thesis.

Signed: 

Name: Muhsincan Sesen

Date: 5th August 2016

Publications

Articles in peer-reviewed journals

1. Sesen, M., Alan, T., and Neild, A., Microfluidic on-demand droplet merging using surface acoustic waves, *Lab on a Chip*, 2014, Vol. 14, Iss. 17, pp. 3325-3333 [26].

2. Sesen, M., Alan, T., and Neild, A., Microfluidic plug steering using surface acoustic waves, *Lab on a Chip*, 2015, Vol. 15, Iss. 14, pp. 3030-3038 [18].

3. Sesen, M., Devendran, C., Malikides, S., Alan, T., and Neild, A., Towards an ordered library of droplets: Plug sensing, splitting and merging using surface acoustic waves. *Lab Chip*, (Manuscript in prep.)

4. Phan, H. V., Coskun, M. B., Sesen, M., Pandraud, G., Neild, A., and Alan, T., Vibrating membrane with discontinuities for rapid and efficient microfluidic mixing, *Lab on a Chip*, 2015, Vol. 15, Iss. 21, pp. 3030-3038 [39].

5. Phan, H. V., Sesen, M., Alan, T., and Neild, A., Single line particle focusing using a vibrating bubble, *Applied Physics Letters*, 2014, Vol. 105 (19), 193507 [40].

6. Sivanantha, N., Ma, C., Collins, D. J., Sesen, M., Brenker, J., Coppel, R. L., Neild, A., and Alan, T., Characterization of adhesive properties of red blood cells using surface acoustic wave induced flows for rapid diagnostics, *Applied Physics Letters*, 2014, Vol. 105, 103704 [41].

Chapter 1

Introduction

This chapter will introduce the general concept of microfluidics and discuss why it has become such a prominent field of research. This will be followed by a brief overview of the thesis outline and upcoming chapters.

1.1 Introduction to Microfluidics

1.1.1 Microfluidics

Microfluidics is the study of fluid flow at the sub-millimetre scale. Biological life, as we know it, is built upon on fluid transport and manipulation at the microscale. The unique nature of microscale fluid physics is responsible for nutrient transport to the leaves of a tall tree, filtration of blood at the kidneys, blood flow in our veins, sperm motility and many more phenomena. Microfluidics was the cornerstone of evolution billions of years ago, however, microfluidic research started and bloomed in the 1990s [42–44]. This was due to a growing interest in molecular biology, micro-scale analytical chemistry [45] and the development of micro-fabrication techniques by the thriving microelectronics industry [46]. Over the last two decades; microfluidics has already revolutionised the medical industry and taken first steps to realise hand-held, affordable point-of-care diagnostic devices for everyone [47, 48].

Standard laboratory procedures such as pipetting, mixing, centrifugation and incubation require expensive and bulky equipment, and large amounts of consumables and high maintenance space while being relatively slow processes. Microfluidics promises to outperform such laboratory procedures on disposable, inexpensive microchips which has given rise to the concept of lab-on-a-chip (LOC) devices. What makes LOC devices so attractive is that they offer sample and reagent reduction, high throughput analysis, faster reaction times, higher sensitivity and overall cost reduction.

Furthermore, microfluidics finds numerous applications in a wide variety of fields like forensic science [49], molecular diagnosis [50], analytical chemistry [51], cell biology [52], environmental studies [53], energy [54] and the food industry [55, 56].

Fluid flow at the microscale is substantially different than its macroscale counterpart. As the size decreases, body forces such as gravity lose their significance and give way to

surface forces such as interfacial tension and capillary action. Viscous forces take over inertial forces, therefore the laminar flow regime is dominant in microfluidics. Moreover; external pumps, valves and actuators can hardly be scaled and attached to microfluidic channels of hundreds of micrometers wide and high. These dissimilarities are sometimes advantageous but more often they pose significant challenges in the design process. This lead researchers to come up with new methods applicable to microfluidics such as the use of dielectrophoresis (DEP) [57,58], acoustic forces [59], deterministic lateral displacement [60], magnetic forces [61], centrifugal forces [62], membrane deformation [63] and many more. Microfluidics, today, remains a young and fertile topic which is why it's such an active and evolving research subject.

1.1.2 Droplet Microfluidics

A promising subdivision of microfluidics is digital microfluidics dealing with droplet based systems. These are two-phase microfluidic systems where digitised droplets of certain composition are dispersed in an immiscible carrier fluid. In this way, microfluidic reaction compartments of nanoliter (nL) to femtoliter (fL) volumes are chemically and physically isolated from each other. Such systems promise accurate control of droplet volumes, single-cell analysis capabilities, repeatable and reliable droplet manipulation, high throughput capability and automation. Its applications encompass protein crystallization [64, 65], chemical and biological assays [66, 67] and inorganic chemistry [68].

It has also been argued that lab-on-a-chip (LOC) devices, especially digital microfluidic devices could potentially revolutionise high throughput screening (HTS) technology [69–71]. HTS is the widespread method for early drug screening studies carried out by pharmaceutical companies. It is an empirical method to test disease-carrying targets (such as cells and proteins) against a library of compounds. HTS has gone through its own miniaturisation period by increasing the number of wells on micro titre plates to save on amount of fluids used and time spent. This is now approximated to save 130 million dollars and 0.8 years for the commercialisation of one drug [72]. However, this miniaturisation has reached its limits imposed by evaporation in such open systems [70, 73] and the accuracy of robotic dispensing.

A strong candidate for replacing HTS technology [14] is the usage of droplet microfluidics since they can offer ultra miniaturization with increased throughputs, lower costs and no evaporation problems [74]. However, there still exists a number of shortcomings associated with this paradigm shift, especially given the fact that droplet microfluidic systems are enclosed, planar and driven by continuous flow with higher throughputs. Even the most common and straightforward laboratory procedures such as pipetting and mixing can prove to be quite challenging when working with droplets in closed channels with rates up to tens of thousands per second. Therefore, droplet manipulation techniques have been extensively studied in the literature to address such issues and to improve the existing methods.

Droplet manipulation can be achieved by various microchannel designs that make use of hydrodynamic forces to manipulate droplets such as splitting and trapping. Alternatively, droplets could be subjected to forces such as acoustic, electric or magnetic to achieve droplet manipulation within microfluidic systems. A comprehensive literature review of droplet microfluidics with emphasis on droplet manipulation techniques will be presented in the upcoming chapter 2. Furthermore, droplet microfluidic devices capable of performing multiple manipulation techniques utilising surface acoustic waves will be introduced as the core of this thesis.

1.2 Thesis Overview

This thesis explores unique ways of manipulating droplets and plugs in microfluidic devices using surface acoustic waves (SAWs) as the actuation method. SAWs hold many advantages over other actuation methods such as seamless integration, portable actuation [75] and contact-free manipulation. Furthermore, several studies have performed successful viability studies for cells [76] and other biological components [77] manipulated with specific SAW microfluidic platforms. These are some of the many reasons why SAWs have been chosen as the primary actuation method for the presented work.

Additionally; research has shown that droplets can be manipulated to perform certain tasks using various actuation methods [78], however, it's challenging to combine these techniques into one integrated platform due to fabrication differences. As engineers, we should come up with designs that are cross-compatible in order to be able to carry out specific studies with minimal extra characterisation.

The scope of this thesis is to investigate various droplet manipulation tasks using SAWs with an end goal to design a modular lab-on-a-chip (LOC) device that could be easily altered to meet specific needs in order to perform a full scale laboratory assay. More specifically; droplet merging, steering and splitting with integrated sensing will be demonstrated using SAWs in the upcoming chapters 4, 5 and 6, respectively.

1.2.1 Chapter 2: Background and Research Aims

Chapter 2 will extend the aforementioned concepts of lab-on-a-chip (LOC) devices and droplet microfluidics. This will be followed by a detailed introduction to various actuation techniques suitable for microfluidics. After the available techniques are introduced, an in-depth review of different methods for manipulating droplets will be presented. To conclude, the research gap will be discussed and the research aims of this thesis will be stated.

1.2.2 Chapter 3: Theory and Fabrication

In chapter 3, theory of acoustics and principles of surface acoustic waves (SAWs) will be introduced. SAWs give rise to a number of distinct phenomena when they couple into fluids, three of which will be discussed in detail, namely acoustic streaming, interface deformation and acoustic radiation forces. Furthermore, heating due to generation and

attenuation of surface acoustic waves will be investigated. This is followed by a review of the micro-fabrication techniques used to fabricate devices used in this study.

1.2.3 Chapter 4: Microfluidic on-demand Droplet Merging using Surface Acoustic Waves

In this chapter, a pioneering microfluidic device capable of merging consecutive droplets on-demand is developed. Droplet coalescence enables reactions to be studied within droplets and exhibits highest demand amongst droplet manipulation techniques in microfluidic systems. This method is easily integrable to existing microfluidic devices and offers enhanced control over the merging process allowing users to merge from two up to four consecutive droplets for further manipulation or analysis.

The designed system makes use of surface acoustic wave induced acoustic radiation forces to trap droplets within an expansion chamber. The acoustic waves, upon interaction with a droplet, result in a net force applied on the droplet that counteracts the drag forces on it and holds it in the high pressure zone. As a consecutive droplet approaches the trapped droplet and collides with it, coalescence takes place. The fused droplet, due to its enlarged volume and constricted nature, experiences intensified drag force. This process repeats until the acoustic radiation forces are overcome by drag forces. A predetermined number of droplets are successfully merged with the developed method depending on initial droplet volume, velocity and the amplitude of the acoustic energy.

This chapter comprises literature review on droplet coalescence, the working principle, fabrication and characterisation of the microfluidic device along with detailed analysis of the factors affecting the droplet merging process.

1.2.4 Chapter 5: Microfluidic Plug Steering using Surface Acoustic Waves

Most droplet microfluidic studies necessitate the ability to sort droplets on demand. For this reason, a novel microfluidic system capable of steering plugs at a specifically designed Y-junction is designed and presented in this chapter. This on-demand plug sorting method utilises surface acoustic waves and offers precise control of the steering process. Moreover, the developed system offers controlled plug splitting at the Y-junction as well as robustness and easy integration to existing systems.

In this study, electrodes implemented to opposing sides of a Y-junction channel are used to generate surface acoustic waves. These waves impinge on an approaching plug interface due to acoustic impedance mismatch and deform it towards one of the outlets which forces the plug to steer into that outlet. In this way, plugs can be directed to desired outlets (e.g waste and collect outlets) for further manipulation or analysis. Furthermore, depending on plug volume and velocity, plugs can be split with control at the Y-junction by tuning the applied electrical energy.

This chapter contains literature review on droplet sorting techniques as well as the working principle, fabrication and characterisation of the microfluidic device. This is followed by a detailed analysis of the factors affecting the droplet sorting and splitting process.

1.2.5 Chapter 6: Towards an Ordered Library of Droplets: Plug Sensing, Splitting and Merging using Surface Acoustic Waves

An advanced microfluidic platform is presented in this chapter. The developed platform is capable of electrically sensing a plug and splitting it using surface acoustic waves (SAWs) directed at a by-pass loop. The designed platform is programmable and modular offering accurate control of split volume as small as hundreds of picoliters. Furthermore, the platform is transformed to accommodate a hydrodynamic merging chamber as a showcase study where the split droplets are coalesced demonstrating on-chip combinatorial analysis capabilities.

The by-pass loop is designed in such a way that it does not cause splitting in the absence of actuation, however, when SAWs couple into the top section of the by-pass loop, acoustic streaming takes place reinforcing fluid flow in that section. This leads to the suction of the plug interface into the by-pass channel allowing splitting to occur. The extent of splitting is controlled by the duration of SAW actuation as well as the applied power.

This chapter consists of a comprehensive literature review on high throughput screening and droplet microfluidics, working principle, fabrication and characterisation of the microfluidic device along with a thorough analysis of the factors affecting the splitting process.

1.2.6 Chapter 7: Conclusion and Future Work

The conclusions attained from the developed microfluidic platforms are discussed within chapter 7. Outcomes and contributions of this study are detailed afterwards. Finally, future work is presented.

Chapter 2

Background and Research Aims

This chapter will introduce microfluidics and microfluidic concepts especially focusing on droplet microfluidics. This will be followed by a comprehensive literature review of droplet manipulation techniques. To conclude, a discussion of the presented literature and the research aims of this thesis will be presented.

2.1 Microfluidics

Over recent years, microfluidics, the study of fluid flow at the micro-scale, has grown to be a prominent research field owing to the wide spectrum of applications it offers. Microfluidics enticed researchers from physics, chemistry, biology and engineering and quickly became an important interdisciplinary field of study. What microfluidics offers is simple yet highly beneficial: nanolitre scale fluid consumption with minimal operation times. It also opened up opportunities to perform brand new experiments which were not possible before such as reaction kinetics [79], whole genome sequencing [80] and fabrication of new materials [81]. A remarkable technical outlook was designing microfluidic chips capable of replicating a series of laboratory tasks such as centrifugation, dilution and mixing. Such microfluidic chips are often referred to as lab-on-a-chip (LOC) devices [82].

Today, it is widely known that the emergence of microfluidics paved the way for scaling down of conventional bench-top laboratory equipment. The miniaturisation of analytical equipment into lab-on-a-chip (LOC) devices alleviates the shortcomings associated with large and expensive instrumentation such as large initial investment, high operational cost due to consumption of large quantities of fluids, maintenance due to moving parts and machinery, and poor sensitivity. Microfluidics offers miniaturisation of such equipment through the reduction in sample and reagent volumes, therefore resulting in lower analysis costs, shorter reaction times with higher resolution and sensitivity. Furthermore; microfluidics, owing to batch-fabrication capabilities enabled by micro-fabrication techniques, is capable of mass-producing low-cost, disposable instruments [45,83]. Such LOC devices are ideal for point-of-care diagnostics [84–86] and environmental sensors [87].

Although microfluidics seemingly brings about many advantages over its macroscale counterparts, it inherently comes with a significant number of challenges. This is mainly due to the fact that equipoise of forces change dramatically leading to new phenomena as

the length scale decreases. A common approach to better understanding the fluid behaviour is to look at some dimensionless numbers because such numbers can express the relative importance of various competing phenomena such as inertia, diffusion, viscosity, buoyancy and surface tension.

A good starting point is to look at the balance of inertial forces and viscous forces. Reynolds number, Re, is a non-dimensional number quantifying the importance of these forces. It's given by:

$$Re = \frac{\rho u L}{\mu} = \frac{inertial}{viscous} \tag{2.1}$$

where ρ is the density, u is the velocity, and μ is the viscosity of the fluid and L stands for the characteristic length scale.

Fluid flow can be categorised into three distinct regimes by looking at the intricate balance of inertial to viscous forces:

- Laminar flow where Re$<$2000
- Unstable flow where 2000$<$Re$<$4000
- Turbulent flow where Re$>$4000

In order to better understand the Reynolds number, a typical microfluidic system is considered in table 2.1:

Description	**Value**
Viscosity of water, μ	10^{-3} kg/ms
Density of water, ρ	10^3 kg/m^3
Microfluidic channel width, w	100 µm
Flow velocity, u	1 mm/s
Re	0.1

Table 2.1: Reynolds number calculation for a typical microfluidic device.

Typical Reynolds number for microfluidics is Re$\ll$1 which implies that viscous dissipation will be dominant whereas inertial effects can be ignored in microfluidic devices. Another significance of Reynolds number is that it emerges as a key parameter when Navier-Stokes equations are non-dimensionalised. Applying the continuum version of Newton's second law of motion to an incompressible, Newtonian, isotropic fluid element on a per unit volume basis, we get the Navier-Stokes equations:

$$\rho(\frac{\partial \mathbf{u}}{\partial t} + \mathbf{u} \cdot \nabla \mathbf{u}) = -\nabla p + \mu \nabla^2 \mathbf{u} + \mathbf{F} \tag{2.2}$$

and incompressibility, simplified from conservation of mass by assuming constant density, applies as:

$$\nabla \cdot \mathbf{u} = 0 \tag{2.3}$$

where t represents time, p is pressure, $\mathbf{u}$ is the velocity vector and $\mathbf{F}$ stands for body forces (per unit volume) such as gravitational, magnetic, etc.

Non-dimensionalisation of the variables of Navier-Stokes equations leads to the appearance of Reynolds number as a factor of the inertial components:

$$Re(\frac{\partial \mathbf{u}^*}{\partial t^*} + \mathbf{u}^* \cdot \nabla \mathbf{u}^*) = -\nabla p^* + \nabla^2 \mathbf{u}^* + \frac{\mathbf{F} L^2}{\mu u} \tag{2.4}$$

where the superscript asterisk ('*') indicates a non-dimensional version of the original term. Detailed steps to the non-dimensionalisation can be found in the book by Nguyen and Wereley [88].

As previously discussed, typical microfluidic systems exhibit very low Reynolds number flows (Re$\ll$1) which verifies that inertial components in equation 2.4 can be neglected, in fact this is applicable up to Re $\approx$ 1 [88]. Hence, the Navier-Stokes equations are linearised and simplified to the non-dimensional Stokes equation:

$$0 = -\nabla p^* + \nabla^2 \mathbf{u}^* + \frac{\mathbf{F} L^2}{\mu u} \tag{2.5}$$

A few conclusions can be drawn from this study. First of all, if we consider a typical microfluidic device and use the parameters in table 2.1, we immediately notice that the body force term, $\mathbf{F}$, has a coefficient of 10^{-2}. This is the reason why body forces lose their effectiveness as the length scale decreases. For example, it is well-known that gravity does not play much of a role in microfluidics [88], except for certain special cases [89]. This does not strictly imply that body forces are not used in microfluidics; they can be used as long as they overcome this disadvantage. For example, the use of dielectrophoretic [15,32,90], centrifugal [83,91–93] and magnetic [94,95] forces are quite common in microfluidic systems. Moreover; acoustic streaming, a method used in this thesis, arises from a body force.

Another conclusion that takes attention is that when we neglect the body force term (i.e no external actuation) in equation 2.5, it simplifies to the linear Stokes equation:

$$\nabla p = \mu \nabla^2 \mathbf{u} \tag{2.6}$$

This equation can be solved quite easily and solutions can be found in textbooks [96,97]. Once the velocity field for a certain geometry is obtained either analytically or experimentally, that field and the streamlines associated with it does not change as the pressure increases. Moreover, if there's a spherical particle flowing in an infinite body of fluid in this regime, the particle will experience Stokes drag force, $\mathbf{F_d}$, given by

$$\mathbf{F_d} = 6\pi\mu r \mathbf{u} \tag{2.7}$$

where r is the radius of the particle. Stokes drag is applicable to droplets flowing a wide microfluidic channel and this will be further discussed in chapter 4.

A final remark about equation 2.6 is that the non-linearity in the original Navier-Stokes equations (eqn. 2.2) existed due to inertia. Non-linearity leads to chaos, turbulence

and flow instabilities which are quite common in the macroscale world and our daily observations such as river falls, ocean waves, flushing a toilet or gardening with a hose. Advective transport and mixing are fuelled by inertia and are hard to avoid in macroscopic world.

In contrast; when the inertial effects diminish and are deemed negligible, diffusive transport is left alone and mixing becomes really hard to achieve because molecular diffusion in microchannels (Brownian motion) is quite slow. In order to understand the interplay between advective and diffusive transport, the dimensionless Péclet number (Pe) is often used. Péclet number is given as:

$$Pe = \frac{uL}{D} = \frac{advective}{diffusive} \tag{2.8}$$

where D is the mass diffusion coefficient. As the velocity and length scale decreases, advective transport decreases and diffusive transport becomes dominant in which case diffusion time, τ, is given by:

$$\tau = \frac{L^2}{2D} \tag{2.9}$$

In a typical microfluidic system, mixing is rather slow and likely to occur at relatively long distances downstream within a few minutes [89] (Fig. 2.1). Depending on the specific application, pure diffusion could be advantageous or not. In most cases, when studying chemical reactions in microfluidic channel, it is desirable to mix chemicals rapidly so that the reaction kinetics could be probed. This is usually achieved by designing serpentine microfluidic channels that stretch and fold fluid elements chaotically and result in faster mixing times by chaotic advection [79]. Mixing in droplets will be further discussed in section 2.2.2 - Droplet Mixing.

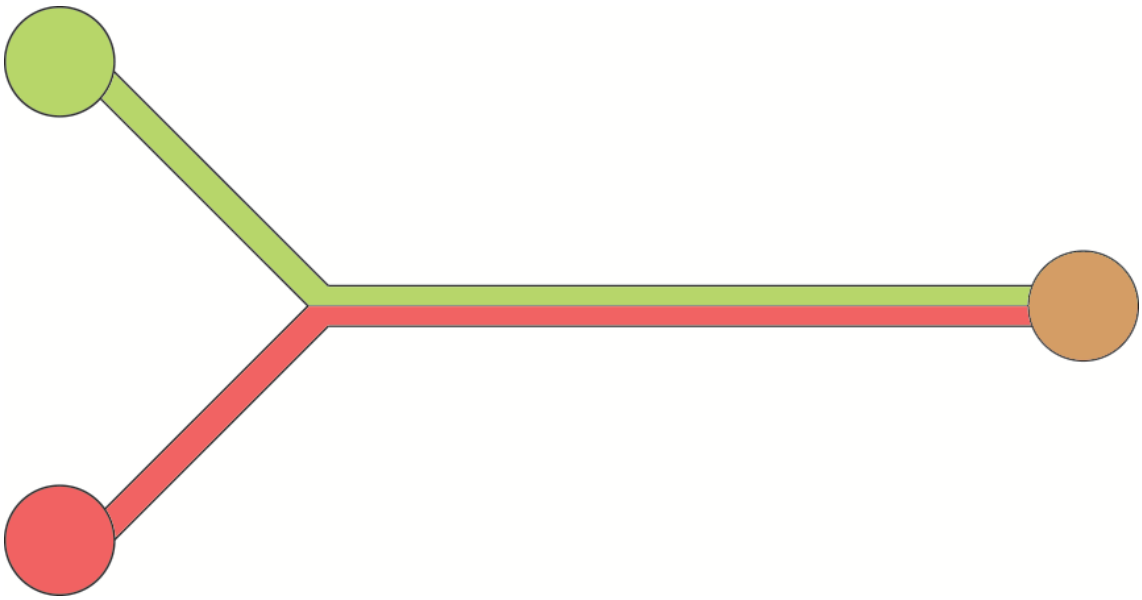

Figure 2.1: Non-mixing in a Y-channel microfluidic device

Between two immiscible fluids, interfacial tension, γ, defines the dynamics of the free surfaces and it plays an important role in two phase microfluidics. Interfacial tension acts

to minimise the total surface area of an interface. In the absence of confinements, the minimum surface area is achieved by forming spheres, the shape of droplets in sufficiently big channels. Another key parameter is the Capillary number which defines the balance of viscous forces to interfacial forces and it's given as:

$$Ca = \frac{\mu_{max} u}{\gamma} = \frac{viscous}{interfacial} \tag{2.10}$$

where μ_{max} is the viscosity of the more viscous fluid amongst the two immiscible phases. Capillary number plays an important role, especially in the generation of droplets; a technique used in the presented work, discussed in detail within section 2.2.2 - Droplet Formation.

The physics of fluid flow at the microscale is substantially different than macroscale fluid flow and it is quite rich, especially because microfluidic devices make use of electrostatics, magnetism, acoustics and thermodynamics. Moreover, micro-fabrication techniques involve polymers which brings about mechanics of materials, elasticity and polymer physics allowing the manufacturing of deformable membranes [98], valves [10] and flaps [99].

Overall, microfluidics is a relatively new field of research but its unique physics and wide range of applications has allowed it to prosper and brought it to prominence. It should be noted here that although the majority of the research into microfluidics goes to chemical and biological studies, it also finds diverse applications in cooling systems [100], energy [101, 102], robotics [103] and many more. As mentioned priorly, a promising subdivision of microfluidics is called droplet microfluidics where two phase fluidic systems are studied. The upcoming chapter discusses the concept and applications of droplet microfluidics in detail.

2.2 Droplet Microfluidics

Another important aspect of microfluidics is the study of multiphase (segmented) flows. Monodisperse droplets of nL to pL volume can be generated in a carrier liquid successively at rates exceeding 20kHz [104], allowing exhaustive studies to be carried out in rapid succession in microfluidic devices. Often termed droplet or digital microfluidics, it offers chemical and physical isolation of droplets to avoid cross-contamination because such droplets are segmented by an immiscible carrier fluid. The wetting properties of the channel walls are usually selected or modified in such a way that droplets do not come into contact because of a thin layer of carrier fluid which wets the walls and surrounds the droplets at all times (Fig. 2.2(a)). Furthermore, surfactants could be used to prevent droplet merging on contact thereby allowing droplets to be closely packed but yet isolated from each other (Fig. 2.2(b)). One of the main reasons why it's called digital microfluidics is the possibility of creating a microfluidic computer chip using droplets as digital bits. Researchers have taken the first steps to realise such a system and shown that simple Boolean logic functions [105–108] could be performed on chip.

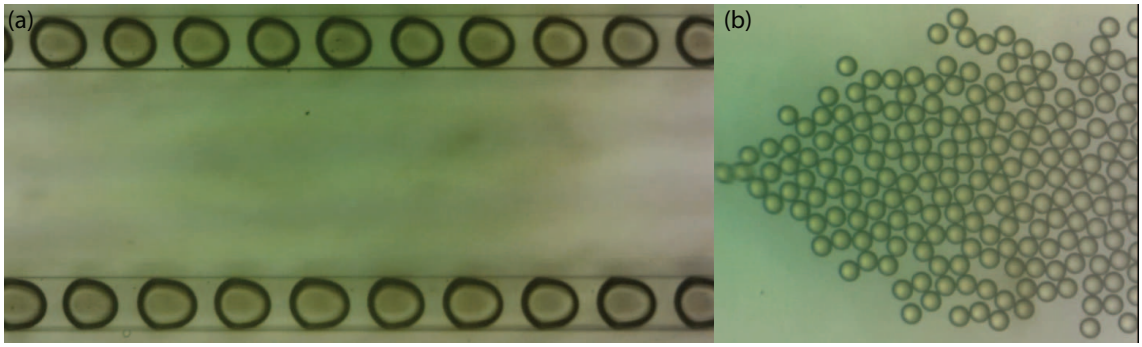

Figure 2.2: (a) Dyed water droplets in olive oil and (b) water droplets in FC-40 stabilized by 2% surfactant (Pico-Surf™1, Sphere Fluidics, UK)

Every single droplet can be identified as a mini reaction compartment. Controlled droplet formation and further manipulation allows a multitude of studies to be carried out with these systems. Furthermore, single cells could be trapped in these droplets to study cell viability after exposure to chemicals or external excitation like ultraviolet (UV) light or thermal cycling. If microfluidic droplets are formed using a cell culture with random distribution as the dispersed phase, the number of cells trapped in a droplet agrees with Poisson distribution (Fig. 2.3(a)) [1]. Efforts to improve the probability of trapping one cell per droplet include squeezing particles into single file to achieve ordered formation (Fig. 2.3(b)) [2] and designing a long entrance channel so that cells arrange themselves in an equally spaced manner due to hydrodynamic forces (Fig. 2.3(c)) [3]. High droplet formation rates and the encapsulation of single cells wihtin droplets allow very large screens to be processed with low volumes of fluids used to find unique cell types in a heterogeneous population or to carry out a directed evolution experiment. Applications of single-cell analysis in droplet-based microfluidics range from gene expression and cytotoxicity to polymerase chain reaction (PCR) and antibody secretion studies [109, 110].

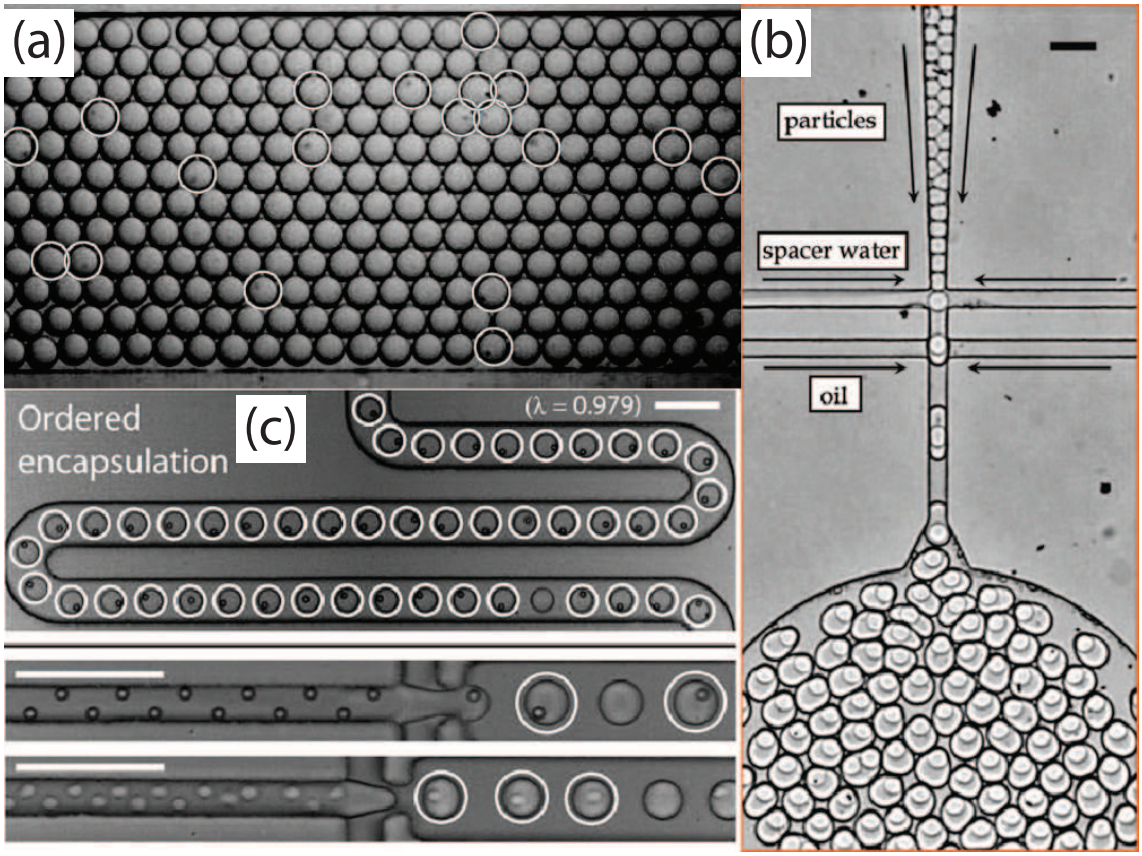

Figure 2.3: (a) Cells in droplets (Poisson distribution) incubated for 3 days are still viable. Reproduced in part from [1] with permission of The Royal Society of Chemistry. (b) Squeezing particles into single file to make droplets achieves single-particle per droplet. Reproduced in part from [2] with permission of The Royal Society of Chemistry. (c) Long entrance length hydrodynamically spaces particles and cells equally to be dispensed in droplets. Reproduced in part from [3] with permission of The Royal Society of Chemistry.

In the context of designing a digital microfluidics device, determining required droplet manipulation techniques and the pre or post-analysis of the proposed system is of paramount importance. Devices need to be designed and optimised on a per study basis because unique process flows are required for every application with multiple steps involving various droplet manipulations and post-processing capabilities. For example, a PCR study needs rapid and accurate thermal cycling whereas a single-cell study might need droplet steering and fluorescent viability assay. A literature survey of droplet manipulation techniques is presented in section 2.2.2.

Moreover, detailed pre and post-analysis of microfluidic systems is essential for rapid design and optimisation of devices. More often than not, 2D numerical studies are unable to capture complex (multi)physics of a proposed system and 3D numerical studies require immense processing capabilities. A simple and efficient tool is to make use of hydraulic-electric circuit analogy. A generally applicable case study of this analogy is presented in the upcoming section.

2.2.1 Electrical Analogy

In order to capture the physics of an unfamiliar concept, a useful approach is to develop a physical analogy. Through this analogy, the information from the familiar subject could be conveyed to the other field of study. This powerful technique allows us to understand complex physics in a simplified manner. In this context, a well-known analogy that has helped us understand fluid behaviour and electricity is the hydraulic-electric circuit analogy (Fig. 2.4) [111–114]. A simple example of this analogy considering a common droplet microfluidic system will be presented in this section.

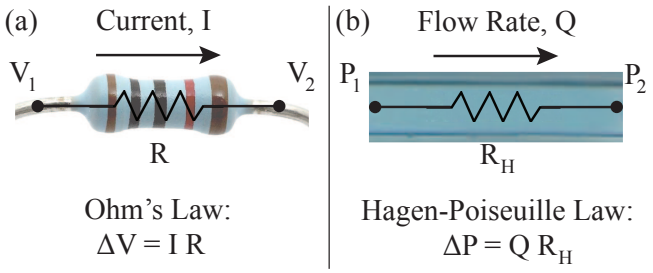

Figure 2.4: Schematics showing the physical similarities of electron flow (a) and fluid flow (b).

Microfluidic networks can be considered analogous to a resistor network in an electrical circuit to simplify analysis [111]. The familiar Ohm's law (Fig. 2.4(a)) in electrical circuit analysis relates the electrical current, I, passing through a resistor of resistance R with a voltage change of V across the resistor:

$$V = IR \tag{2.11}$$

This is analogous to a pressure-driven Hagen-Poiseuille flow (Fig. 2.4(b)) in a circular channel where pressure drop, ΔP, across the channel is equivalent to voltage drop; flow

rate, Q, within the channel is analogous to electrical current and hydraulic resistance, R_H, is similar to electrical resistance:

$$\Delta P = QR_H \tag{2.12}$$

Hydraulic resistance, R_H, for a rectangular cross section microchannel with close to unity aspect ratio (i.e w≈h) is given by:

$$R_H = \frac{8L(w+h)^4\mu}{(wh)^4\pi} \tag{2.13}$$

where w and h are the width and the height of the channel, respectively. Hydraulic resistance could be found for different aspect ratio channels as the summation of a Fourier series [115]. These relationships could be derived firstly by solving the linear Stokes equation 2.6 to find the parabolic velocity profile of the flow inside a circular channel. Once the velocity function is obtained, integrating it over the channel cross sectional area gives the volumetric flow rate, Q, and finally replacing circular channel radius with hydraulic diameter of a rectangular channel leads to equation 2.13. Detailed steps can be found in previous work by Oh et al. [116].

This analogy provides researchers a useful tool to linearise and analyse microfluidic network problems using electrical circuit analogies involving but not limited to resistance coupling (series or parallel), Kirchhoff's laws, capacitors and inductors. However, when we consider droplets within microchannels, these analogies get a little bit more complicated due the addition of interfacial tension and the role of droplet viscosity. In order to better understand this complication, a typical pressure distribution inside a microchannel with a viscous plug could be observed in Fig. 2.5.

Droplet microfluidic systems can be simplified and analysed with a hydraulic-electric circuit analogy with a few modifications [117–119]. If we consider a simple droplet microfluidic system with one plug, inlet pressure P_i, outlet pressure P_o and hydrodynamic resistances R_i, R_o and R_p at the back of the plug, the front of the plug and within the plug, respectively (referring to Fig. 2.5); we can formulate the pressure balance in the channel as (analogous to resistors in series):

$$P_i - R_iQ + 2\gamma H_i = P_o + R_oQ + 2\gamma H_o + R_pQ \tag{2.14}$$

where γ is the interfacial tension between the two mediums and H represents the mean curvature of the interface given by $H = w^{-1} + h^{-1}$ where w is the width and h is the height of the microfluidic channel. Unless the front or the back end of the plug has a different H (e.g plug is in an expansion zone), the pressures associated with interfacial tension will be the same (i.e $\gamma H_i = \gamma H_o$). This is generally the case so we can rearrange equation 2.14 as:

$$\Delta P = Q(R_i + R_o + R_p) \tag{2.15}$$

where $\Delta P = P_i - P_o$. Furthermore, as mentioned earlier, hydraulic resistance in a rectangular microchannel is given by equation 2.13 and all the parameters are common for the

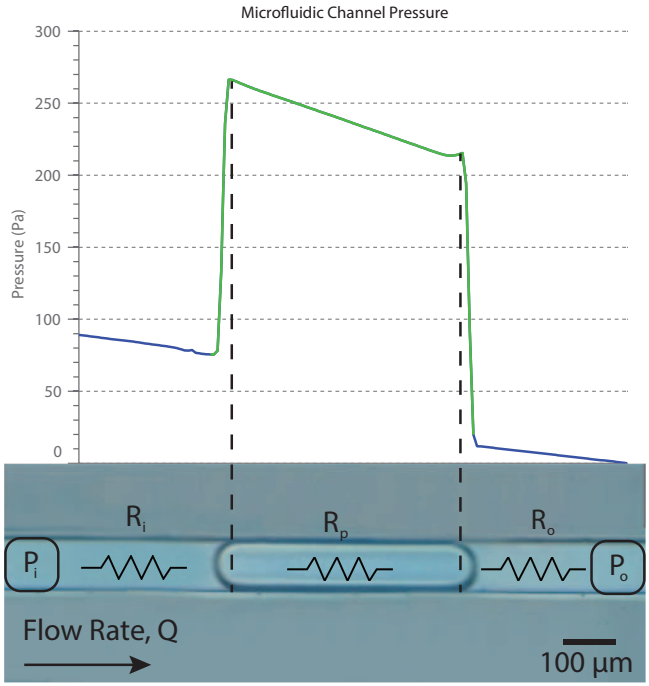

Figure 2.5: Pressure distribution along a microchannel with a water-in-oil plug. Numerical analysis carried out by using COMSOL Multiphysics software.

carrier fluid (i.e R_i and R_o) except for channel length, L. Considering common microfluidic devices; we can assume that there will be multiple plugs of equal volume spaced sufficiently apart [118] in a microfluidic device to finally get:

$$\Delta P = Q(R_{cp} + nR_p) \tag{2.16}$$

where n is the number of plugs in the channel and R_{cp} is the hydrodynamic resistance associated with the entire continuous phase in the system. R_{cp} can be obtained by substituting the total length of the carrier fluid, L, and its viscosity, μ, into equation 2.13.

A generally applicable hydraulic-electric analogy was presented for a microfluidic device entartaining multiple monodisperse plugs with sufficient spacing. Further modifications or simplifications could be made depending on the specific study [18, 112, 116–119]. A study specific in-depth analysis can be found in chapters 5 and 6.

Now that we have the basics for pre or post analysis of a digital microfluidics system using hydraulic-electric analogy, we can move on to another important aspect of droplet microfluidics, namely, droplet manipulation techniques. Droplet manipulation techniques are in high demand when designing study specific devices, therefore a multitude of methods have been developed utilising various active manipulation techniques as well as many passive methods. A literature review of microfluidic droplet manipulation techniques will be discussed in the upcoming section.

2.2.2 Droplet Manipulation

Droplet manipulation is a key factor in droplet microfluidics devices. Many reactions or assays studied in droplets require timely control of reagent injection to initiate, alter or end the reaction and this requires droplet fusion. Similarly, a form of filtering or sorting of the droplets are desired by majority of droplet microfluidics studies to get rid of unwanted droplets. These are just a few examples amongst a number of requirements, this section focuses on most of the major droplet manipulation techniques that have been developed to date such as droplet formation, sorting, merging, mixing and more.

Droplet manipulation can be achieved by active or passive methods. Passive systems exploit hydrodynamic forces by using clever channel designs and can usually be analysed using hydraulic-electric analogy presented earlier in section 2.2.1 - Electrical Analogy. Passive systems are usually able to yield faster throughputs whilst active systems work with a number of different forcing mechanisms and can offer programmability and on demand actuation. Some of the common actuation methods will be briefly explained first so that droplet manipulation techniques are better understood.

Membrane Deformation

A common active droplet manipulation technique is to use membrane deformation for creating pressure fluctuations in the fluidic channel. Integrating membranes at specific locations of a microfluidic device allows researchers to manipulate the flow at those places and to control them actively. Such locations behave like valves in microfluidic devices therefore they are often referred to as micro-valves.

Micro-valves can be integrated to microfluidic devices via a double layer polydimethylsiloxane (PDMS) approach where one layer incorporates microfluidic channels and the other has air ports crossing the microfluidic channels at desired locations to form a PDMS membrane (Fig. 2.6(a)). The air ports are usually connected to solenoid valves for quick on/off regulation. Since PDMS is an elastic polymer, when air pressure is applied to the PDMS membrane, the membrane deforms and almost closes the microfluidic channels (Fig. 2.6(b)). Conversely when negative pressure is applied, the PDMS deforms inward to create a suction effect in the fluidic channels (Fig. 2.6(c)). The closing and opening action acts like a micro-valve which can be used to turn flow on or off at desired locations. Moreover, the membrane could be fluctuated to promote mixing [10].

Surface Acoustic Waves (SAWs)

Another method of actuating droplets is by harnessing the energy of surface acoustic waves (SAWs). SAWs are nm-scale amplitude acoustic waves that propagate at MHz frequencies on the near surface of piezoelectric substrates. They can be generated by actuation of electrode pairs deposited on piezoelectric substrate with constant spacing, often referred to as inter-digital transducers (IDTs) (Fig. 2.7). When a signal with matching frequency is applied across the electrode pairs, an electric field coupled to the piezoelectric material is produced which gives rise to SAWs. The resonant frequency of the IDTs, f, can be

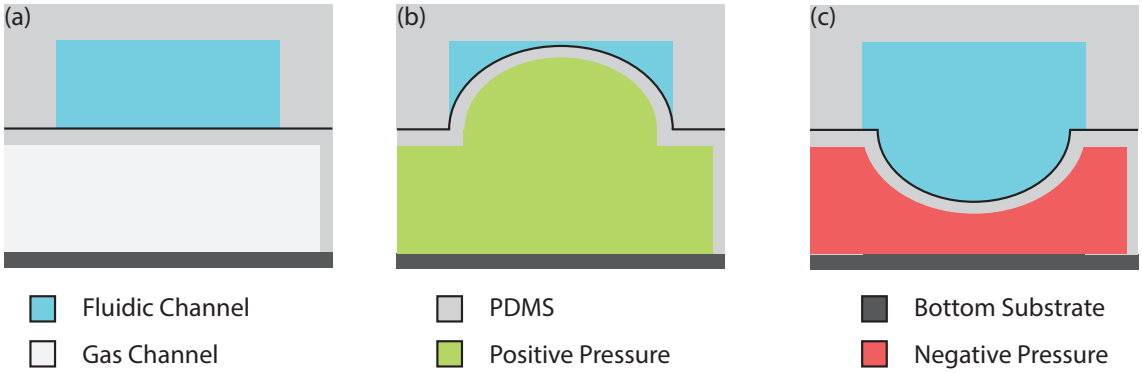

Figure 2.6: Cross sectional view of a representative microfluidic device demonstrating micro-valve working mechanism. (a) The membrane is at rest when the pressure is neutral in the gas layer. (b) The membrane deforms outward and blocks the flow in the fluidic layer when positive pressure is applied and (c) the membrane deforms inward when negative pressure is applied.

determined by using distance between each transducer pair, λ, (Fig. 2.7) and the speed of sound in the piezoelectric substrate, c_s:

$$f = c_s/\lambda \tag{2.17}$$

SAWs are classified as Rayleigh waves which do not penetrate deep into the substrate so they do not attenuate much in the absence of other substrates or liquids. Therefore they travel efficiently and easily couple into the fluids within microfluidic channels and transfer momentum to them (Fig. 2.7). This leads to interesting phenomena; to name a few relevant to the content of the presented thesis, acoustic streaming, acoustic radiation forces (ARF) and interface deformation.

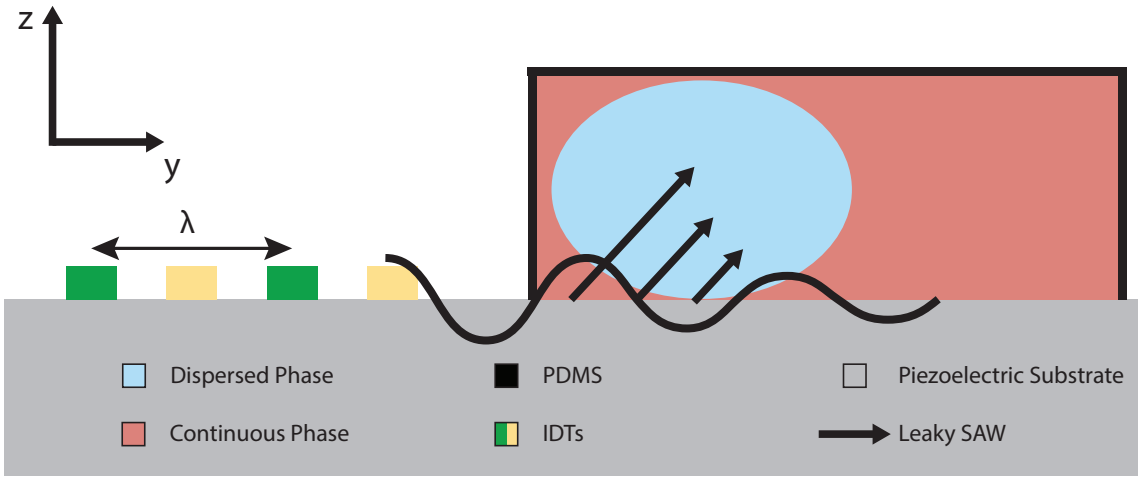

Figure 2.7: Surface acoustic waves generated by IDTs travel on piezoelectric substrate and couple into the fluid giving rise to pressure waves. SAWs can be used to manipulate droplets on demand.

Acoustic streaming takes place when SAWs couple into a single phase fluid media. SAWs refract upon contact with the fluid due to mismatch of sound speed in the media

and they decay rapidly; often referred to as leaky SAW (Fig. 2.7), this leads to higher pressure zones close to the source of actuation thereby creating a circulatory flow away from the IDTs. Acoustic radiation force (ARF), however, is a second-order, time-averaged effect on spherical particles or droplets immersed in an immiscible medium within a microfluidic channel. The acoustic waves reflect and refract upon interaction with spherical objects and results in a net force, ARF, which can move the object relative to pressure extrema. Another important phenomenon arises when an acoustic wave interacts with a fluid-fluid interface. If there's an acoustic impedance mismatch amongst the fluids that form the interface, a net radiation force is observed [120,121] that can deform the interface towards or away from the incident wave depending on the properties of the fluids.

SAWs, in general, exhibit lower acoustic energy losses and power consumption, and, as such, are highly suitable for microfluidic actuation [122]. Acoustic droplet actuation method could effortlessly be integrated to a lab-on-a-chip (LOC) device and it does not involve any moving parts. Moreover, it could be operated accurately and easily with basic programming.

Droplets have been actuated using surface acoustic waves within this work utilising some of the above mentioned phenomena or their coupled effects so these will be discussed with a more in-depth review in section 3.1.1.

Electric Fields

Intense electric fields can also be used to actuate droplets in microfluidic channels. Electric fields can easily be generated within lab-on-a-chip (LOC) devices by depositing electrodes on the substrate. Either direct current (DC) or alternating current (AC) can be applied to generate localised electric fields. Two of the commonly used droplet manipulation techniques utilising electric fields are electrophoresis and dielectrophoresis (DEP).

DC electric fields can be used to attract or repel droplets, however, the resulting body force is really small if the droplets do not carry a charge. For this reason, researchers have attempted to pre-charge droplets where one example shows that if an anode and a cathode are placed oppositely at a droplet splitting junction, the daughter droplets get charged up [16,123]. The charged droplets can then be significantly influenced by DC electric fields where they move towards the opposite charge while moving away from the same charge (Fig. 2.8(a)), this is referred to as electrophoresis [124].

The droplet charging step may not be ideal for a number of studies where charging a droplet might be harmful for droplet content, in such cases dielectrophoresis (DEP) can be preferred. When a droplet is subjected to an AC electric field, dipoles are created and they interact with the gradient of the electric field [124] (Fig 2.8(b)). This gives rise to DEP force, $\mathbf{F_{DEP}}$, a type of body force (see section 2.1) given as:

$$\mathbf{F_{DEP}} = 2\pi\epsilon_1 Re|\underline{K}(\omega)|r^3\nabla\mathbf{E}^2 \tag{2.18}$$

where ϵ_1 is the dielectric permittivity of the continuous media, $Re|\underline{K}(\omega)|$ is the real part of the Clausius-Mossotti function, $K(w)$, r is the droplet radius and $\mathbf{E}$ is electric field. It is important to note here that the attraction or repulsion depends on the sign of the real

part of the Clausius-Mossotti function which almost always works to pull towards the high intensity region in the case of droplets. They could, however, push or pull depending on the AC frequency in the case of particles which will not be covered in this thesis.

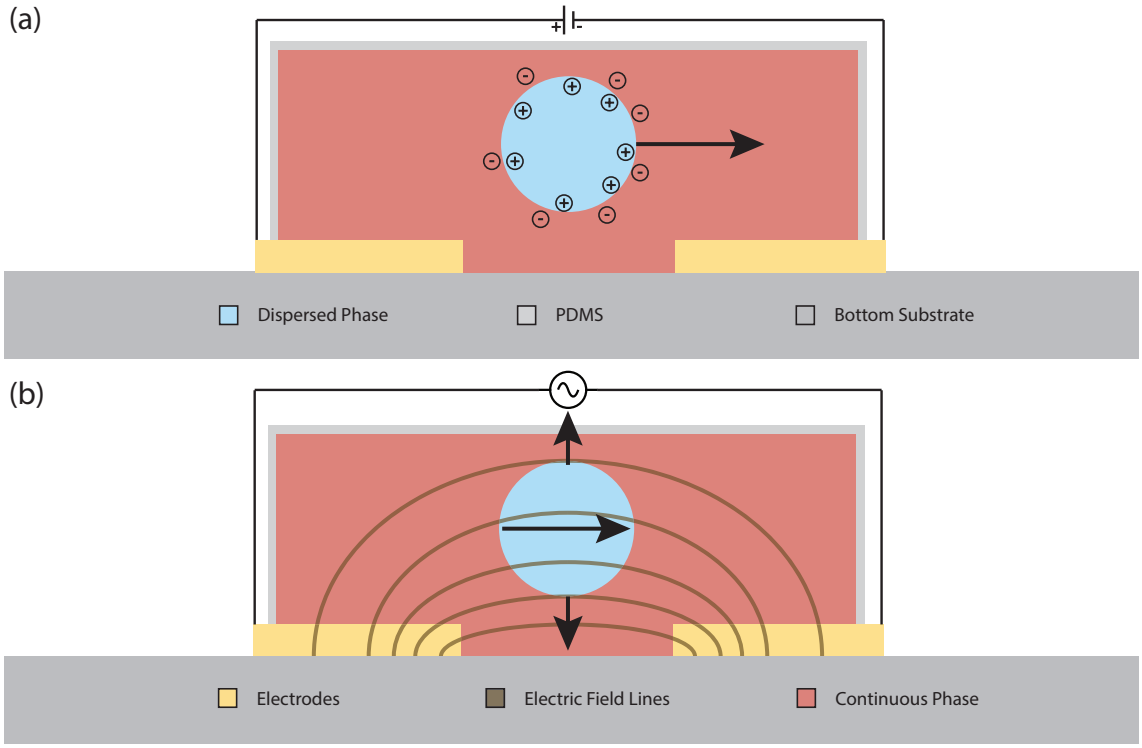

Figure 2.8: (a) Electrophoresis: Charged droplets migrate towards the electrode they are attracted to in a DC field. (b) Dielectrophoresis: Higher AC field intensity attracts droplets.

Having established some fundamentals of droplet manipulation using techniques such as membrane deformation, electric fields and SAWs; we will turn our focus to different droplet manipulation techniques in the upcoming sections.

Droplet Formation

The starting point for a droplet based lab-on-a-chip (LOC) device is the accurate and uniform generation of a mono-disperse droplet stream. Droplet formation is usually achieved through passive techniques which take advantage of the flow field to deform the interface and promote the natural growth of interfacial instabilities [4]. There exists three main passive techniques which are widely used by researchers to generate droplets, namely, T-junctions (Fig. 2.9(a)), flow focusing devices (Fig. 2.9(b)) and co-flowing streams (Fig. 2.9(c)). Moreover, some active droplet formation techniques exist where droplet production could be triggered and the volume of the droplets produced can be altered on demand using membrane deformation (micro-valves) [7, 10], heating [9, 125], SAWs [5, 8] (Fig. 2.9(d)) or vibration [126].

T-junctions

The formation of droplets in T-junctions was first observed by Thorsen et al. [127] who propelled two immiscible fluids through two perpendicular micro-channels and examined

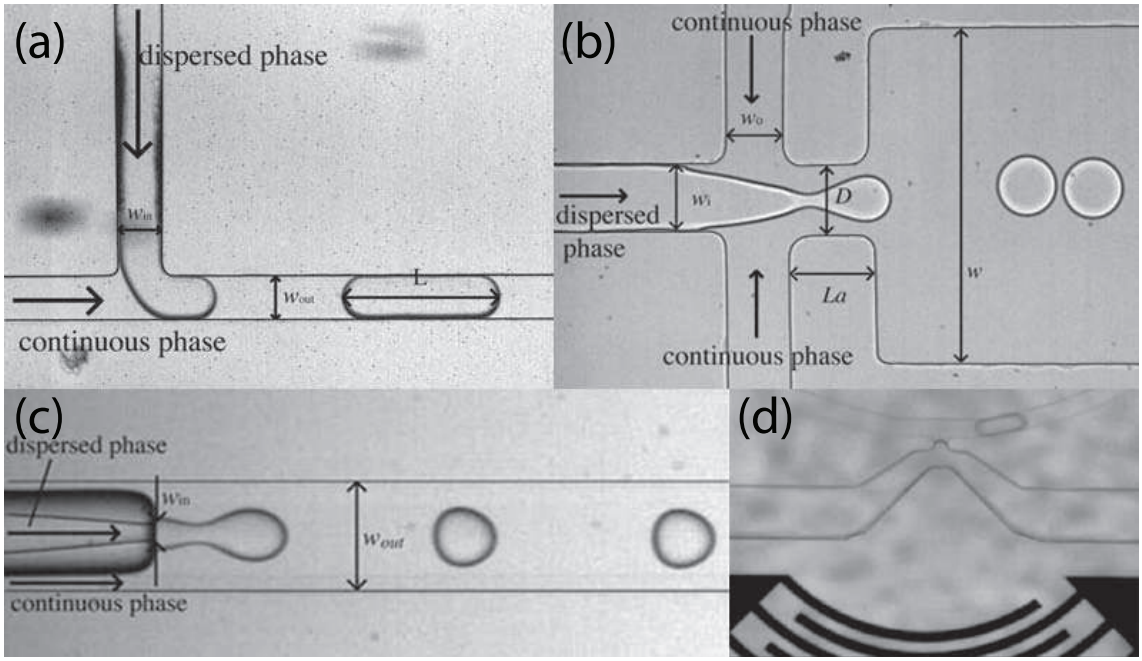

Figure 2.9: Droplet generation using (a) T-junction, (b) flow focusing geometry and (c) co-flowing streams. Reproduced from [4] with permission of The Royal Society of Chemistry. (d) On-demand droplet generation using surface acoustic waves. Reproduced in part from [5] with permission of The Royal Society of Chemistry.

the formation of stable droplet streams where the flows meet. T-junction droplet formation has been widely used in droplet microfluidic systems since then and consequently it was thoroughly characterised and understood by researchers via numerical and experimental studies [128–131]. A number of parameters affect droplet formation in T-junctions:

- Capillary number, Ca (see section 2.1)
- Interfacial tension, σ (see section 2.1)
- Flow rate ratio of two streams, (Q_1/Q_2)
- Viscosity ratio of the fluids, (μ_1/μ_2)
- Wetting characteristics of the fluids with the channel walls (Contact angle)
- T-junction geometry
- Channel aspect ratio (h/w)
- Surfactants added to the fluids

The production of droplets using T-junction geometries can be categorised into three separate regimes; squeezing, dripping and jetting regime. When the capillary number is lower than a critical capillary number $Ca \approx 0.015$ [130,132,133], indicating that interfacial tension is significantly larger than viscous shear, the droplets grow to fill up the entire channel unobstructed by the viscous shear stress and block the continuous phase flow until the dynamic pressure builds up in the trailing end of the droplet. This pressure build up thins the interface as the droplet grows and finally ruptures the interface to form a droplet.

Sequential images of the process can be obversed in Fig. 2.10. Such droplets formed are usually not spherical and sometimes referred to as plugs meaning the droplet diameter is larger than the channel width. This is the regime and method used to form droplets or plugs within this study.

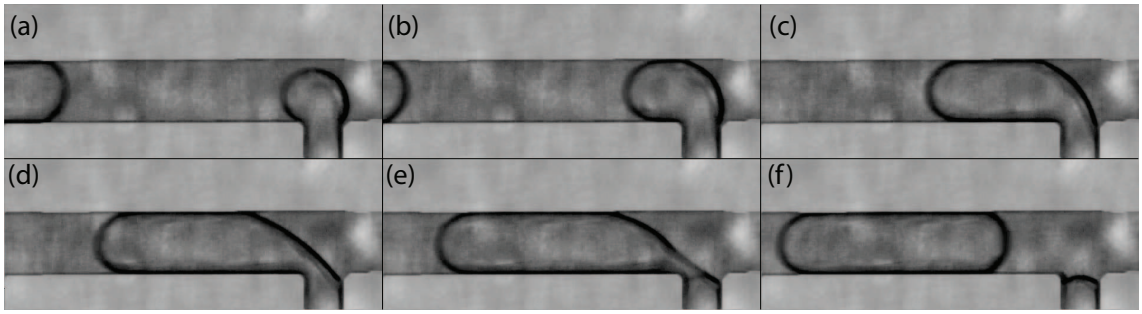

Figure 2.10: Sequential images of droplet generation using a T-junction where (a) droplets grows and (b) fills the channel completely to block the continuous phase flow. (c) Pressure in the carrier fluid upstream builds up as the droplet grows and (d) thins the interface at the corner of the T-junction (e) until it ruptures (f) to form a droplet.

An important observation to note about this regime is that flow rate ratio ($Q1/Q2$) and droplet length, therefore droplet volume (V_d), are proportional to each other independent of the oil viscosity (i.e $Q1/Q2 \propto V_d$) as observed by Garstecki et al. [128]. This property significantly reduces the complexity of droplet production and allows researchers to conduct studies with different droplet volumes for better characterisation.

Furthermore, Steijn et al. [6] have developed a by-pass channel geometry which forces droplets to be of the same size regardless of the imposed flow rates and fluid properties. The by-pass channel is designed around the T-junction site so that the continuous phase flow is not obstructed while the droplet grows thereby preventing the rapid pressure build up mentioned earlier. The droplet grows freely until the by-pass channel is completely blocked, after which the droplet pinches off. Sequential images of the process can be observed in Fig. 2.11.

Such a design allows a LOC device to produce mono-disperse droplets without the need for expensive and bulky equipment because cheaper and smaller syringe pumps incur pressure fluctuations in microfluidic devices leading to poly-disperse and irregular droplet production. This also moves a device away from the much argued chip-in-a-lab concept [134] closer to the original lab-on-a-chip idea by decreasing the footprint of the auxiliary devices needed for operation, especially in remote areas.

The second regime is the dripping regime where Capillary number is high enough so that viscous shear breaks off the interface to form a droplet before the droplet constricts the oil flow. In this regime, the flow rates and therefore the throughput is significantly higher. Moreover, the produced droplets are usually spherical and smaller than the channel width and highly mono-disperse. This regime is suitable for studying high throughput screens and single-cell studies.

The jetting regime is observed when the flow rates are increased further; in this case, the dispersed phase protrude into the main channel like a jet stream initially. Further

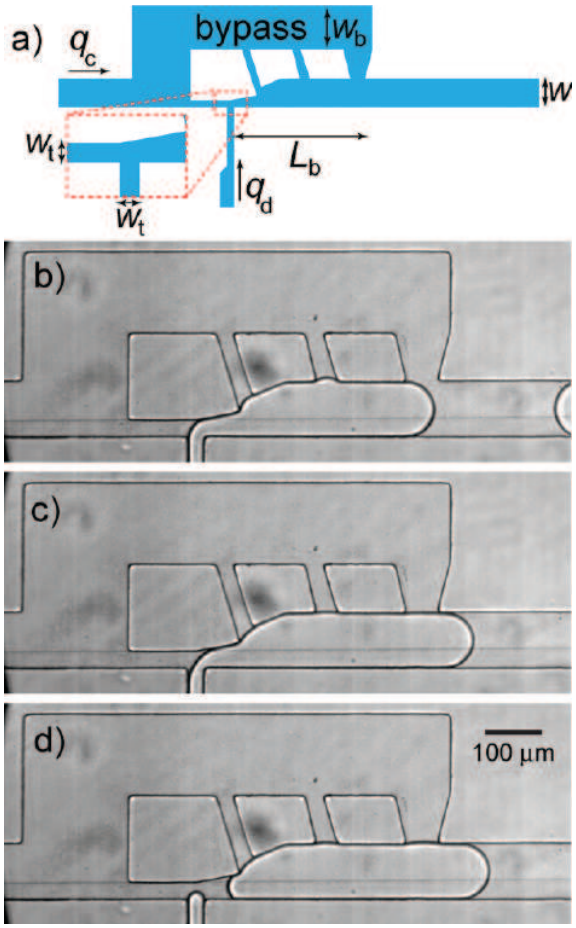

Figure 2.11: (a) Schematics of the fixed volume droplet generator design. (b)-(d) Sequential images of the droplet generation process. Reprinted with permission from [6]. Copyright 2013, AIP Publishing LLC.

downstream, due to high shear stress, the interface destabilises (Rayleigh-Plateau instability) and breaks-off to form spherical mono-disperse droplets. The jetting regime is usually preferred for particle or fiber synthesis studies [135] because the jetting length could be controlled by varying the flow parameters.

Co-flow

Flow focusing geometries (Fig. 2.9(b)) were first proposed by Anna et al. [136] and Dreyfus et al. [137] where the dispersed phase is pinched orthogonally by two continuous phase streams that are flowing in towards each other. On the other hand, co-flowing streams (Fig. 2.9(c)) were introduced by Cramer et al. [138] and they exploited the instabilities arising from the continuous phase flowing from an outer ring merging with the dispersed phase flowing through an inner ring. The physics of flow focusing and co-flowing droplet generation are quite similar yet it's often studied separately in the literature [78].

In a co-flowing system, the dispersed phase is injected into the continuous phase (Fig. 2.9(c)) where it forms a thread. This thread quickly thins due to hydrodynamic shearing and becomes unstable. As a result, the thread decays into droplets in order to minimize the total surface area thereby reducing the free energy of the interface [4]. In a flow focusing system, the co-flowing liquids are further forced through an orifice. This stretches and thins the thread resulting in smaller droplets produced. Similar to T-junctions, the size and frequency of the generated droplets depends on a number of parameters. Since flow focusing geometries are more complex, it is hard to formulate or estimate the final size and frequency using analytical approaches.

While flow focusing and co-flowing geometries are slightly more complicated to fabricate and operate, they offer enhanced mono-dispersity and higher throughputs compared to T-junction geometries. Double-emulsion studies, where single or multiple droplets are confined within bigger droplets, are usually carried out with flow focusing geometries [139,140]. It has also been argued that these geometries are preferred while working with fragile biological samples [78].

Active Droplet Formation

As an alternative to passive droplet formation techniques, researchers have come up with designs that either allow the production of droplets on demand or modify the droplet volume and frequency actively, sometimes both [5, 7–10]. This technique holds promise for exhaustive assays where multiple chemicals need to be screened in a search to find the optimum ingredients. It has been challenging to produce droplets from multiple inlets to create a combinatorial study like high throughput screening (HTS) because microfluidic devices are planar and driven by continuous flows. Moreover, it is sometimes necessary to finely tune the reacting chemicals with respect to their quantities. Active droplet generation designs address these issues by offering droplet volume control and on/off switching capabilities. Some of these techniques will be presented in this section.

One of the active droplet formation methods makes use of a micro-valve (see section 2.2.2 - Membrane Deformation) implemented at a droplet forming T-junction in order to vary the output droplet volumes [7]. As the actuation period of a micro-valve is extended, resulting droplet volume increases (Fig. 2.12(a)).

Similarly, by applying surface acoustic waves (SAWs) (see section 2.2.2 - Surface Acoustic Waves) at a droplet forming flow focusing geometry, the droplet volume and frequency could be altered on the fly [8]. In this case, as the SAW power is increased, droplet volume decreases whereas their formation frequency increases (Fig. 2.12(b)).

Moreover, heating the fluids changes their viscosity and interfacial tension. An electrical heating element was implemented at a flow focusing interface to change the final droplet volume [9]. As the temperature at the junction is increased, fluid viscosity and interfacial tension decrease thereby increasing the volume of the droplets dispensed into the microfluidic device (Fig. 2.12(c)).

Finally, micro-valves were integrated at multiple droplet formation inlets to alternate between them programmatically [10]. This resulted in the formation of a combinatorial matrix where droplets from four different inlets were mixed and matched with each other to realise all possible combinations (Fig. 2.12(d)).

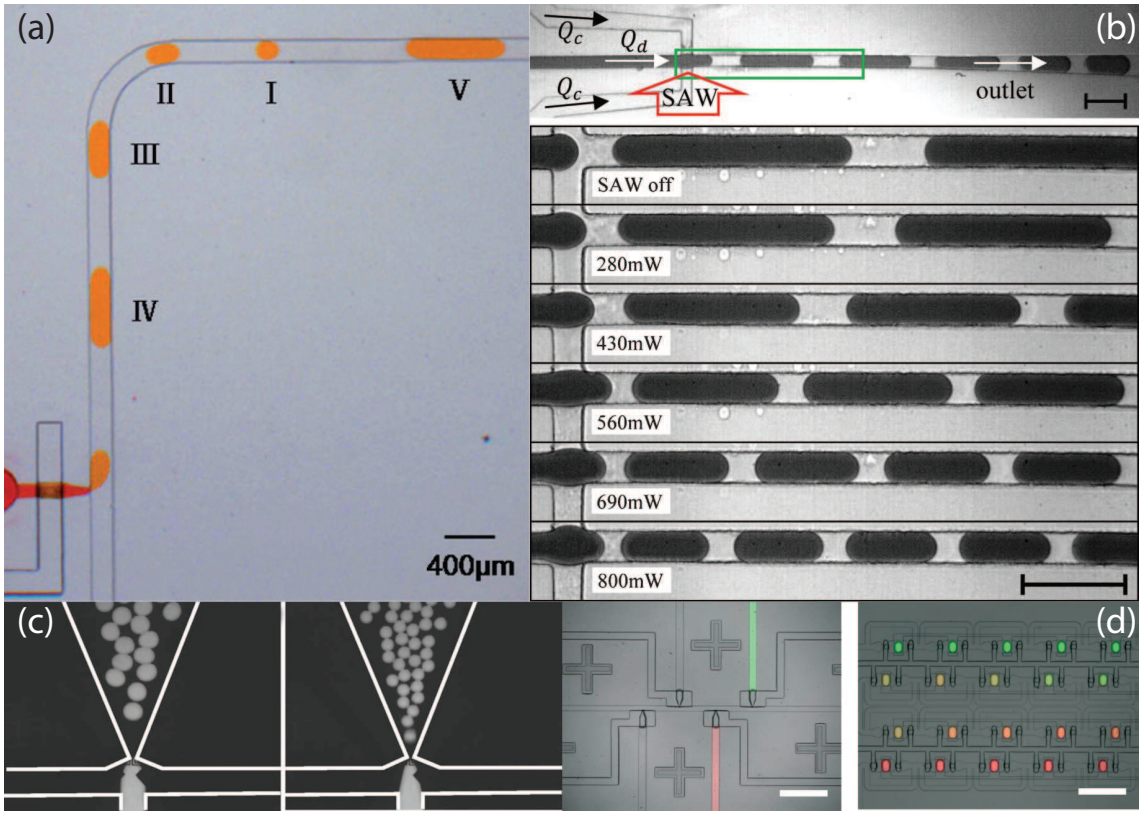

Figure 2.12: (a) Droplet formation using deforming membranes. Reproduced in part from [7] with permission of The Royal Society of Chemistry. (b) On the fly droplet volume and frequency modulation using surface acoustic waves (SAWs). Reproduced in part from [8] with permission of The Royal Society of Chemistry. (c) Droplet volume adjustment using heating. Reprinted with permission from [9]. Copyright 2007, AIP Publishing LLC. (d) Droplet formation from different inlets using membrane deformation. Reproduced in part from [10] with permission of The Royal Society of Chemistry.

Having discussed different ways of generating droplets, we will briefly go over techniques to sense the existence of these droplets. Although droplet generation is often robust and reliable, sometimes a microfluidic system gets exposed to unforeseen fluctuations that

could lead to the production of unwanted droplets in an untimely manner. In such cases, droplet sensing and sorting can be implemented to improve the system efficiency at the cost of increased complexity.

Droplet Sensing

Sensing droplets is of utmost importance when performing time-dependent studies where a droplet's exact arrival time to a specific section of the microfluidic chip is required for further manipulation such as droplet sorting. Similarly, in the case of a quantitative study where the exact number of droplets passing through a section is required, droplet sensing can provide useful information about the system. Furthermore, it is sometimes possible to sense the content or volume of a droplet while sensing as well and this can be very useful if there are certain physical or chemical requirements on the droplets. There are two primary methods for sensing droplets in closed microfluidic channels; namely, optical and electrical detection.

Optical detection methods make use of light passing through a droplet at various wavelengths. An easy to implement optical detection method is a microscope-integrated high speed CCD camera with image processing where the droplets can be processed quantitatively and qualitatively by measuring their occurrence, pixel area and light refraction intensity. However, real time image processing usually requires a significant amount of computing power therefore throughputs are usually low. Jakiela et al. [11] made use of a linear camera to sense droplets within a microfluidic channel. The linear camera records as low as 2048 pixels instead of the several mega-pixels recorded with standard CCD cameras so that the required computing power is significantly reduced and the throughput is improved. The linear camera can detect the front and the back end of the droplet by analysing light intensity, thereby providing droplet velocity and volume information as well as their occurrence frequency [11] (Fig. 2.13(a)).

Another technique is to use a photodiode for counting or timing droplets within a microfluidic system [12, 13]. Nguyen et al. [12] integrated an optical fibre across the microfluidic channel to sense the droplets via a photodiode (Fig. 2.13(b)). Robert de Saint Vincent et al. [13] took this further and implemented a pair of photodiodes connected head to tail which produces a differential signal. This signal can be interpreted at high throughputs to acquire droplet information such as size, velocity and frequency (Fig. 2.13(c)).

Moreover, light wavelength could be changed to fluorescent light and fluorescence intensity could be measured in order to distinguish between droplets by comparing their fluorescence [141,142]. Overall, optical droplet detection methods can achieve high throughputs and capture qualitative droplet information but they usually requires expensive and bulky equipment such as laser beams to operate.

Electrical detection methods, on the other hand, can be implemented as electrodes on a chip where the output could be measured by microchips and analysed by computers. Two similar examples of electrical detection are resistive [143] and conductive sensing [144] where the electrodes are in contact with the fluid in the microchannel. The conductivity of the dispersed phase is usually much higher than that of the continuous phase so once the

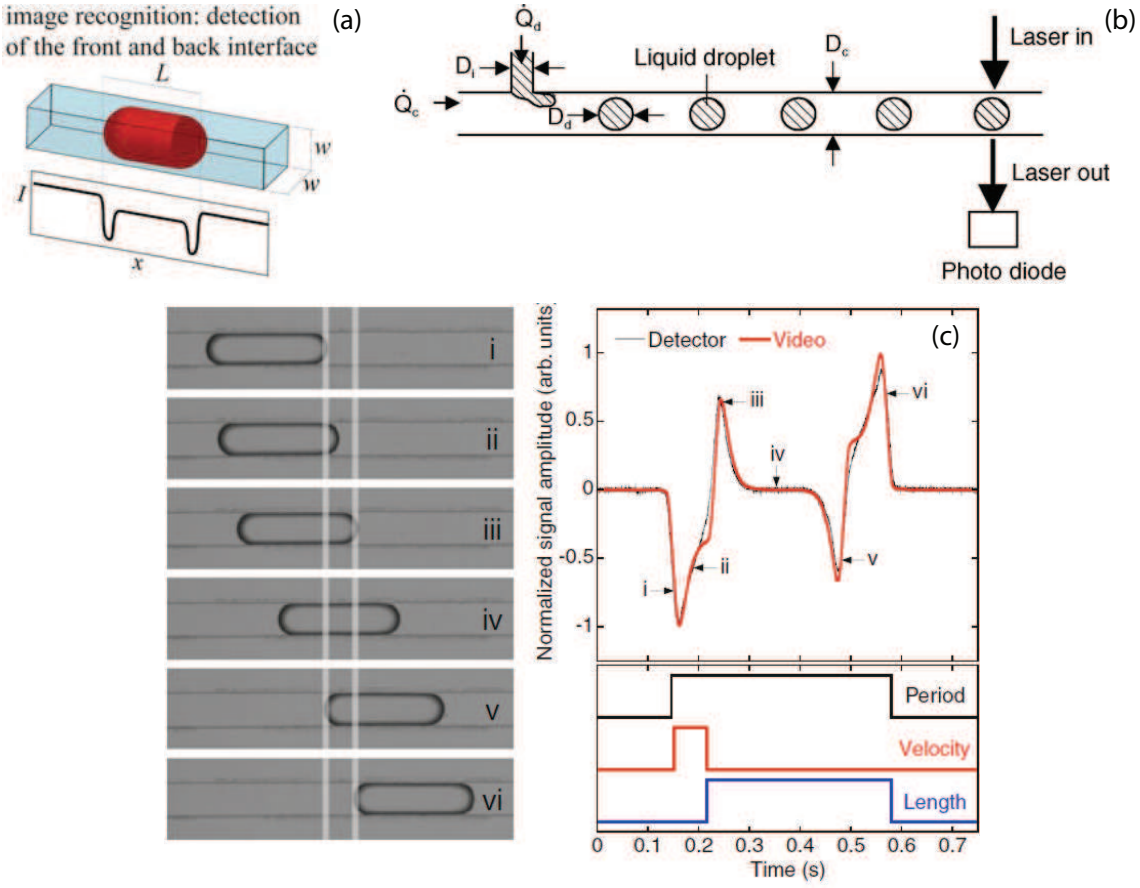

Figure 2.13: (a) Using a linear camera to sense droplets. Reproduced in part from [11] with permission of The Royal Society of Chemistry. (b) Detecting droplets with a photodiode. Reprinted from [12], Copyright (2006), with permission from Elsevier. (c) A pair of photodiodes connected head to tail to sense droplets and determine their size, velocity and frequency. Reprinted from [13] with permission of Springer.

dispersed phase comes into contact with two open electrodes, the circuit is complete and this could easily be picked up by a microchip. Similarly with resistive sensing [143]; when a conductive droplet passes over a high resistance section of the electrodes, the resistance of the sensor decreases and this can be tuned to detect droplets passing over the electrodes. Resistive and conductive methods offer superior sensitivity but require contact with the droplets in which case cross-contamination can be an issue.

Capacitive sensors, however, are fabricated with a passivation layer to eliminate cross-contamination at the expense of sensitivity. Commonly, the dielectric constant of the aqueous dispersed phase is significantly higher than its oil based counterpart, this makes conductive sensing applicable for droplet detection. One example is microwave sensing [145] where a droplet passing over a spiral sensor changes its resonant frequency which can be picked up by a microwave circuit that measures the reflection coefficient of the sensor. The preferred method of electrical detection, however, is capacitive sensing [146–149] where a passing droplet increases the capacitance of the electrodes usually integrated underneath a microchannel (Fig. 2.14). This is because of the fact that the permittivity of the droplet is higher than the continuous phase.

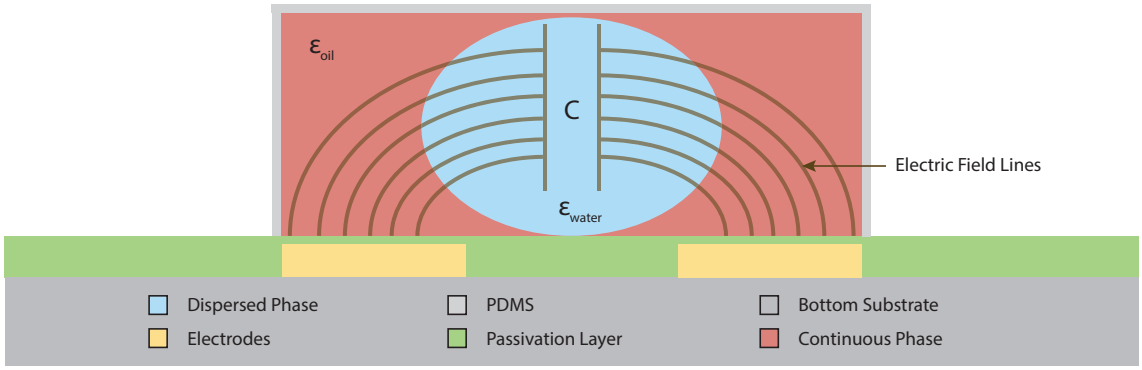

Figure 2.14: Cross sectional view of a representative microfluidic device demonstrating capacitive droplet sensing. Once a droplet with high permittivity passes over the capacitive electrodes, the capacitance increases. This can be picked up by a microchip to sense the droplet.

The design of the electrodes play an important role in the capacitive sensing of droplets. Sensing electrodes usually exhibit capacitances of a few picofarads (pF), therefore the sensor capacitance change should be adjusted to best the microchip's sensitivity. Moreover, instead of just a pair of electrodes, multiple IDT-like electrodes can be designed to obtain information about droplet size, velocity and even content [147, 149].

In the system created in chapter 6, methods from Elbuken et al.'s capacitive sensor [147] were adopted due to their robustness, ease of integration and readily available, affordable components. The fabrication techniques were slightly altered to achieve compatibility with fabrication methods of SAW inducing inter-digital transducers (IDTs) deposited on piezoelectric substrate. Finally, for the capacitive electrodes; the designs tested and optimized for a fringing field capacitive pH sensor [150] were preferred. Further details can be found in chapter 6.

Once the droplets are sensed via any of the above mentioned methods, they could be further manipulated depending on specific chip requirements. Sometimes unwanted droplets could exist in the system such as with single-cell encapsulation in droplets where cells usually are distributed into droplets according to Poisson's distribution (see Fig. 2.3(a)). In such cases; in order to get rid of the unwanted droplets or to collect desired droplets, droplets could be sorted at Y-junctions. Different techniques to sort droplets at junctions will be discussed in the upcoming section.

Droplet Sorting

The ability to sort the generated droplets on demand is crucial in the design of lab-on-a-chip (LOC) devices. Some droplet microfluidics studies require droplets to be sorted into different outlets thereby getting rid of unwanted droplets or collecting wanted droplets into one specific channel. More often than not, the distinction between wanted and unwanted droplets are achieved by droplet sensing systems which was discussed in the previous section.

A common method to achieve droplet sorting starts with biasing one of the two outlets so that the droplets automatically steer into the low resistance channel in the absence of external actuation. Once a droplet is identified as unwanted or desired, however, the information can be used to trigger an actuation mechanism which would then work to steer that droplet to the unbiased higher resistance channel.

Microfluidic droplet sorting devices have been designed with mechanical actuation [151] but they were prone to slow response times due to the large relaxation times of pumping systems [17]. One of the most promising droplet sorting technique utilises dielectrophoresis [14,15,141] (Fig. 2.15(a),(b)) where the droplets are attracted into the unbiased channels by DEP forces (see section 2.2.2 - Electric Fields). However, due to its dependence on the gradient of an electric field, high voltage (several kV's) is needed to provide sufficient forces with these applications [16].

Droplet sorting can also be achieved by pre-charging the droplets and then steering them under an electric field [16, 123] (Fig. 2.15(c)) (see section 2.2.2 - Electric Fields). This reduces the high voltage requirement for steering droplets because they are charged, however, charging droplets requires an additional splitting step and can sometimes be harmful for the content of the droplets.

Magnetic sorting can be achieved with magnetic labelling [15]. The labelled droplets respond to magnetic fields generated inside microfluidic devices due to their magnetic content. Higher sorting rates can be achieved with magnetic sorting but magnetic labelling can be undesired especially when working with delicate biological samples.

Additionally, droplets could be sorted with surface acoustic waves (SAWs) [17] (Fig. 2.15(d)) (see section 2.2.2 - Surface Acoustic Waves). In this case, Franke et al. [17] made use of a Y-junction design where the droplets preferentially followed the upper channel (low resistance) in the absence of SAWs. When the IDTs are excited, however, SAWs couple into the continuous medium and induce acoustic streaming. This streaming agitates the

continuous medium which in turn displaces droplets laterally and forces them to be steered into the high resistance outlet channel.

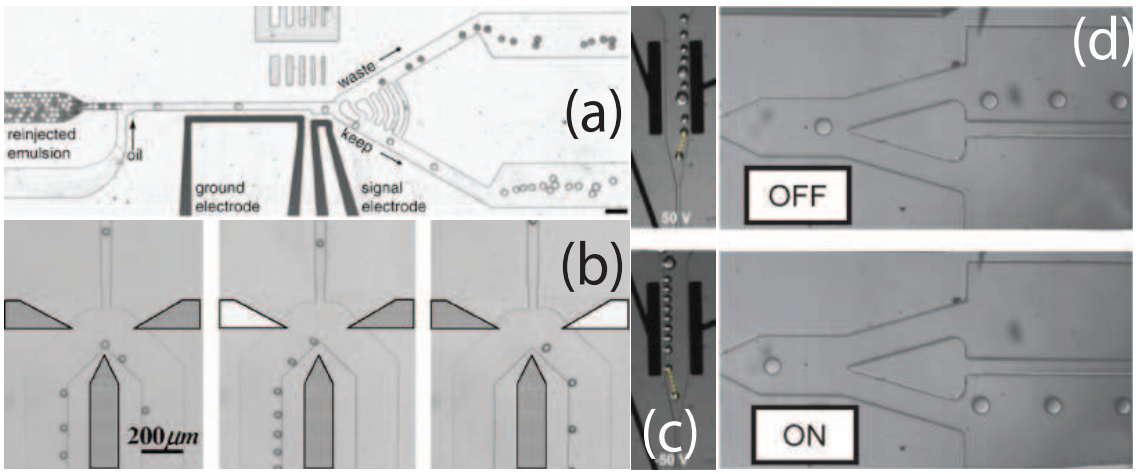

Figure 2.15: (a) Dielectrophoretic sorting of droplets. Reproduced from [14].Copyright 2010 National Academy of Sciences, USA. (b) Microfluidic sorting of droplets utilising dielectrophoresis. Reprinted with permission from [15]. Copyright 2006, AIP Publishing LLC. (c) Sorting of pre-charged droplets subjected to transverse electric field. Reproduced in part from [16] with permission of The Royal Society of Chemistry. (d) Sorting of droplets with surface acoustic waves. Reproduced in part from [17] with permission of The Royal Society of Chemistry.

In the presented thesis, plugs have been steered completely or split unevenly at a specially designed Y-junction (Fig. 2.16). SAWs have been directed to the interface of the plugs to displace them into one or the other outlet which were not biased during the study. Although biasing is a convenient method for steering droplets, the outlet resistances have to be carefully maintained in order for the system to work. The system demonstrated here can sort larger plugs into any of the outlets (Fig. 2.16(a),(b)) without losing valuable sequence information. Moreover, it offers control of even (Fig. 2.16(c)) or uneven (Fig. 2.16(d)) splitting of the plug at the Y-junction in a programmable manner.

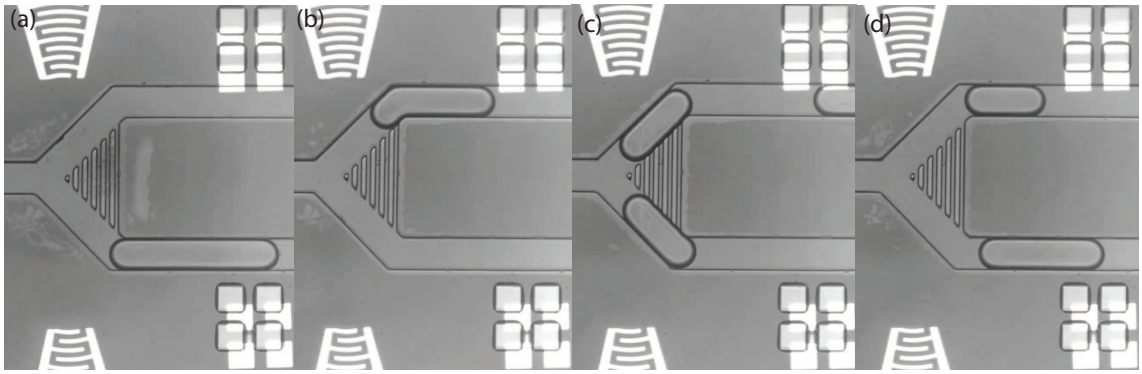

Figure 2.16: Microfluidic plug steering using surface acoustic waves (SAWs). (a) The plug can be completely steered into lower channel if top IDTs are actuated. (b) The plug can be completely steered into upper channel if bottom IDTs are actuated. (c) The plug evenly splits if the SAWs are not actuated due to equal outlet conditions. (d) The plug unevenly splits if the SAW actuation power is low [18].

Microfluidic plug steering using surface acoustic waves is presented in more detail in chapter 5 where in-depth analysis and characterisation of the system is carried out.

Droplet Merging

Chemical and biological analysis commonly needs coalescence of different liquids (e.g., samples and reagents) to complete the reactions [152]. Reactions in droplets can be used for a number of applications, including the formation of particles, chemical synthesis, kinetics studies, or for the synthesis of biomolecules [153]. Droplet microfluidic systems offer the advantage of isolated droplets which could be merged to serve as compartments in which to study fast organic reactions [45]. This is why another essential component of a potential versatile LOC device would be the on demand merging of consecutive droplets so that the desired samples and reagents could readily be merged.

There are multiple factors that affect droplet coalescence such as wall wetting properties, microchannel geometry, capillary number, surfactants, liquid viscosities and impact velocity but they have not yet been characterised thoroughly [19]. The most commonly used model to predict droplet coalescence is the film drainage model which will be explained with a brief overview.

Without Surfactants

Aqueous droplets without any surfactants merge spontaneously upon contact or within close proximity due to film drainage effects (Fig. 2.17 (a)). There exists a film of continuous medium between two adjacent droplets which prevents coalescence and the time it takes for this film to reduce its thickness by half is given as [154]:

$$t_{drainage} = 40r\sqrt{\frac{\mu_c}{\gamma u}} \tag{2.19}$$

where r is droplet radius, μ_c is the viscosity of the continuous medium, γ denotes the interfacial tension between the liquids and u is the constant approach velocity. As soon as the liquid film thins out, intermolecular forces come into play and rupture the interface, allowing merging to take place [19]. The work presented in chapter 4 describes a microfluidic droplet merging system without the use of surfactants. If the parameters from this study are applied to equation 2.19, $t_{drainage}$ turns out to be 0.12 s. This exemplifies how quickly the merging takes place with the absence of surfactants.

Furthermore, it has been shown that there exists a critical capillary number (see Eqn. 2.10), $Ca_c \approx 10^{-2}$, that determines the threshold for droplet merging to succeed [19,155]. If the capillary number is less than this critical value (i.e $Ca < Ca_c$), then droplet coalescence is more likely to occur. Similarly, the capillary number in the droplet merging study (chapter 4) was calculated and it was found as $Ca = 4 \times 10^{-3}$ satisfying this theoretical condition.

With Surfactants

Most often than not, surfactants are added to the continuous phase to carry out microfluidic studies. The addition of surfactants finds widespread usage by researchers because it reduces interfacial tension for easy droplet generation and transport, prolongs stability in

a closely packed droplet formation (see Fig. 2.3(a)) and prevents cross-contamination so droplets can be used as individual micro-reactors.

The downside of adding surfactants is that it undermines the spontaneity of droplet coalescence due to two main phenomena; surfactant repulsion and Marangoni effect. Surfactants coat the interface of the droplets and they strongly repel each other, in this way the liquid film thickness does not thin out and the droplets maintain stability. Moreover, Marangoni effect takes place which creates a counter-flow in the liquid film thereby slowing down the liquid film drainage process. This effect is shown in Fig. 2.17(b) where the red arrows indicate the direction of Marangoni flow.

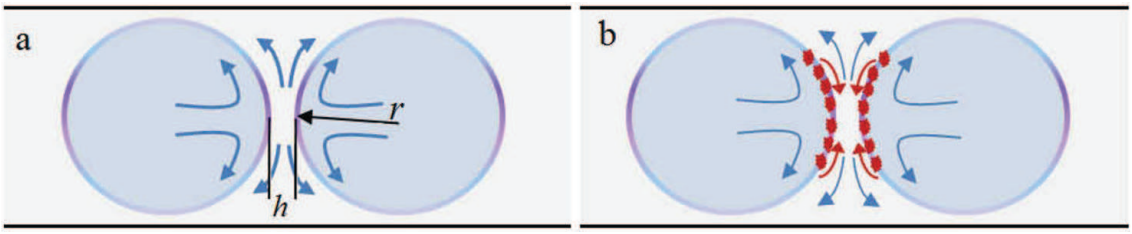

Figure 2.17: (a) Film drainage (blue arrows) schematic with the absence of surfactant and (b) with the surfactant where Marangoni stress (red arrows) counteracts film drainage. Reprinted from [19] Copyright (2015), with permission from Elsevier.

Marangoni flow occurs due to discontinuities in the surface tension of the interface where a higher surface tension will pull its surrounding liquid more strongly compared to a lower value. Since the surfactant is responsible for altering the surface tension of the droplets, the surfactant concentration near the droplet interface plays an important role in modifying the local surface tension of individual droplets. The immediate surfactant concentration at the liquid film interface can become uneven due to factors such as flow and molecular diffusion [19] thereby leading to discrepancies in the surface tension around the droplet which results in Marangoni flows that delay the film drainage and consequently increase droplet stability.

Since coalescence of microfluidic droplets is usually not spontaneous, researchers have come up with methods to ensure that fusion takes place. Two main methods find widespread usage for microfluidic droplet merging, namely, electrocoalescence [20,21,123,156] (Fig. 2.18(a),(b)) and hydrodynamic methods [22,23] (Fig. 2.18(c),(d)).

It's widely known that if a droplet-droplet interface is subjected to intense electric field, the interface ruptures and droplets fuse even in the presence of surfactants. This is termed electrocoalescence. The physical principles behind electrocoalescence are believed to be the interaction between the electric field and the droplets, leading to droplet charging by induction and contact, and then aggregation and coalescence through electric field-induced droplet-droplet interactions which do not require the droplets to be charged [157]. Generally, an electric field is applied to promote contact between the dispersed aqueous droplets, facilitate aqueous droplet-droplet coalescence and promote aqueous droplet interface rupture and consequent coalescence with free aqueous liquid at a plane interface [158]. This requires the conductivity and permeability between two immiscible fluids to be different which is usually the case [157,159–162].

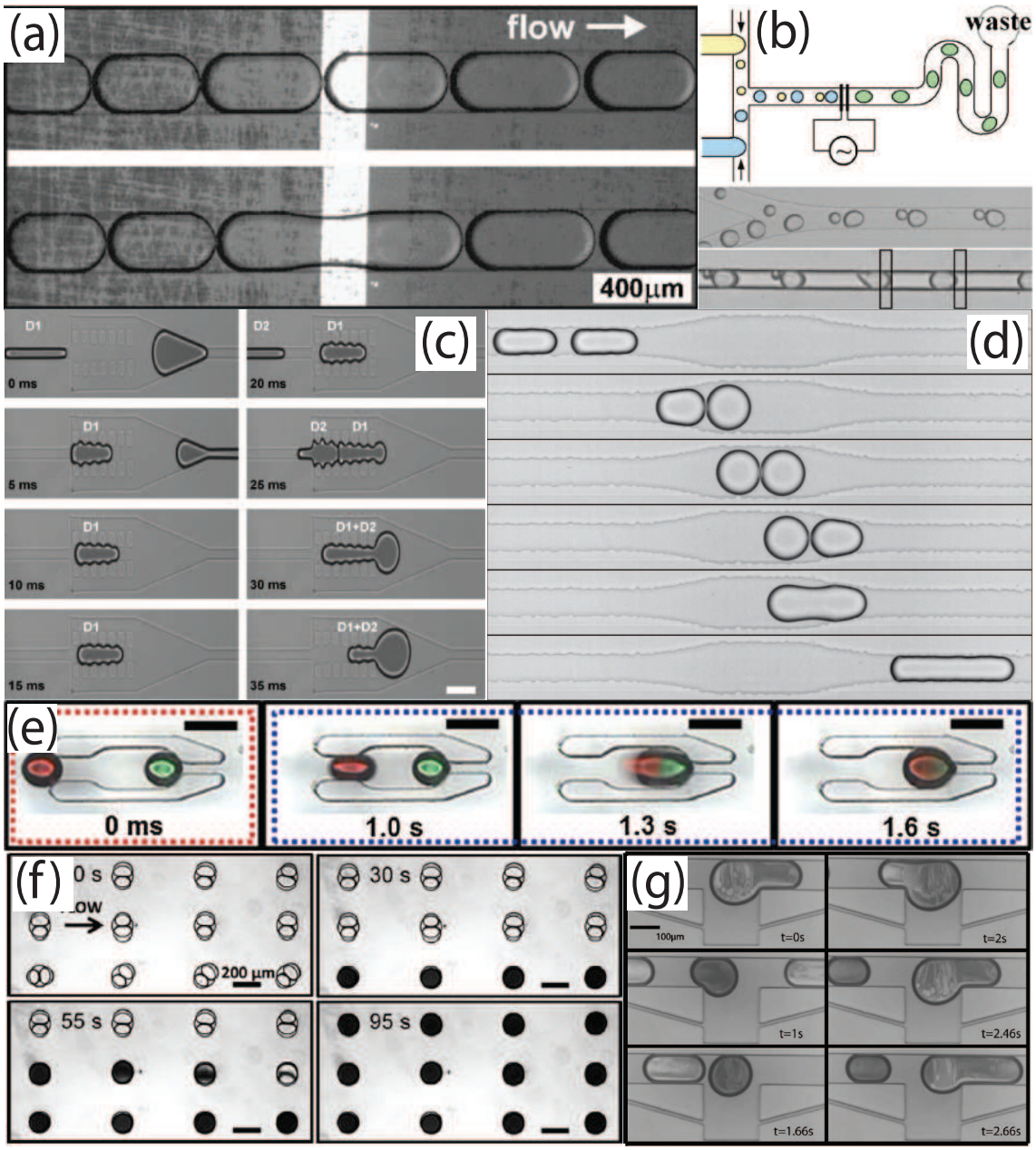

Figure 2.18: (a) Droplet merging with electrocoalescence. Reprinted with permission from [20]. Copyright 2006, AIP Publishing LLC. (b) Electrocoalescence of synchronized droplets. Reprinted with permission from [21]. Copyright 2006, AIP Publishing LLC. (c) Pillar droplet merging where the droplet is trapped within pillars until a second one comes and physically merges with the trapped droplet. Reproduced in part from [22] with permission of The Royal Society of Chemistry. (d) Droplet merging with the aid of an expansion where the droplets slow down due to expanding microchannel geometry and the successive droplet merges with the slow one. Reprinted figure with permission from [23], Copyright (2008) by the American Physical Society. (e) Droplet trapping and merging within microfluidic traps using pressure bursts induced by deforming membranes. Reprinted from [24] with permission of Springer. (f) Droplet trapping into surface energy wells followed by flushing with no surfactant carrier fluid leads to coalescence of trapped droplets. Reproduced in part from [25] with permission of The Royal Society of Chemistry. (g) Droplet merging using surface acoustic waves where the droplets is trapped within the acoustic field until the next droplet comes and merges with the trapped one. Reproduced in part from [26] with permission of The Royal Society of Chemistry.

Hydrodynamic merging of droplets, however, relies on high impact velocity of droplets and is achieved through clever microchannel geometry designs and requires no external actuation. Generally, a speed bump is introduced further downstream to the formed train of droplets. When a droplet flows through the speed bump zone, its velocity decreases either due to designed physical restrictions [22] (Fig. 2.18(c)) or due to an expansion in the channel [23,163,164] (Fig. 2.18(d)). The trailing droplet comes in fast and then fusion takes place between the two droplets or more. However, it is not possible to accomplish merging on demand with the passive hydrodynamic methods developed so far.

More recently, droplet merging has been achieved by the aid of membrane deformation (see section 2.2.2 - Membrane Deformation) which can induce pressure bursts to trap multiple droplets in storage chambers [10,24] (Fig. 2.18(e)). Furthermore, Tullis et al. [25] managed to trap multiple droplets in surface energy wells and flushed the system with oil without surfactant to induce fusion (Fig. 2.18(f)). In both of these recent studies, since the droplets are already trapped prior to fusion, fast reaction kinetics studies could be performed with high accuracy because the merging could be controlled.

As part of the work presented in this thesis, droplet merging was achieved by acoustically trapping incoming droplets within a micro groove until successive droplets coalesced with the trapped one [26] (Fig. 2.18(g)). Surface acoustic waves (SAWs) were directed to the droplets in the micro expansion chamber which lead to acoustic-tweezers-type trapping of the droplets in the high pressure zone. As consecutive droplets reached the chamber and collided into the trapped droplet, fusion took place. Once the droplet in the chamber reached a certain size limit, acoustic forces were overcome by drag forces and the merged droplets exited the trapping chamber. This technique allows on-demand, controlled merging of consecutive droplets where the sequential formation of various droplets could be utilised to carry out a combinatorial droplet library study. Droplet merging with SAWs will be presented with full detail entailing analysis and characterisation of the system in chapter 4.

Droplet Splitting

Yet another essential droplet manipulation technique is the opposite of droplet merging called droplet splitting or sometimes droplet fission. This technique has also been extensively studied in droplet-based microfluidics systems. Droplet splitting attracts high demand because it helps to reduce the droplet volume [152], to control the concentration of chemicals inside the droplets [165] and to produce arrays of droplets for high-throughput applications [28]. Since each droplet can serve as a vessel for reagents, by splitting the single droplet into two or more droplets, the experimental capacity can easily be scaled up [153].

Droplet splitting methods do not rely on external components or power, they usually involve single or multiple bifurcating junctions. As a droplet is flowing through a bifurcating junction, it is affected by the shear forces occurring due to channel design. If the interfacial tension could be overcome by the shear forces, droplets split into two or more daughter droplets. The symmetry of the junction could be modified to adjust the relative sizes of the daughter droplets. A perfectly symmetric junction would lead to the break up

of a droplet into two equal sized droplets [27, 28, 166] (Fig. 2.19(a),(b)), whereas with an asymmetric junction, the droplet will be divided into two unequal daughter droplets [167] (Fig. 2.19(c),(d)). It has also been shown that two daughter droplets of different concentrations could be obtained by an asymmetric bifurcation junction [165].

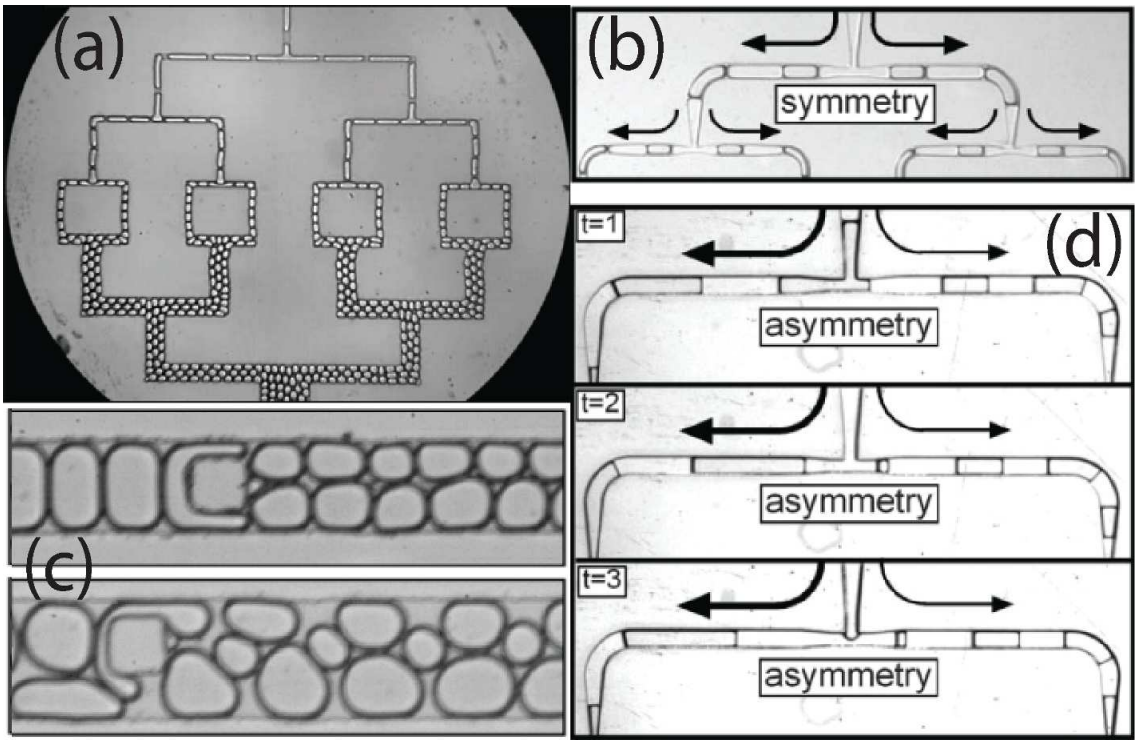

Figure 2.19: (a) Symmetric droplet splitting. Reprinted figure with permission from [27], Copyright (2004) by the American Physical Society. (b) Symmetric droplet splitting. Reproduced in part from [28] with permission of The Royal Society of Chemistry. (c) Asymmetric droplet splitting. Reprinted figure with permission from [27], Copyright (2004) by the American Physical Society. (d) Asymmetric droplet splitting. Reproduced in part from [28] with permission of The Royal Society of Chemistry.

Two novel, active and controlled plug splitting methods will be presented in this thesis. Plug splitting has been achieved by utilising surface acoustic waves (SAWs) in two different microfluidic systems. In the first one, SAWs are directed at the plug interface whilst approaching a Y-junction (Fig. 2.20(a)) to achieve uneven plug splitting. When the travelling SAWs (TSAWs) act on the interface of a plug, they deform and push the interface away from the TSAWs into the desired outlet channel. Depending on the power of the applied TSAWs, the splitting can be controlled to an accuracy of 15% [18]. An incoming plug, at the extremes, can be split into two daughter droplets consisting of 86% and 14% of the original plug volume with this method. This method has a potential to prove extremely useful whilst studying volume dependant reaction kinetics. In-depth analysis and characterisation of the proposed system can be found in chapter 5.

As an advancement to this plug splitting method, a better microfluidic system is proposed in this thesis where the splitting could be controlled much more accurately. In this design, a by-pass loop is integrated to the main microfluidic channel which does not induce splitting in the absence of SAWs. Once the SAWs are generated, they propel the

continuous medium in the upper section of the by-pass loop which leads to a strong suction effect at the by-pass entrance junction when a plug is passing through. Depending on the duration of the applied SAWs, a part of the main plug is split into the by-pass channel (Fig. 2.20(b)). Additionally, a plug sensor is integrated upstream of the T-junction to accurately time the application of the SAWs. This automated system also allows the user to select which plugs should be split by how much into the by-pass channel where they can be further manipulated (i.e merged or trapped). Further analysis and system characterisation can be found in chapter 6.

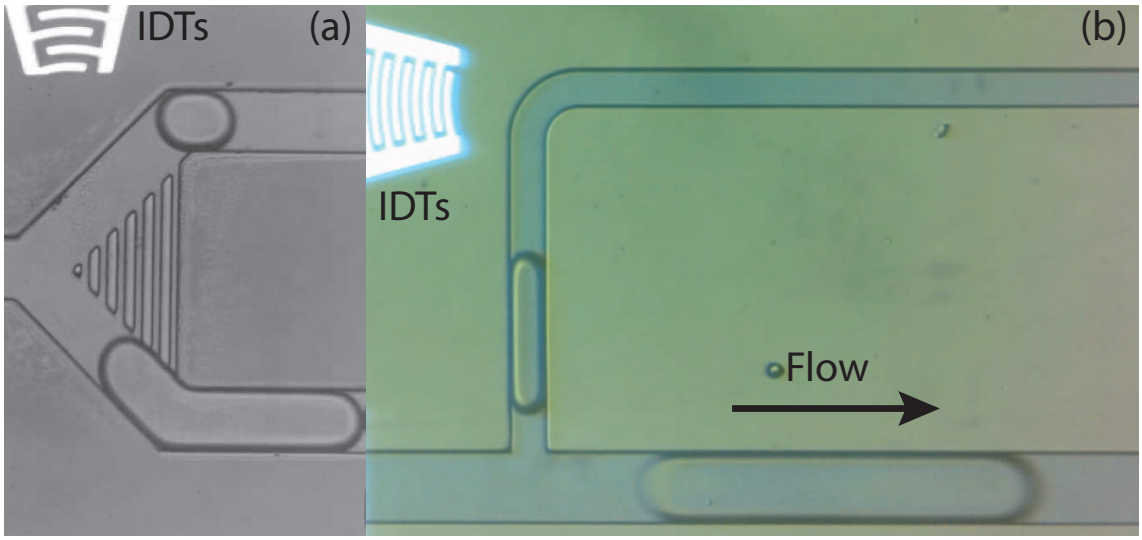

Figure 2.20: (a) SAWs generated by the IDTs deform and push the plug interface into the bottom channel at a specially designed Y-junction leading to asymmetric splitting of the plug depending on the intensity of applied acoustic energy [18]. (b) SAWs directed at a by-pass channel propel the continuous fluid to induce suction of a plug into the by-pass channel controlled by the duration of applied SAWs.

Droplet Trapping

Given the fast nature of high throughput screening (HTS) applications, it would be unintuitive to track a single droplet to observe the reaction occurring within. A better approach is to trap a droplet, observe while the droplet is immobile and then release the droplet for further manipulation. However, given that microdroplets of pL size are highly mobile and not rigid, it is quite hard to trap them. Researchers have developed various novel methods to overcome this problem.

One method is to design appropriate micro parking spaces for droplets within the microfluidic device [29,30,168] (Fig. 2.21(a),(b)). When the droplets arrive at the parking spaces, they passively get trapped usually due to higher interfacial tension imposed by the small channel geometry.

Abbyad et al [31] demonstrated successful trapping and releasing of droplets in surface energy wells (Fig. 2.21(c)). Surface energy wells can be achieved by microfabricating small holes or railways at the roof of a microfluidic device [25,31]. When a droplet encounters a surface energy well, it's local surface tension increases due to small channel dimensions.

The higher surface tension in the energy well counteracts the fluid drag on the droplet; in this way the droplet stays trapped in the desired area. However, such designs might lead to the loss of sequence information which is crucial to high throughput screening applications like drug screening [169].

Furthermore, Wang et al [32,90] managed to selectively trap droplets into micro chambers by utilising dielectrophoretic (DEP) forces (see section 2.2.2 - Electric Fields) (Fig. 2.21(d)). The droplets were subjected to DEP forces when passing near the electrodes, therefore they were polarised and pushed into micro chambers where further observation could take place. It should be noted that this method is dependant on fluid properties, can be damaging to biological media and requires voltages of several kVs.

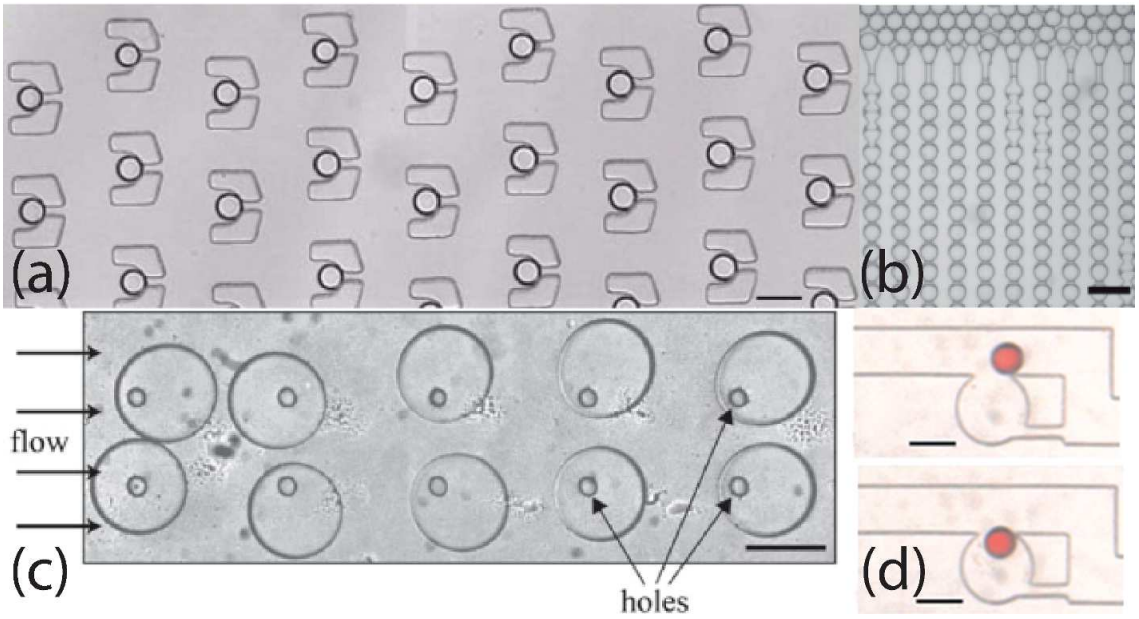

Figure 2.21: (a) Static droplet traps. Reproduced in part from [29] with permission of The Royal Society of Chemistry. (b) Droplet trapping at micro parking spaces. Reproduced in part from [30] with permission of The Royal Society of Chemistry. (c) Droplet trapping at surface energy wells Reproduced in part from [31] with permission of The Royal Society of Chemistry. (d) Droplet trapping in micro chambers with dielectrophoresis. Reproduced in part from [32] with permission of The Royal Society of Chemistry.

We have also designed similar micro chambers and successfully trapped droplets by selectively displacing them inside these chambers using SAWs (Fig. 2.22). Similar to pushing plug interfaces at a Y-junction (see previous section), droplets can be forced into trapping chambers where there's a by-pass channel integrated so that the continuous medium can vacate the chamber whilst a droplet is coming in. This work will not be presented as a part of this thesis, its sole purpose is to demonstrate that we can achieve all of the above mentioned droplet manipulation techniques using SAWs.

Droplet Dilution

Another fundamental component of a LOC would be the generation of droplets with varying concentrations in a rapid and controllable manner. This is usually required when screening

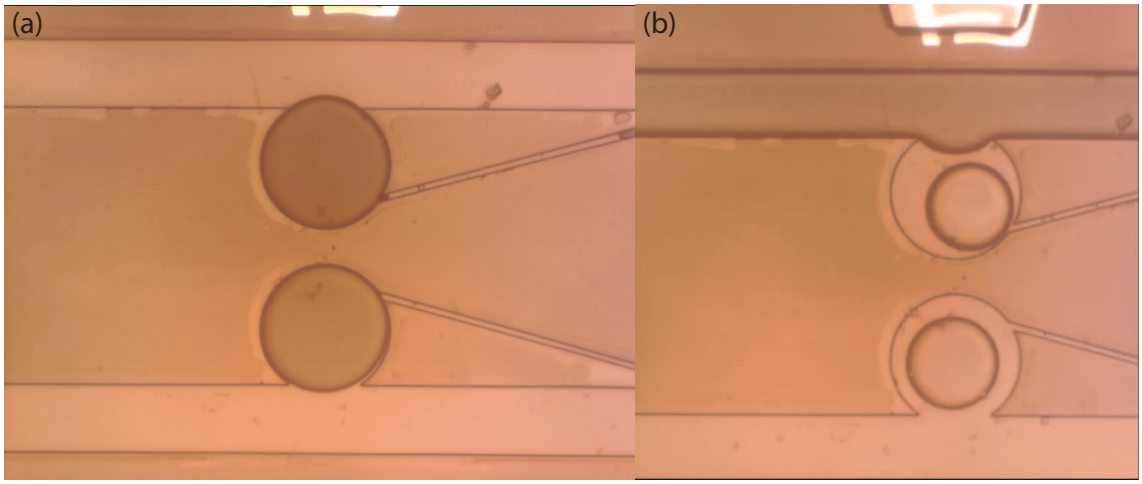

Figure 2.22: Droplet trapping into micro chambers by using surface acoustic waves.

or assaying rare biological samples [170]. While this is a standard and easy task for a macroscale environment, it is quite a challenging operation in closed microfluidic channels.

An early attempt at generating a concentration gradient in a continuous flow microfluidic system exploits on the fact that flow is always laminar in a microfluidic channel due to low Reynolds number (see eqn. 2.1). A carefully designed network of microchannels enables controlled diffusive mixing of species flowing in parallel fluid streams [33] (Fig. 2.23(a)). More recently, this concept was used in a multi-layer microfluidic device where the continuous concentration gradient produced was used to create droplets [34] (Fig. 2.23(b)).

Another attempt at creating concentration gradients was accomplished by utilising controlled exchange of materials between moving plugs and stationary drops [35] (Fig. 2.23(c)). As the moving plug was diffusively mixing with the stationary droplets, a concentration gradient was formed. Furthermore, Niu et al. [36] designed a droplet dilution module using droplet microfluidics. The diluted droplets were formed through merging with a highly concentrated reservoir, diffusing to a certain extent and then splitting from the reservoir at the other end (Fig. 2.23(d)). As the reservoir is diluted, the produced droplets had less and less concentrations of the reservoir content (Fig. 2.23(e)). As the reservoir gets depleted, however, it needs to be replaced which might prove to be time consuming for high throughput applications.

Droplet Mixing

As mentioned earlier, the small size of the microchannels in a microfluidic system imposes that the flow always stays in the laminar regime. The laminar flow poses a problem when it is desired to mix the fluids inside a microchannel. Especially when studying the kinetics of biological and chemical reactions [153], the degree of mixing becomes quite important. Diffusive mixing still takes place inside a droplet, however, such mixing takes a relatively long time and is not suitable for high throughput applications.

Researchers have come up with several designs to promote rapid mixing in microchannels by exploiting the fact that droplet movement through a channel creates a recirculating flow in each half of the droplet that touches the channel wall [153,171]. As a droplet takes

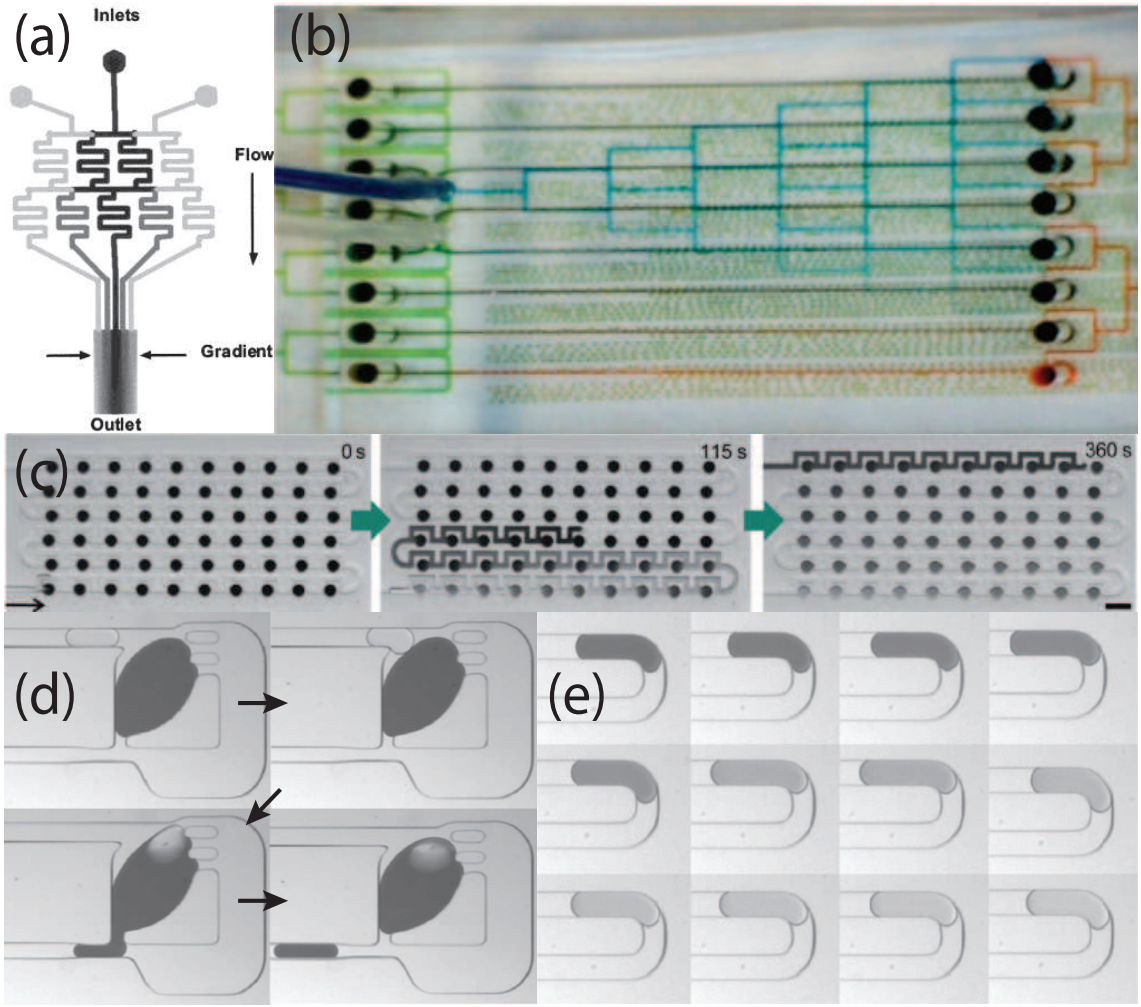

Figure 2.23: (a) Continuous flow gradient formation using diffusive mixing of species. Reprinted with permission from [33]. Copyright (2000) American Chemical Society. (b) Multi-layered microfluidic device that can generate droplets from a continuous concentration gradient formed in the upper layers. Reprinted with permission from [34]. Copyright (2015) American Chemical Society. (c) A library of concentration gradients created by utilising controlled exchange of materials between moving plugs and stationary droplets. Reproduced in part from [35] with permission of The Royal Society of Chemistry. (d), (e) Generation of diluted droplet gradients by sequential mixing with a reservoir. Reprinted by permission from Macmillan Publishers Ltd: Nature Chemistry [36], copyright (2011).

a turn in a microchannel, each part of the droplet is exposed to different lengths of channel wall, therefore creating chaotic advection inside the droplet and enhancing mixing. A winding microchannel geometry leads to iterative folding and stretching of the droplet to maximise mixing with chaotic advection [172] (Fig. 2.24(a)). Moreover, the length of the serpentine microchannel geometry could be modified to achieve the desired level of mixing required for the intended study. Furthermore, introducing artificial roughness along the channel wall was also reported to enhance mixing in microfluidic devices [38](Fig. 2.24(b)).

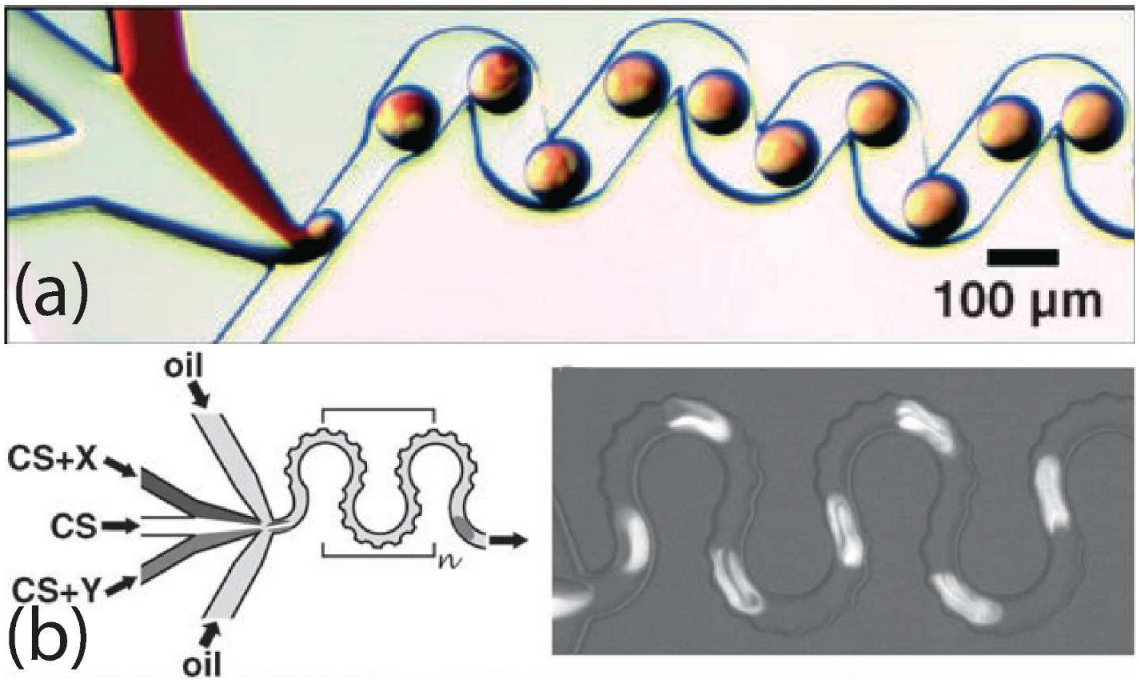

Figure 2.24: (a) Mixing of individual droplets in a serpentine channel by chaotic advection. Reprinted with permission from [37]. Copyright 2003, AIP Publishing LLC. (b) Droplet mixing with bumpy serpentine mixer. Reprinted with permission from [38]. Copyright (2005) American Chemical Society.

2.3 Conclusion and Research Aims

Now that we have looked at the literature on microfluidics, especially focusing on droplet microfluidics and different droplet manipulation techniques, we can jump to specific conclusions and clearly indicate the research aims of this thesis.

Despite the fact that some of the proposed devices were modified and used in specific studies such as acoustic loading of virus-like particles (VLPs), trapping and recovery of photodegradable hydrogels and reconstructing ternary phase diagram of water-ethanol-hexanol mixtures; this thesis focuses on the engineering aspect of the proposed microfluidic devices and how this can greatly contribute to the available knowledge. In this sense, a direct conclusion to draw from the explored droplet manipulation techniques is that they all utilise various actuation methods that could be achieved with specific and usually not cross-compatible fabrication techniques. Due to this fact, they are very specific to what kind of droplet operations they can perform and do not offer much flexibility.

We, on the other hand, have adopted surface acoustic waves (SAWs) as our primary actuation method and shown that we can outperform most the above mentioned droplet manipulation techniques. Furthermore, we have developed these methods separately while keeping making sure not to impose any restricting flow characteristics (i.e specific inlet or outlet pressure) or specific fabrication techniques so that all the developed methods could be mixed and matched like LEGO® blocks to build a system suiting every specific studies' needs. A passive "plug-n-play" modular microfluidic system, SmartBuild [173], has been developed with similar qualities and it can be upgraded with active manipulation capabilities. We have, overall, shown that droplets can be sensed, sorted, split, merged and trapped using SAWs. It is also important to note here that our group has previously shown that droplets could be formed on demand using SAWs [5]. This leaves dilution and mixing which can be integrated to any system as passive methods and they have been thoroughly characterised.

Apart from the above mentioned research goals, we have also taken on a challenge that existed since the 2000s. It is widely believed that droplet-based microfluidics for carrying out biochemical and cell-based assays has the potential for triggering a complete paradigm shift in the evolution of high throughput screening (HTS) technology [69–71]. For this matter, being able to create a matrix of droplets from two distinct libraries is of utmost importance. Proposed in this thesis is a plug splitting microfluidic device which can achieve this task because it can be programmed to split predefined plugs. Since consecutive plugs of various content can be formed using a Serial Sample Loading (SSL) system [174], with the proposed plug splitting system, a combinatorial study could easily be realised. The throughput of the system needs yet to be improved in order to compete with current HTS systems but we believe this is a substantial step towards a remarkable goal.

Chapter 3

Theory and Fabrication

This chapter will focus on the theory of acoustics with emphasis on surface acoustic waves (SAWs), the technique used throughout this thesis, detailing the mechanisms associated. This will be followed by an exploration of the microfabrication techniques utilised to produce microfluidic devices capable of generating SAWs.

3.1 Acoustics

Acoustics is the study of mechanical waves propagating in media such as solids, liquids and gases. Acoustic research dates back to Pythagoras who was studying musical harmonics as early as 6^{th} century BC. Modern acoustics is now a vast field of study encompassing, but not limited to, earthquakes, ultrasound imaging, sonar, mechanical vibration, musical acoustics, soundscapes and speech recognition. Since every wave has a frequency associated with it, we can categorise waves depending on their frequencies such as audible sound, ultrasound and infrasound (Fig. 3.1).

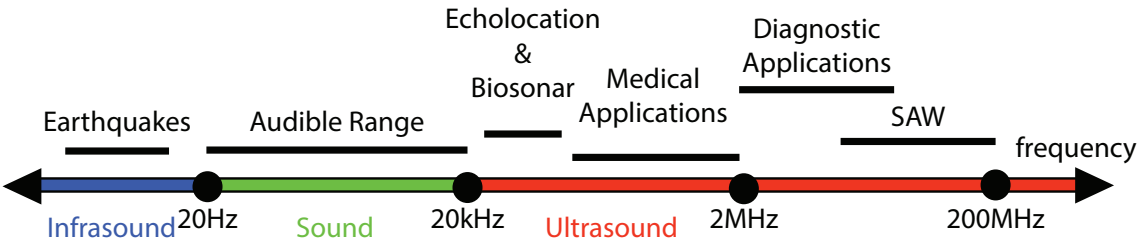

Figure 3.1: Approximate sound frequency ranges and their applications or occurrences.

Ultrasound waves are defined as sound waves with frequencies exceeding the audible range (i.e $f > 20kHz$). Although inaudible by humans, ultrasound is used by bats to hunt prey (echolocation) and by dolphins to navigate (biosonar). Ultrasound technologies that find widespread usage today include shock wave lithotripsy for kidney stone treatment [175], ultrasonic cleaning, ultrasonic imaging, sonochemistry [176] and non-destructive testing [177].

Ultrasound also finds widespread usage in microfluidic applications [89] owing to the rapid progression of nanofabrication techniques and its safe usage with biological samples

[178]; usually termed "Acoustofluidics", it can be used to perform particle manipulation [40, 179–185], cell manipulation [186,187], gene therapy [188], droplet manipulation [17,18,26], microfluidic mixing [39,189,190] and bone fracture healing [191].

This chapter will focus on the theory of acoustofluidics with emphasis on surface acoustic waves (SAWs), the method used in this thesis to manipulate droplets and plugs.

3.1.1 Surface Acoustic Waves

Surface acoustic waves (SAWs) are nm-scale amplitude, MHz frequency acoustic waves propagating on a piezoelectric substrate. SAWs have been widely employed in microfluidic applications [5,8,76,192–197] addressing tasks including particle manipulation [198–202], cell manipulation [41,203,204], microfluidic pumping [205], droplet manipulation [17,18,26] and drug delivery [75]. Some of the major advantages of using SAWs in microfluidic systems stems from their energy efficient and portable nature as well as their ease of fabrication and seamless integration. On the contrary, SAWs can only be generated on relatively expensive piezoelectric substrates where unwanted heating might occur. Heating in surface acoustic wave devices will be discussed in detail later this section.

Direct piezoelectric surface wave transduction was first introduced in the micro-scale [206] in the form of inter-digital transducers (IDTs) which are equidistant electrodes deposited on piezoelectric substrate. When a radio frequency signal is applied to the IDTs, a periodic electric field matching the operating frequency of the IDTs is produced. This field electromechanically couples with the piezoelectric material to generate travelling surface acoustic waves. The distance between each successive transducer determines the resonant frequency, f, of the device according to $f = c_s/\lambda$, where c_s is the sound speed on the substrate surface and $\lambda/2$ is the distance between successive IDT fingers (Fig. 3.2).

Since the thickness of the substrate (500 μm) is much larger than the amplitude of the travelling waves, these waves can be classified as Rayleigh waves [207]. Rayleigh waves are special waves that travel along the near surface of a solid medium; an earthquake, for example, is a macroscale Rayleigh wave. Rayleigh waves are energy efficient since the majority of the acoustic energy travels along the surface without dissipating into the solid more than a few wavelengths. This is also why earthquakes can affect a significant area surrounding their point of origin.

When the surface acoustic waves travelling along the piezoelectric substrate with a sound speed of c_s come into contact with the fluid medium with a sound speed of c_l, a certain fraction of the acoustic energy is transferred to the liquid medium due to the mismatch of sound speeds in the media with the Rayleigh angle found by $\theta_R = sin^{-1}(c_l/c_s)$. This acoustic energy leakage into the liquid leads to an exponential decay of the propagating SAW power [208], morphing SAWs into what is known as leaky SAWs (LSAWs) (Fig. 3.2).

This coupling results in pressure waves generated in the liquid media giving rise to interesting phenomena. Three such phenomena that are relevant to the studies presented in this thesis will be discussed individually in the upcoming sections. Firstly, the acoustic energy transfer from the leaky SAW to the fluid results in a pressure wave that creates recirculation within the fluid medium and this is referred to as acoustic streaming [209–212]

(section 3.1.1 - Acoustic Streaming). Secondly, if the SAWs meet an interface with an acoustic impedance mismatch, it induces a net radiation force applied on the interface which deforms the interface [120, 121] (section 3.1.1 - Interface Deformation). Finally, if there's a particle or a droplet within the fluid medium excited by SAWs, they experience acoustic radiation force (ARF) [213–215] (section 3.1.1 - Acoustic Radiation Forces) which is a non-linear force arising from the second-order time-averaged terms existing in the pressure field generated by SAWs.

Acoustic Streaming

Acoustic streaming is the term used to identify steady streaming effects occurring in a fluid medium arising from viscous attenuation of an acoustic wave. Acoustic streaming can be generated by a number of different acoustic excitation methods such as piezoelectric transducers [185, 189, 216], oscillating gas bubbles [40, 217] or microstructures [190] and surface acoustic waves (SAWs) [17, 218]. Depending on the mechanism of the acoustic actuation, different type of acoustic streaming can be realised such as Rayleigh streaming [209] and Eckart streaming [210].

SAW induced acoustic streaming is a separate phenomenon by itself and cannot be classified as any of the above mentioned types [219]. SAW induced acoustic streaming arises mainly from the exponential decay of the above mentioned leaky SAW (LSAW). As soon as the SAW couples into the fluid medium, it attenuates and decays exponentially leading to a significant gradient in the sound amplitude. This gradient induces a driving force in the coupled liquid which is called acoustic streaming (Fig. 3.2). SAW induced acoustic streaming force, $\mathbf{F_{st}}$, which is a body force (see section 2.1), can be expressed with a time average using the sound velocity field, $\mathbf{u_s}$, in the coupled fluid as [220, 221]:

$$\mathbf{F_{st}} = \rho \langle (\mathbf{u_s} \cdot \nabla)\mathbf{u_s} + \mathbf{u_s}(\nabla \cdot \mathbf{u_s}) \rangle \tag{3.1}$$

SAW induced acoustic streaming finds a number of applications in microfluidics such as mixing [222], droplet translation [218], jetting [223], micropumping [205,220] and droplet sorting [17]. In chapter 6 of this thesis, a microfluidic device capable of splitting plugs is developed where acoustic streaming was used to augment fluid flow in a by-pass channel leading to plug interface protrusion into the by-pass loop so that controlled splitting takes place.

Interface Deformation

As discussed earlier, when surface acoustic waves (SAWs) come into contact with a fluid medium, they couple and propagate within the medium as acoustic waves. When such an acoustic wave meets a fluid-fluid interface, however, its behaviour depends on the acoustic impedance mismatch of the media. Although analytical studies of non-linear acoustics regarding this phenomenon have usually focussed on 1D waves impinging normally on perfectly absorbing or reflecting interfaces [224,225] as well as partially reflecting ones [120, 121, 226, 227], typДçcally the waves are neither one dimensional, nor do they

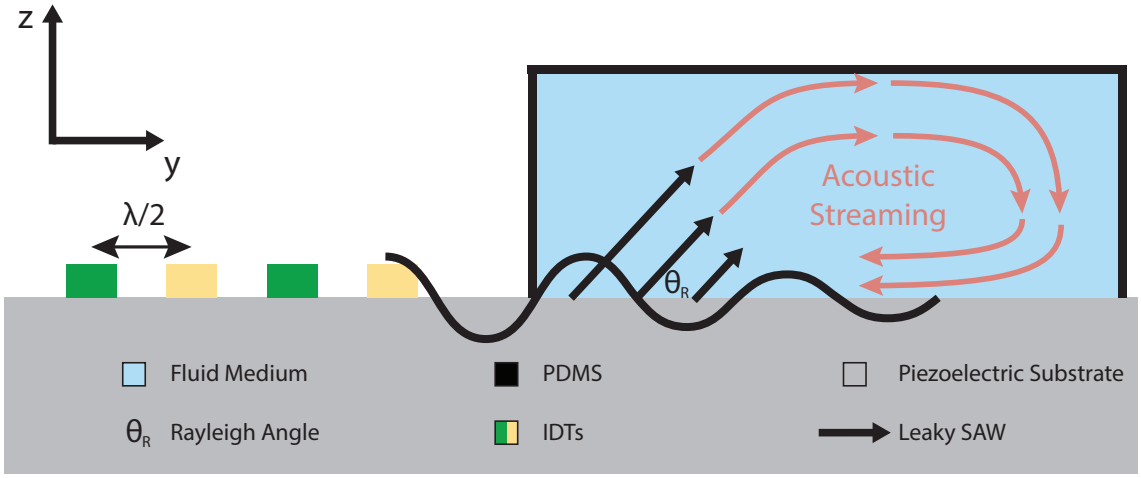

Figure 3.2: Schematic plot showing surface acoustic wave propagation, fluid coupling, Rayleigh angle, leaky SAW and SAW induced acoustic streaming.

impinge normally on an interface in real life applications. Instead, such acoustic waves are complex 3D waves that can interact with curved interfaces especially in the case of droplet microfluidics.

Nevertheless; in order to understand how an acoustic wave interacts with an interface, we consider a plane progressive wave in medium 1 of energy density E_1 impinging normally on a partially reflecting interface. The resulting acoustic radiation pressure, P_{ARP}, acting on the interface is given by: [226]

$$P_{ARP} = E_1(1 - \frac{c_1}{c_2} + R_c(\frac{c_1 + c_2}{c_2})) \tag{3.2}$$

where c_i is the speed of sound in fluid i and R_c is the acoustic reflection coefficient given by: [226]

$$R_c = (\frac{Z_1 - Z_2}{Z_1 + Z_2})^2 \tag{3.3}$$

where Z_i is the acoustic impedance of medium i found by multiplying the density of the fluid with the speed of sound in the medium (i.e $Z_i = \rho_i c_i$).

A quick observation emerging from equation 3.2 is that depending on the fluid properties, acoustic radiation pressure could turn out to be positive or negative meaning the interface could be deformed towards or away from the incoming acoustic wave. In fact; when fluid properties from the work discussed in chapter 4, where the interface tends to deform towards the acoustic wave, are substituted, P_{ARP} is calculated as $P_{ARP} = 0.0034E_1$. On the contrary; when we look at the work detailed in chapter 5 where the opposite holds, we conclude that $P_{ARP} = -1.13E_1$. This is attributed to the distinct oils used in these studies exhibiting different densities and sound speeds.

Alternatively; if the pressure field, $P_0(x, y, z)$, arising from the acoustic transducer in the vicinity of the interface is known, the acoustic radiation pressure on the interface could be found using: [121]

$$P_{ARP}(x,y,z) = P_0^2(x,y,z)\frac{Z_1^2 + Z_2^2 - 2Z_1c_1\rho_2}{Z_1c_1(Z_1+Z_2)^2} \tag{3.4}$$

the direction of the deformation can also be determined using equation 3.4.

It is important to mention that other forces usually come into play when acoustic radiation pressure on an interface is considered. Most importantly; surface tension force acts to minimise the surface energy of an interface at all times which leads to well-known Laplace pressure, P_{LAP}, given by:

$$P_{LAP} = \gamma H \tag{3.5}$$

where γ is the interfacial tension between the two mediums and H represents the mean curvature of the interface, commonly simplified to height, h, and width, w of a microchannel in the case of microfluidic droplets (i.e $H = w^{-1} + h^{-1}$) (also see eqn. 2.14). Moreover; acoustic streaming (see 3.1.1 - Acoustic Streaming) can also act on such an interface exerting a normal viscous stress depending on fluid properties and geometry [121], however, it was calculated and experimentally shown that this effect is negligible in the studies detailed in chapters 4 and 5.

To conclude; even though the analytical examples detailed above focus on 1D waves, they provide valuable insight to the theory of interface deformation arising from the acoustic radiation pressure. Using this interface deformation, microfluidic plugs can be steered into different outlet channels at a specially designed Y-junction. The results of this work are discussed in chapter 5 of this thesis.

Acoustic Radiation Forces

Following the previous discussions, if a spherical object is placed within a fluid medium that is subject to acoustic waves, they experience a net force called acoustic radiation force (ARF). These forces arise due the interaction of the incident wave and the object. The acoustic waves undergo diffraction, refraction, reflection or absorption; usually a combination of all four upon interaction with the spherical object. This nature of this interaction gives rise to a resultant pressure field which might move the object in the surrounding medium. Such a movement highly depends on the physical properties of the object.

When an acoustic wave propagates in a fluid volume, its state can be understood by analysing pressure and velocity oscillations. Since the waves studied in this thesis are surface acoustic waves, they oscillate at very high frequencies on the order of MHz. As a result of this, we can only observe time-averaged effects of such oscillations. Due to the harmonic nature of these oscillations, the time-averaged first-order pressure, P, and velocity, $\mathbf{v}$, terms cancel each other out whereas the second-order terms lead to a net force applied on the object. This acoustic radiation force, $\mathbf{F_{ARF}}$, could be found by integrating over the surface, S, of an object moving in a fluid medium with properties ρ and c: [228]

$$\mathbf{F_{ARF}} = \frac{1}{2}\rho\int_S \left[\langle \mathbf{v^2}\rangle - \frac{1}{\rho^2 c^2}\langle P^2\rangle\right]\mathbf{n}dS - \rho\int_S \langle(\mathbf{n}\cdot\mathbf{v})\mathbf{v}\rangle dS \tag{3.6}$$

where **n** is the normal vector and the brackets indicate a time-averaged value.

Analytical solutions to equation 3.6 exist when an object with radius much smaller than the acoustic wavelength is considered (i.e. $r \ll \lambda$) [228, 229]; often referred to as the Gor'kov's potential [215]. However; in regards to the work discussed in chapter 4, the droplet size is larger than the wavelength of the excitation and as such no analytical solutions exist.

In the case of a 1D wave, however, Yosioka and Kawasima [214] provide an analytical solution applicable to inhomogeneities larger than the acoustic wavelength where they predict that the object will always move in the direction of wave propagation. We have experimentally shown that this is not true for droplets dispersed in a carrier medium subjected to complex sound fields. Depending on the acoustic impedance mismatch of the dispersed and the continuous medium, the droplets were able to move against the direction of wave propagation. This is best explained by considering droplets acting analogous to concave or convex mirrors as incident waves impinge and refract.

2D numerical simulations using COMSOL Multiphysics® software have been carried out to better understand this phenomena. A water droplet placed in various mediums was subjected to a radiating pressure wave and the resulting second-order time-averaged presure field was plotted in figure 3.3. In figure 3.3(a) where the continuous medium has a lower speed of sound and higher density than that of water, the droplet acts like a convex lens and mostly diffracts the sound waves leading to a high pressure zones at the front of the droplet. The acoustic radiation pressure, P_{ARP}, on the interface, due to impedance mismatch (see eqn. 3.4), is integrated over the entire droplet surface to find the net force applied on the droplet. This force is called acoustic radiation force (ARF) and in this case, due to the high pressure regions observed in figure 3.3(a), ARF pushes the droplet away from the direction of wave propagation. On the contrary, in figure 3.3(b) where the continuous medium has a higher speed of sound and lower density, the droplet acts like a concave lens and focusses the incident waves within itself leading to a high pressure zone at the far end of the droplet. This results in an acoustic radiation force acting against the waves, moving the droplet towards the source of actuation.

It was this second method that was used to attract and trap droplets within high intensity acoustic pressure zones until successive droplets arrived and coalesced with the trapped one. Since the droplet size increased after coalescence, the acoustic radiation forces were unable to overcome the increasing drag force leading to the ejection of the merged droplet from the trapped zone. The reader is referred to chapter 4 for further discussion on this work.

Heating due to Surface Acoustic Waves

Microfluidic systems incorporating surface acoustic waves (SAWs) are susceptible to heating due to two major reasons; generation and attenuation of SAWs. SAWs are generated as a result of the conversion of electrical energy into mechanical waves, however, some of this electrical energy is dissipated. Moreover, SAWs attenuate into the PDMS block and the

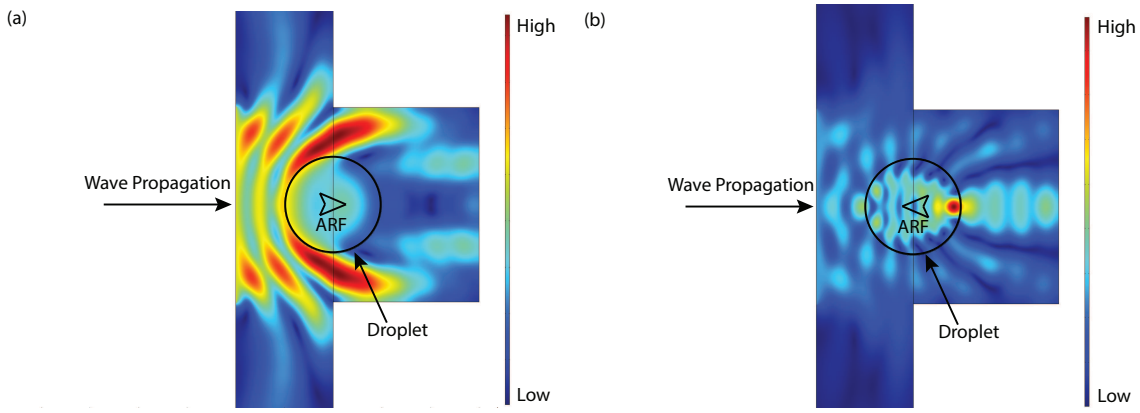

Figure 3.3: Numerical simulation (COMSOL Multiphysics®) results showing time-averaged pressure distribution when a water droplet is placed in an acoustic field surrounded by continuous medium exhibiting (a) lower speed of sound and higher density versus (b) higher speed of sound and lower density values.

fluids, which also results in heating. While some studies utilise the latter effect for micro-droplet heating [230–233] and PDMS hotspots [234,235], the former is often undesirable as it leads to overheating [236]. Overheating could be detrimental for biological samples as well as experimental data due to temperature dependent physical properties of fluids. For that reason, the chips were mounted on a thermoelectric cooler (TEC) and heat sink system during the experiments reported in this thesis. This helped maintain the microfluidic devices at a constant temperature throughout the experiments.

Electrical power and duty cycle are two key parameters for quantifying energy supplied to SAW devices. Some of the electrical power is immediately reflected back due to impedance mismatch which is quantified by the S_{11} parameter. PowerSAW (BelektroniG GmbH) measures this parameter, therefore, all power values reported in the experiments exclude these losses in the first place because they do not contribute to heating.

Duty cycle measures the relative duration of activation within a full period of operation. For example, if the IDTs are actuated for 1 second every 2 seconds, a duty cycle of 50% can be measured. In order to ensure constant temperature operation, duty cycles were kept low during the experiments. However, heating is a common issue experienced during the operation of SAW microfluidic devices, therefore more work needs to be carried out in order to better understand the parameters influencing heating in SAW microfluidics. For that reason, preliminary heat transfer experiments have been undertaken to provide insight into various heating mechanisms and their precedence. This section first investigates heating caused by the generation of SAWs followed by heating due to SAW attenuation into PDMS and fluids.

Generation

When an AC signal with matching frequency is applied to the electrodes, mechanical surface waves are generated on the substrate which propagate and attenuate. When this transient process is experimentally observed via a thermal imaging camera where the substrate is relatively larger compared to the size of the IDTs, it was seen that heating occurs along the propagation path decaying away from the IDTs [237]. This evidence suggests

that most of the heating occurs due to dissipation such as vibrational damping of SAWs and friction associated with oscillating surface molecules. However, there might be further reasons for heat generation during SAW generation such as dielectric heating which will be briefly investigated later. The complexity of the underlying physics for these mechanisms is sufficient for dissertations on their own, however, in an attempt to uncover their roles, preliminary experiments have been conducted.

A 16x16x0.5 mm^3 (LxWxH) lithium niobate ($LiNbO_3$)(128°Y-cut) substrate, with patterned electrodes is considered, identical to the chips used in the experiments throughout this thesis. The chip is placed on the cold side of TEC1-12706, which has dimensions of 40x40x4 mm^3 (LxWxH), and pressed down with spring loaded contact pins. The hot side is interfaced with thermal paste to an aluminium, machined heat sink that houses a 12 V fan. Two sets of experiments have been conducted for preliminary heat transfer characterisation; passive and active cooling.

Passive Cooling

Steady state surface temperatures of the chip were recorded after 5 minutes during passive cooling experiments and fed into a simplified heat transfer model in order to estimate the heat removed by the passive system. Due to thermodynamic equilibrium, it can be concluded that heat removed by the system must be equal to the heat generated by the IDTs. The heat transfer model is constructed analogous to a resistive network where three resistances are considered in series; conduction resistance, R_{cond}, contact resistance, R_{cont}, and convection resistance, R_{conv}. In this case, heat flux, $\vec{q}$, can be found as a function of surface temperature, T_s:

$$\vec{q}(T_s) = \frac{T_s - T_a}{A_s(R_{cond} + R_{cont} + R_{conv})} \tag{3.7}$$

where A_s is the surface area of the substrate and T_a is the ambient temperature.

Firstly, the excess heat generated at the top surface of the substrate is conducted through the thickness of the substrate to the TEC surface. The thermal resistance of this conduction, R_{cond}, can be found by $R_{cond} = t_s/(k_s A_s)$ using the thickness of the substrate, t_s, and its thermal conductivity, k_s.

Second thermal resistance arises from imperfect contact at the physical interface of TEC and substrate due to surface roughness. Contact thermal resistance can be calculated by $R_{cont} = R_i/A_s$ where contact resistance, R_i, depends on a number of parameters such as surface finish, material, roughness and temperature. It is approximated as 0.5x10^{-3} m^2K/W for the current study based on figure 1.20 of the textbook "Principles of Heat Transfer" by Kreith et al. [238].

Finally, heat is naturally convected from the TEC surface to the environment. Convective thermal resistance, R_{conv}, is given by $(hA_s)^{-1}$ where h stands for the heat transfer coefficient from TEC surface. Heat transfer coefficient is a key parameter in heat transfer applications, it is found by:

$$h = \frac{Nuk_{TEC}}{D_h} \tag{3.8}$$

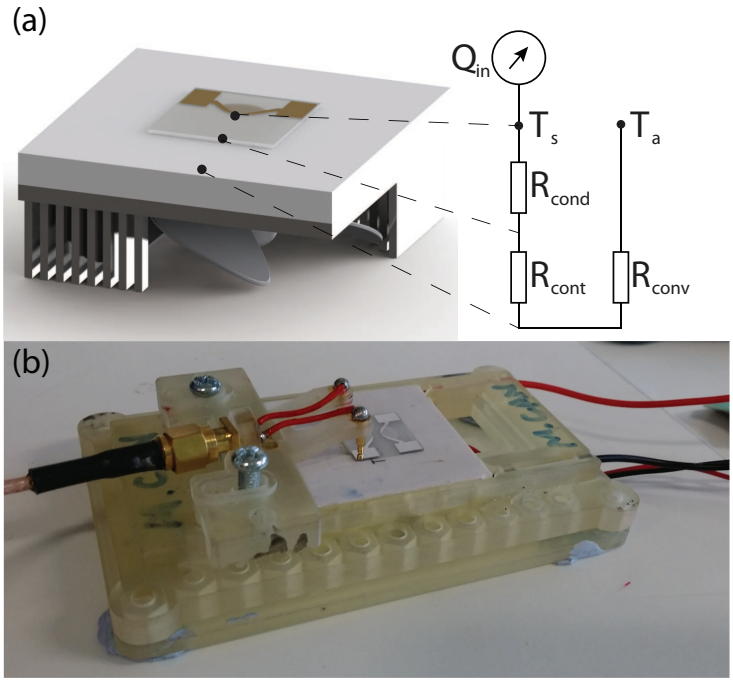

Figure 3.4: (a) Passive cooling heat transfer model. (b) Experimental setup.

where k_{TEC} is the thermal conductivity and D_h is the hydraulic diameter of TEC surface. Nusselt number, Nu, is a dimensionless number that quantifies the ratio of convective to conductive heat transfer. Nusselt number has been approximated as $0.766Ra^{0.195}$. This is in agreement with experimental results obtained by Goldstein et al. [239] investigating natural convection near heated horizontal surfaces at low Rayleigh numbers, Ra.

A few more noteworthy assumptions:

- TEC surface temperature was assumed to be uniform (i.e. horizontal heat conduction neglected, $k_{TEC} = 150$ W/mK).
- TEC bottom surface and its sides were assumed to be thermally insulated.
- Heat was assumed to be generated uniformly on the surface of the substrate.

Steady state surface temperatures, T_s, after 5 minutes were measured for incremental input power up to 2 W with duty cycle 100% using the thermal imaging infrared camera (FLIR i7, FLIR Systems, Inc.) and substituted into equation 3.7 to obtain heat flux, $\vec{q}$. Heat generated by SAWs, Q_{in}, is equal to the heat removed by natural convection in steady state and it's simply given by $Q_{in} = \vec{q}A_s$.

The results of the passive cooling experiments, detailed above, are shown on figure 3.5 (a). Heat generated by the IDTs linearly increases as the applied power is amplified in agreement with results from previous studies [235,237]. It was calculated that, on average, $15\% \pm 3\%$ of the supplied power was lost as heat. The rest is converted into mechanical surface waves propagating on the substrate strengthening the statement that SAWs are energy efficient. Figure 3.5 (b) will be discussed later.

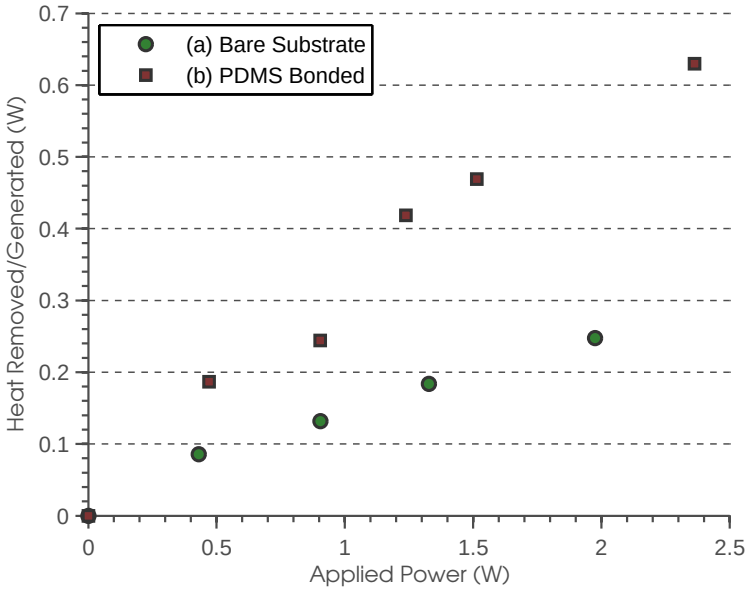

Figure 3.5: (a) Heat removed by natural convection (equivalent of heat generated by SAWs) and (b) heat removed by natural convection (equivalent of heat generated by SAWs + acoustic energy absorbed by PDMS) as a function of the applied power during passive cooling experiments with a (a) bare substrate and (b) PDMS bonded substrate.

Active Cooling

Active cooling experiments have been conducted in the same way as passive cooling experiments except for the fact that the thermoelectric cooler (TEC) and the fan were operated at 3.25 W and 12 V, respectively. While the fan and the heat sink was used to remove heat from the hot side of the TEC, the cold side was used to cool down the substrate. Steady state temperature difference, $\Delta T = T_s - T_a$, with passive and active cooling as a function of the applied input power is presented in figure 3.6 (a)-(b). It can be observed that temperature increase can be significantly decreased using the active cooling system, thus device temperature increase could be maintained within < 10°C up to 2 W even with 100% duty cycle. In the case of more demanding applications or working with sensitive biological samples, cooling system can be upgraded at the expense of size and total power consumption. Figure 3.6 (c)-(d) will be discussed later.

Dielectric Heating

Another potential heating mechanism during the generation of SAWs is dielectric heating. Lithium niobate (LN) is a dielectric material with a high electrical resistivity [240], therefore, it has the potential to absorb electromagnetic (EM) energy when subjected to a time-varying electric field. The absorbed EM energy is uniformly converted to heat in this process called dielectric heating. Dielectric heating is the result of periodic molecular rotation where induced and intrinsic dipole moments in the material constantly (try to) align with the electric field [241]. Their ability to do so is quantified by the loss tangent, $\tan\delta$, of a material; in that case, the heat flux due to dipole heating, $\vec{q}_{DH}$ is given by: [242]

$$\vec{q}_{DH} = \omega|\vec{E}|^2\epsilon_r\epsilon_0\tan\delta h_s \tag{3.9}$$

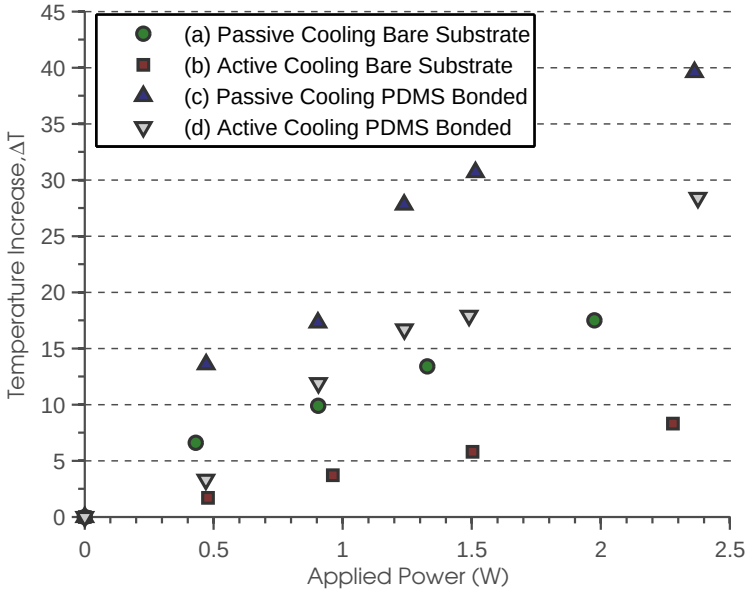

Figure 3.6: Temperature increase as a function of input power with (a) passive cooling and bare substrate, (b) active cooling and bare substrate, (c) passive cooling and PDMS bonded substrate and (d) active cooling and PDMS bonded substrate.

where ω is the angular frequency, E is the electric field strength, h_s is the height of the substrate and ϵ_r, ϵ_0 are the relative permittivity of the material and free space, respectively. When typical values from the experiments are substituted into the equation, a maximum heat flux of 20 W/m^2 (Q_{in} = 6x10^{-3} W) can be estimated due to dipole heating. This value is negligible based on previous calculations (see figure 3.5) therefore we can rule out dipole heating. This was further backed by experiments where the electrodes were actuated with non-resonant frequencies and surface temperatures did not change.

It is worthwhile to mention that dielectric or microwave heating has been used in a number of studies [241, 243–245] to heat up and/or sense a water-based droplet and its temperature owing to water's unique properties (loss tangent of 0.157 at 3 GHz) that allow it to absorb microwave energy quite efficiently especially at frequencies between 3 and 20 GHz. This is exactly the same technology used in commercial microwave ovens.

Attenuation

Now that we have looked into heating associated with the generation of SAWs, we will discuss heating caused by attenuation of SAWs into mediums. As previously mentioned, SAWs refract with Rayleigh angle into mediums placed along the propagation path. This gives rise to longitudinal pressure waves (LWs) that radiate into the medium such as PDMS or liquids leading to heating, vibration, streaming and atomisation. The heating of liquids and PDMS will be discussed separately.

There are a number of open system studies investigating the heating of droplets (1-10 µL) deposited onto substrates and subjected to SAWs [230–233]. Key findings of these studies are:

- Droplets absorb more energy at lower frequencies with longer wavelengths [233].

- Dielectric heating of water droplets at MHz frequencies is negligible [231].
- The extent of LW absorption depends on attenuation based on liquid properties such as sound speed, density, viscosity, heat capacity and thermal conductivity [232, 246].
- LWs induced in water by 200 μm wavelength SAWs dissipate 95% of their energy after travelling 35 cm [232].

The experiments carried out in this thesis involved closed microfluidic channels of 50 μm height where the instantaneous liquid volume within SAW propagation region would not exceed 1 nL which gets fully replenished every 200 ms. In light of the above findings and experimental conditions stated, LW absorption of liquids can be neglected as its effect will be minor compared to other heating mechanisms. Nonetheless, further studies are required for a better understanding of the underlying physics of liquid LW absorption and its conversion to heat.

LWs can also dissipate within an elastic medium such as PDMS. In fact, previous work suggests that PDMS is an acoustic energy absorber that can efficiently convert it to thermal energy [234, 235]. There's also evidence suggesting that PDMS absorbs certain wavelengths within SAW frequency band better than others [234, 235]. These properties have recently been exploited in order to design microheater arrays [234, 235].

For a better understanding of SAW attenuation into PDMS and its subsequent heating effects, the bare substrate used in the previous heat transfer experiments was bonded to a typical PDMS block, approximately 16x5x4 mm^3 (LxWxH), and same experiments were repeated. Passive cooling experiments with PDMS revealed that the estimated average heat generation of a substrate bonded to PDMS (see Fig. 3.5 (b)) was $32\% \pm 5\%$ of the original supplied input power. Compared to the experiments with the bare substrate, the electrical energy lost as heat almost doubled due to attenuation of acoustic energy into PDMS. It should be noted that passive cooling was significantly hindered by the PDMS block due to its insulating nature which enabled storage of heat, especially at 100% duty cycle, leading to temperature increase over time. PDMS properties causing this are its very low thermal conductivity, 0.15 W/mK, and its quite large specific heat capacity, 1460 J/kgK.

Substrate surface temperature increase in the presence and absence of active cooling is shown on figure 3.6 (c)-(d). Surface temperatures were brought down about 10°C with the aid of the active cooling system. Unlike experiments performed with the bare substrate, the surface temperature distribution was not uniform in steady state; localised high temperatures were observed in the PDMS block. This is attributed to the unique PDMS properties discussed earlier. There's a clear need for future work in order to fully comprehend acoustic energy absorption of PDMS.

The effects of duty cycling were also investigated. For this reason, same experiments were repeated with the PDMS block using active and passive cooling where 2.4 W of electrical power was applied and the duty cycle was varied. Steady state surface temperature increases after 5 minutes as a function of duty factor are shown on figure 3.7. A linearly

increasing trend is observed which agrees with previous experiments that analysed effects of duty factor [231, 233].

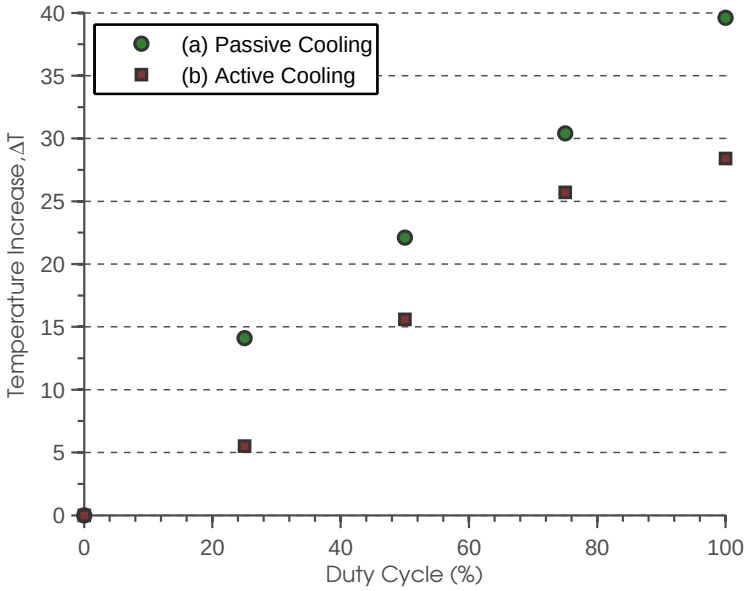

Figure 3.7: Steady state surface temperature increase at 2.4 W as a function of duty cycle with (a) passive cooling and (b) active cooling.

Conclusion

Surface acoustic wave (SAW) devices are known to generate excess heat, often undesired for biological samples and flow stability. However, there's a lack of research regarding SAW heating mechanisms and optimisation. A thorough literature review supported by a series of preliminary heat transfer studies were presented looking into heat generation in SAW microfluidic devices, specifically the ones used in this thesis. Maximum power, duty cycle and temperature increase during experiments have been measured as:

- Chapter 4: Power < 2.5 W, duty cycle $< 40\%$, active cooling, $\Delta T < 10$°C.
- Chapter 5: Power < 300 mW, duty cycle 100%, passive cooling, $\Delta T < 5$°C.
- Chapter 6: Power < 1 W, duty cycle $< 10\%$, passive cooling, $\Delta T < 5$°C.

With the above information, it is safe to say that heating effects and temperature change were minimal for the studies reported in this thesis. Temperature increase was controlled via active cooling and low duty cycling during the studies presented here. At higher applied power levels, duty factor was further decreased in order to maintain surface temperature stability. Failure to do so would result in flow instability due to physical property change of working liquids.

Evidence from literature backed by verification experiments suggests that the main causes of heating observed in SAW microfluidic systems developed in this thesis are the effective acoustic energy absorption of PDMS and its dissipation as well as the mechanical vibration damping and friction associated with the generation and propagation of SAWs on piezoelectric substrate. Additional work is required for further characterisation of heating

mechanisms so that efficient SAW microfluidic devices could be designed that are less prone to heating. Future studies include investigating the effects of IDT design, electrode surface area, SAW wavelength, substrate properties, PDMS properties and size.

3.2 Fabrication

The fabrication steps for making a microfluidic chip capable of generating surface acoustic waves (SAWs) will be discussed in this section. Although the designs are different for each study, the fabrication steps are identical.

3.2.1 CAD to Mask

As a first step of the fabrication process; SAW generating inter-digital transducers (IDTs) and associated microchannel features were designed on Layout Editor (CAD) software. The designed features were exposed onto a glass mask (pre-coated with chromium and a positive photoresist) by using SF-100 XTREME (Intelligent Micro Patterning, LLC) maskless lithography machine. After developing the photoresist, the exposed chromium coating was wet etched for 3:30 minutes with chromium etchant followed by a quick cleaning dip in diluted (%10 v/v) sulphuric acid solution for 10 seconds to get rid of any residues from the chromium etchant. The mask was then rinsed and dried by nitrogen blow gun which completes the mask fabrication steps. Such a mask carries the features designed on the software and they can be reused to fabricate devices over and over again.

3.2.2 Bottom Substrate

For the inter-digital transducers (IDTs) to be able to generate SAWs, they need to deposited on piezoelectric substrate as discussed earlier (see section 3.1.1). For this reason, a 0.5 mm thick, single side polished 128°Y-cut, X-propagating lithium niobate (LN)($LiNbO_3$) substrate was spin coated with the positive photoresist AZ1512 (Microchemicals GmbH) using Delta 80RC (SUSS MicroTec) spinner, baked at 90°C for 1 min and exposed to 75 mJ of UV light through the patterned mask containing the IDT features. The designed SAW propagation direction was carefully aligned with the propagation direction of the substrate because the speed of sound on piezoelectric substrate LN changes as the wafer is rotated.

Following soft lithography, a 10 nm thick adhesion layer of chromium and a 200 nm thick conducting layer of aluminium was deposited onto the substrate using Nanochrome II e-beam evaporator (Intlvac). Electron-beam evaporation is a method of low pressure physical vapour deposition where the material is evaporated using e-beam and deposited onto target substrates. This method coats the entire wafer, therefore it is usually followed by a lift off procedure where the substrate is dipped in ultrasonic acetone bath to remove all the areas with photoresist (Fig. 3.8). Once the photoresist was stripped, the wafer was dried and diced to specific dimensions for the final product using DAD321 (DISCO, Japan) automated dicing saw.

3.2.3 Fluidic Channels

In order to prepare a master polydimethylsiloxane (PDMS) mold for the designed microfluidic channels, the features were patterned onto a single side polished $< 100 >$ silicon wafer by standard soft lithography techniques using the patterned microfluidic channels mask. A 100 nm layer of chromium was deposited onto the silicon wafer to act as etch-stop and the photoresist layer was lifted off after deposition. The silicon wafer with the patterned etch-stop layer was then dry etched using Plasmalab System 100 with ICP380 source (Oxford Instruments) by alternating etching (plasma SF_6) and deposition (plasma C_4F_8) cycles to achieve high aspect ratio structures (Fig. 3.8). This procedure is also known as deep reactive ion etching (DRIE). After etching the mold to the desired depth (usually $\approx$ 50 µm), it was chromium etched to get rid of the chromium etch-stop layer. Finally, silane (SiH_4) was deposited to the mold inside a vacuum desiccator to render the surface hydrophobic for easy PDMS peeling. Once the PDMs mold is ready, it can be reused to cast PDMS many times.

To prepare 10:1 ratio polydimethylsiloxane (PDMS); 10 parts (by weight) SYLGARD® 184 Silicone Elastomer Base (Dow Corning) was mixed with 1 part (by weight) SYLGARD® 184 Elastomer Curing Agent (Dow Corning). The prepared mold was then placed in a petri-dish and the prepared PDMS was poured on top of the silicon mold. This was placed under vacuum for 3 hours for degassing and heat cured for 3 hours at 60°C on a hotplate. As the PDMS is cured, it cross-links and hardens from its viscous form into an elastic polymer. Once it's cured, it could easily be peeled off from the silicon mold since the surface of the mold was rendered hydrophobic.

The cured PDMS with the designed microfluidic features was then diced into desired shapes and punched for access to inlets and outlets. The PDMS chip was carefully aligned and bonded to the diced LN device after exposure to an activated air plasma (Harrick Plasma PDC-32G: 1 mBar, 18 W, 5 minutes for the LN substrate and 20 seconds for the PDMS). As a last step, inlet and outlet tubing was inserted into the punched holes and the interface was sealed with uncured PDMS to prevent leakages.

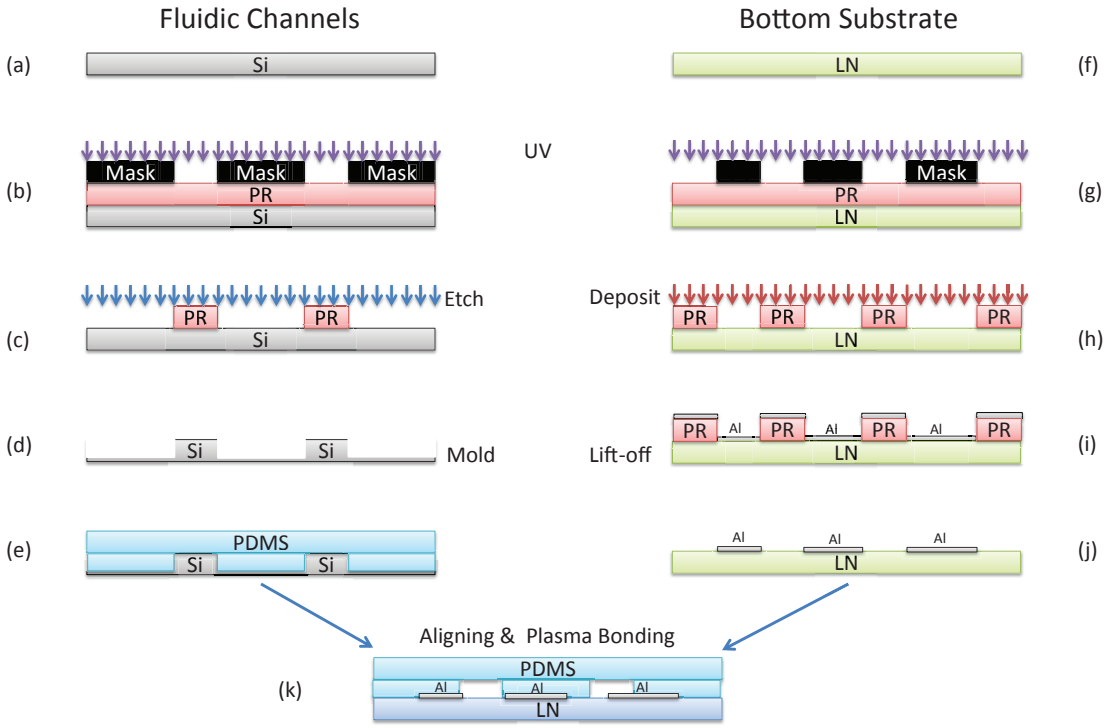

Figure 3.8: Schematics detailing fabrication steps. (a) Silicon wafer is spin-coated with photoresist and (b) exposed to UV light. (c) The patterned wafer is etched using DRIE to (d) make the mold. (e) PDMS is cast using this mold to fabricate the fluidic channels. On the other hand, (f) lithium niobate wafer is similarly patterned by (g) lithography. (h) Chromium and aluminium are deposited onto the wafer which is followed by (i) lift-off to (j) fabricate electrodes on the substrate. Finally, (k) PDMS chips and lithium niobate is exposed to air plasma and bonded irreversibly.

Chapter 4

Microfluidic on-demand Droplet Merging using Surface Acoustic Waves

4.1 Overview

In this chapter, a novel microfluidic device is presented that makes use of surface acoustic waves (SAWs) to merge multiple droplets on-demand. Droplet fusion is one of the key droplet manipulation techniques because a majority of studies require two chemicals to merge so that the resultant reaction can be observed.

Previously; droplets have been shown to coalescence when subjected to intense electric fields (electrocoalescence), when collided into each other using membrane deformation, and when brought together using passive methods. Electrocoalescence requires droplets to be adjacent to each other and high intensity electric fields can be damaging to biological media. Membrane deformation is very complicated to fabricate and operate whereas passive methods are not selective or on-demand. This chapter presents a droplet microfluidic device that is capable of merging multiple droplets on-demand using surface acoustic waves.

The droplets can be immobilised as they pass through an expansion chamber by using surface acoustic wave induced acoustic radiation forces. As the droplets are trapped in the high intensity acoustic pressure zones, successive droplets arrive and coalesce with the trapped one. This takes place as long as the drag force on the droplet doesn't overcome the retaining acoustic radiation forces, however, when this happens, the fused droplet exits the trapping chamber. It was experimentally shown that coalescence depends on initial droplet volume, velocity and the power of acoustic actuation. The system was thoroughly characterised so that it could be easily scaled and integrated to other microfluidic devices.

A review of droplet fusion, fabrication and working principle of the proposed device are presented in this chapter followed by detailed analysis of experimental results and discussion. This new droplet merging system is easy to fabricate and operate which makes it ideal for integration with different designs.

4.2 Publication

The following publication has been published and reprinted from [26].

Monash University

Declaration for Thesis Chapter 4
Declaration by candidate

In the case of Chapter 4, the nature and extent of my contribution to the work was the following:

Nature of contribution	**Extent of contribution**
Design and fabrication of devices, experimentation, development, result analysis, interpretation and writing.	90%

The following co-authors contributed to the work:

Name	**Nature of contribution**	**Extent of contribution**
Dr. Tuncay Alan	Project Supervision, editing	N/A
Assoc. Prof. Adrian Neild	Project Supervision, editing	N/A

The undersigned hereby certify that the above declaration correctly reflects the nature and extent of the candidate's and co-authors' contributions to this work.
s

Candidate's Signature: 

Candidate's Name: Muhsincan Sesen

Date: 5th August 2016

Main Supervisor's Signature: 

Main Supervisors's Name: Assoc. Prof. Adrian Neild

Date: 5th August 2016

Lab on a Chip

PAPER

View Article Online
View Journal | View Issue

Microfluidic on-demand droplet merging using surface acoustic waves†

Cite this: *Lab Chip*, 2014, **14**, 3325

Muhsincan Sesen, Tuncay Alan and Adrian Neild*

Individual droplets can be isolated within microfluidic systems by use of an immiscible carrier layer. This type of two phase systems, often termed "digital microfluidics", find wide ranging applications in chemical synthesis and analysis. To conduct on-chip biochemical analysis, a key step is to be able to merge droplets selectively in order to initiate the required reactions. In this paper, a novel microfluidic chip integrating interdigital transducers is designed to merge multiple droplets on-demand. The approach uses surface acoustic wave induced acoustic radiation forces to immobilize droplets as they pass from a channel into a small expansion chamber, there they can be held until successive droplets arrive. Hence, no requirement is placed on the initial spacing between droplets. When the merged volume reaches a critical size, drag forces exerted by the flowing oil phase act to overcome the retaining acoustic radiation forces, causing the merged volume to exit the chamber. This will occur after a predetermined number of droplets have merged depending on the initial droplet size and selected actuation power.

Received 17th April 2014,
Accepted 20th June 2014

DOI: 10.1039/c4lc00456f

www.rsc.org/loc

1 Introduction

The field of microfluidics is driven by the vast possibilities offered by scaling down conventional benchtop laboratory processes and equipment. The miniaturization of analytical equipment into lab-on-a-chip (LOC) devices overcomes the limitations arising with bulky and expensive instrumentation through the reduction in sample and reagent volumes; resulting in lower analysis costs, shorter reaction times, higher resolution and sensitivity. Furthermore, batch-fabrication techniques provide low cost and disposable instruments ideal for point-of-care diagnostics and environmental sensors.[1]

One class of lab-on-a-chip (LOC) devices, termed digital microfluidics, isolate small droplets of sample fluids by use of an immiscible carrier fluid. In this way, these two phase systems can handle droplet assays whilst ensuring each sample is physically and chemically isolated. These droplets are typically created using hydrodynamic effects which occur when a flowing sample stream meets a flowing oil stream; the result is the production of a large number of monodisperse sample droplets interspaced by volumes of oil.[2–5]

Each droplet can be thought of as being analogous (at a much smaller scale) to a sample deposited in a test tube or the well of micro titre plate, in order to further the analogy, and enable on-chip biochemical assay, a series of additional tasks need to be achievable at the chip scale, these include sorting,[6–10] merging,[10–14] splitting,[15–20] trapping,[21–26] dilution[25,27] and mixing.[28–31] It is essential to assure that such manipulation technologies are easy to integrate, robust, energy efficient and contamination free.

On-chip reaction of small chemical samples can be used for a number of applications, including the formation of particles, chemical synthesis, kinetics studies, biomolecule synthesis,[32] or for the study of fast organic reactions.[33] For the reactions to be initiated, the coalescence or merging of different droplets is required (*e.g.*, samples and reagents). As such, the on-chip merging of specific sample droplets containing different chemicals, dilutions or volumes is a vital component for versatile LOC devices to enable biochemical assays. Two main methods for merging droplets have been explored to date, namely, electrocoalescence[10–12] and hydrodynamic methods.[13,14]

Electrocoalescence has been employed by researchers in order to facilitate merging of two adjacent droplets, it utilizes an electric field applied to high conductivity aqueous droplets immersed in a low conductivity continuous phase. Electrocoalescence method involves the charging of the droplets upon interaction with an electrical field; subsequent aggregation and coalescence then occur due to droplet–droplet interactions.[34] The applied electric field enhances contact between the dispersed aqueous droplets and enables droplet–droplet coalescence through the rupture of droplet-interface.[35] This requires the conductivity and permeability between two immiscible fluids to be different[36,37] and the droplets to be in close proximity.

Department of Mechanical and Aerospace Engineering, Monash University, Clayton, VIC 3800, Australia. E-mail: adrian.neild@monash.edu; Tel: +61 3 990 54655

† Electronic supplementary information (ESI) available. See DOI: 10.1039/c4lc00456f

View Article Online
Paper Lab on a Chip

Hydrodynamic merging of droplets is achieved through clever microchannel geometry designs and requires no external actuation. Generally, a microfabricated speed bump is introduced further downstream to the formed train of droplets. When a droplet flows through the speed bump zone, its velocity decreases either due to designed physical restrictions[13] or due to an expansion in the channel.[14,38,39] The trailing droplet catches up and collides with the slowed droplet after which fusion takes place between the two droplets or more. However, the passive hydrodynamic techniques employed alone are not capable of merging droplets on-demand.

On-demand control is of significant importance for on-chip assays, where a range of reagents need to react with a range of samples (or sample dilutions). Thus, dealing with large numbers of identical droplets created by conventional hydrodynamic effects complicates this task. Recently, surface acoustic waves have been shown to be capable of producing single picolitre droplets on-demand,[40] in this work we demonstrate that the same actuation principle can be applied to merge multiple droplets on-demand; in this way, the easy integration of techniques becomes straightforward.

Ultrasonic waves offer, through non-linear effects, a range of forcing mechanisms which act on a different time scale to the ultrasonic oscillation. For instance, Bjerknes forces can draw particles to oscillating bubbles,[41] acoustic streaming is highly applicable to fluid mixing,[42,43] and acoustic radiation forces can be used to migrate[44–46] and collect[47–50] suspended particles, and to sort droplets.[9]

Surface acoustic waves (SAWs), a special type of ultrasonic wave propagating on the surface of a piezoelectric substrate, have been widely employed in microfluidic applications.[5,9,44,51–58] They offer a cost-effective fast response actuation source which is easy to fabricate and integrate, energy efficient, and safe to biological samples.[59] In this work, SAW generated acoustic radiation forces, arising due to the mismatch in the acoustic impedances (wave speed and density) of the oil and aqueous phases, will be used to stop the progress of a selected droplet, such that successive droplets will merge with the trapped droplet until a certain volume is reached; afterwards the merged droplet will be released from the acoustic trap. As the initial droplet is stationary prior to merging, there is no requirement placed on the spacing between the droplets.

2 Operating principle

The system which has been developed for the purpose of merging droplets using SAW is depicted in Fig. 1. At the inlet, droplets are produced by use of T-junctions of continuous oil and water streams. Most of the experimental results presented here were gathered with two inlets (oil and water); the three inlet (oil, water and dye) design depicted was used to demonstrate merging of two droplets containing different liquids. The channel along which the flow pushes the droplets measures 100 μm wide by 50 μm high, except at the expansion area where the channel width is 300 μm. There are also two

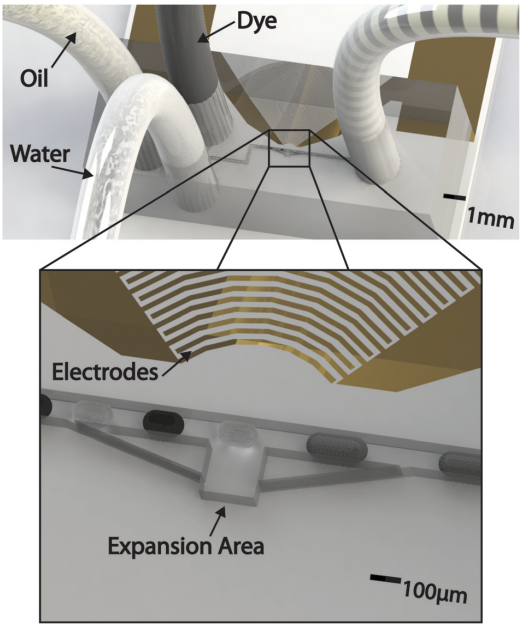

Fig. 1 Microfluidic droplet merging chip design. Water and dye streams are designed to form T-junctions with the oil flow so that alternating droplets are generated. Droplets are trapped right across the electrodes due to surface acoustic waves so that the upcoming droplet can come and merge with the stopped one.

very thin channels which were originally intended to allow a bypass flow when the droplet is held at the expansion in fact, due to issues of feature resolution they were blocked and proved to be unnecessary for the successful operation of the system. Curved aluminum electrodes, deposited on a piezoelectric substrate, are arranged such that the center of curvature coincides with the expansion area in the channel; these electrodes are used to excite the SAW.

SAWs are acoustic waves with nm-scale amplitudes, oscillating in the MHz range and propagating along the surface of a piezoelectric substrate. Direct piezoelectric surface wave transduction was first introduced in the microscale[60] by use of inter-digital transducers (IDTs), such as those used here, consisting of periodic electrodes on a piezoelectric substrate. When an oscillating electrical signal of suitable frequency is applied to the IDTs, constructive interference between the waves generated at each electrode occurs. The required resonant frequency, f, is dictated by the pitch of the electrodes which is equal to half the wavelength, $\lambda/2$, according to $f = c_s/\lambda$, where c_s is the sound speed on the substrate surface.

As the thickness of the substrate (500 μm) is chosen to be much larger than the wavelength, the resultant waves can be classified as Rayleigh waves;[61] these are energy efficient since the majority of the acoustic energy travels along the surface without dissipating into the depth of the solid by more than a few wavelengths. In addition by use of curved IDTs the

View Article Online

Lab on a Chip Paper

waves can be easily focused on the substrate, in our case they are focused at the location of the channel expansion.

When the surface acoustic waves traveling along the piezoelectric substrate with a (Rayleigh) sound speed of c_s comes into contact with the fluid medium with a sound speed of c_l, acoustic energy is coupled to the liquid. The resulting wave in the fluid propagates at the Rayleigh angle found by $\theta_R = \sin^{-1}(c_l/c_s)$ – depicted in Fig. 2(a). The focused nature of the waves on the substrate will give rise to spatial variations in the intensity of the coupled pressure waves. It is these pressure waves in the fluid which will be used to merge the droplets.

In many cases the calculations of the force field which acts on inhomogeneities in the fluid leads simply from knowledge of the pressure field. In the case of a one-dimensional field, for example, expressions are available for both a traveling and standing wave scenario, and some of the expressions are valid for inhomogeneities larger than the wavelength of the pressure field.[62] In the case of more complex sound fields, the equation provided by Gor'kov[63] is widely applied. However this is limited to particles significantly smaller than the wavelength. In this work, the wavelength of the sound waves excited in the continuous medium is 28.86 μm and the droplets vary between 100 μm and 150 μm in diameter, furthermore the field is not one-dimensional, consisting instead of a focused series of substrate waves coupling at a given angle into the fluid. As such no analytical solution is available to move from pressure field to force field. Recently, it was shown that when particles of diameter, d, are subjected to SAW with wavelength, λ, while $\lambda \approx d$, a net acoustic force is induced on the particles due to acoustic scattering.[64]

An analogy can be drawn between a focused acoustic field and that of a focused optical beam, such an analogy has been used by Lee and Shung, with the acoustic beam being generated by an axially focused transducer[65] (Fig. 2(b)). In a single beam optical trap two forces are generated on a particle with different optical properties to those of the suspension medium, they are scattering induced forces and gradient forces.[66] The scattering forces tend to push particles in the direction of the optical propagation, whilst the gradient forces, which arise from spatial intensity variations due to focusing, tend to move particles towards high intensity zones. Hence, one breakthrough in optical trapping was the demonstration that a single optical beam can trap a particle,[67] provided that it is focused, as in this case the gradient forces dominate over the scattering forces (Fig. 2(b)).

A clear and significant shortcoming in this analogy arises when it is considered for a focused SAW beam due to the different wave propagation direction. In an axially focused beam (optical or acoustic) the propagation direction is through the waist of the beam, whilst in the case of the focused SAW beam, the focusing is along x-direction (Fig. 2(c)) and propagation is in the y–z plane (Fig. 2(a)). What this means is that the scattering forces due to propagation direction, can be expected to be at an angle to the focal plane, due to the additional constraint of the droplet being encapsulated in a channel, the scattering forces will simply push the droplet against the roof of the channel, thus we would expect the gradient forces to dictate droplet movement in the x–y plane. Time averaged surface displacement on the lithium niobate substrate shown in Fig. 2(c) was captured using a Laser Doppler Vibrometer, there is a clear intensity variation along the channel, peaking at the location of the expansion chamber.

The droplets used in this work are in the Mie regime where the droplet diameter, D, is of similar magnitude to the wavelength, λ (*i.e.* $\lambda \approx D$). Geometrical (ray) acoustics, where sound is modeled as rays, can be used for modeling acoustic/optical trapping in the Mie regime.[68] In such a case, droplets are attracted towards high intensity ultrasound zones.[69]

The other key force acting on the droplet in the trapping region is that of drag. In its simplest form, *i.e.* when considering a particle in an infinite volume of fluid, Stokes drag is given by

$$F_d = 6\pi\mu r v \quad (1)$$

where μ is the viscosity of the continuous fluid, r is the radius of the droplet and v is the velocity of the flow; provided that the acoustic force is sufficient to overcome this force, the droplet will remain trapped.

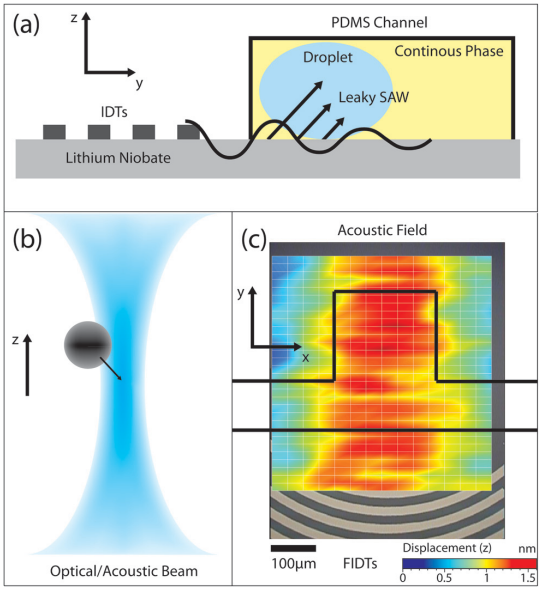

Fig. 2 (a) Leaky SAWs travel on the piezoelectric substrate surface and exponentially decay as they leak into the fluid medium. (b) Optical/acoustic beam lying on z-axis have been shown to attract droplets in the Mie regime towards the focus point where the intensity is maximum.[70,71] (c) The time averaged out-of-plane (z) surface displacement on the lithium niobate substrate captured using a Laser Doppler Vibrometer (LDV) shows that the acoustic field in the x–y plane is focused along the x-direction in the area of the expansion chamber.

3 Fabrication

The IDTs used in this study were 80 μm wavelength (48.5 MHz) focused IDTs composed of 45 finger-pairs, the arc subtends an angle of 90°. Focused IDTs (FIDTs) are a special type of IDTs where finger pairs are formed into concentric circular arcs rather than the conventional straight finger pairs. This was first proposed by Green *et al.*[72] and employed in a number of recent studies.[40,47,73]

A 200 nm thick aluminum layer of FIDT features were deposited onto 0.5 mm thick, double side polished 128° *Y*-cut, *X*-propagating lithium niobate, $LiNbO_3$, substrate. The silicon master mold for the designed microfluidic channels was fabricated using standard lithography and dry etching techniques (50 μm deep). The patterns were transferred to polydimethylsiloxane (PDMS) (SYLGARD® 184, Dow Corning) (10 : 1) using the master mold and individual devices were bonded to the diced lithium niobate devices after exposure to an activated air plasma (Harrick Plasma PDC-32G).

4 Experimental

The tubing for the inlets and outlets were connected to the device and syringes. The syringes were operated by two or three (depending on the number of inlets) NE-1000 (New Era Pump Systems, Inc.) syringe pumps to get the desired flow rates into the microfluidic channel network. The device was stabilized on a 3D-printed platform housing a peltier cooler and a fan. The entire setup was placed on the stage of a microscope (Olympus BX43, Tokyo, Japan) and videos were captured using a 5MP eyepiece camera (Dino-Lite AM7023B, New Taipei City, Taiwan). Olive oil was used as the continuous phase (viscosity, μ = 85 cP, surface tension at oil–water interface, $\sigma_{w/o} \approx 0.024$ N m^{-1} (ref. 74)), whereas the dispersed phase was DI-water (no surfactants used).

SAWs were generated by applying an AC signal across the electrode pads using a SMC100A signal generator (Rohde&Schwarz) amplified by AR 25A250A amplifier (Amplifier Research). The reported power values are measured using a WaveSurfer 454 oscilloscope (Teledyne LeCroy). The operating frequency of each device was determined using Power Signal Generator – F20 (BelektroniG, Bruenig & Guhr Elektronik GbR) by minimizing the reflected power from each device over a range of frequencies. Lithium niobate surface displacement was measured and visualized using a laser Doppler vibrometer (Polytech GmBH UHF-120, Waldbronn, Germany).

5 Results

As a droplet enters the channel expansion it will slow due to hydrodynamic effects but will not come to rest. The velocity of droplets passing through the expansion chamber, under no SAW actuation, is shown for a range of flow rates in Fig. 3(a). Droplet velocities were calculated by measuring the number of pixels traveled by the droplets during the time between each successive frame and a smoothing function

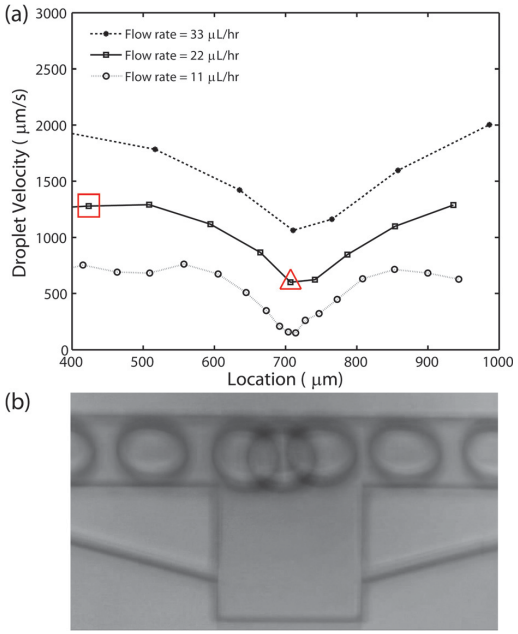

Fig. 3 (a) In-channel droplet velocity profiles for different flow rates. Droplet velocities are calculated along the area of interest and a smoothing function (3-point moving average) was applied using MATLAB software. (b) 7 frames (equally spaced in time) have been superimposed to show the progress of the droplet through the expansion chamber. (The red square and triangle are referred to in the caption for Fig. 5.)

(3-point moving average) was applied to the results with MATLAB software. In Fig. 3(b), the progress of a single droplet can be seen from a composite image which consists of seven superimposed frames (equally spaced in time).

In contrast, Fig. 4 shows, by way of a time series of images, the progress of a droplet under the influence of an acoustic field excited by SAW. It can be seen that the droplet comes to a complete stop at the center line of the focused IDTs (Fig. 4, t = 1.2 s). After the droplet was rendered immobile, the oil phase was able to flow around the droplet through the expansion area (Fig. 4, t = 2.2 s). Subsequently a second droplet enters the expansion chamber and merges with the first (Fig. 4, t = 2.6 s), the resultant larger droplet then moves out of the acoustic trap (Fig. 4, t = 2.8 s).

Having demonstrated the principle of SAW droplet trapping and merging, we now examine the operational conditions required to achieve this. The minimum trapping power required to merge droplets of different velocities was analyzed by conducting a series of experiments in which the power was slowly increased until a droplet in varying fluid flow rates was trapped (Fig. 5). The flow rates applied to the two inlets were increased uniformly, resulting in droplets of equal sizes being formed. The data is plotted in two ways, in that the power is plotted against two sets of droplet velocities; firstly, the square data points use the droplet

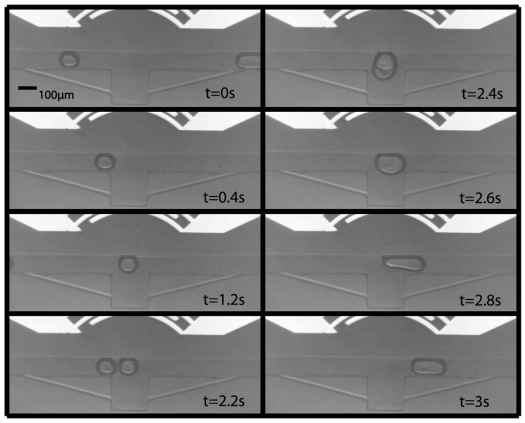

Fig. 4 Time lapse images of the droplet merging experiment. The first droplet is immobilized across the FIDTs while the next droplet comes and merges with the stationary one. The merged droplet travels downstream because the acoustic energy in the system is not enough to hold a bigger volume droplet. The oil flow is from left to right.

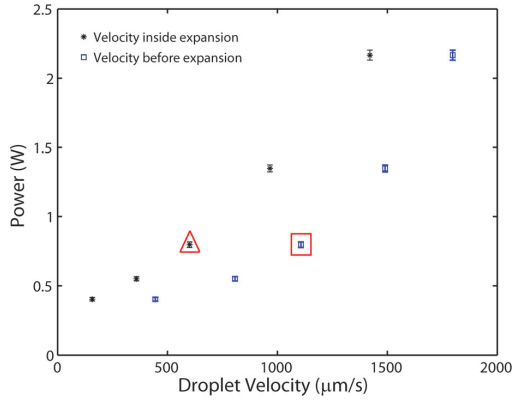

Fig. 5 Minimum trapping power for droplets of 0.447 ± 0.013 nL volume generated at increasing flow rates. Maximum and minimum droplet velocities were calculated and averaged before and inside the expansion area, respectively, while acoustic energy was not present (Fig. 3). The data point highlighted with the red triangle and square use the velocity data points in Fig. 3 which are highlighted the same way.

velocity in the channels before the expansion easily extracted from Fig. 3 (the maximum velocity values). However, it is known from Fig. 3 that the droplets slow due to hydrodynamic effects as they pass through the expansion even when unimpeded by acoustic effects. The second set of droplet velocities are for the velocity at which a droplet travels through the expansion in the absence of ultrasonic effects (*i.e.* the minimum value in the plots shown in Fig. 3). When halting a droplet ultrasonically, the drag force needs to be exceeded by the ultrasonic force. The location at which the droplets are halted is inside the expansion area, hence it is drag related to this velocity which needs to be overcome. It can be seen from this second set of data that there is an almost linear relationship between droplet velocity inside the expansion and required acoustic power for the first three data points (<22 μL h^{-1}) (asterisks in Fig. 5). We believe that the linearity is lost at higher flow rates and higher amplitudes due to experimental difficulties.

In order to understand this outcome, it is worth considering the relationship between parameters affecting the forces concerned:

$$P_i \propto \xi^2 \propto p^2 \propto F \tag{2}$$

It has previously been shown that power input, P_i, is proportional to piezoelectric surface velocity squared,[75] ξ^2. This surface vibration velocity relates directly to pressure amplitude, p, generated in the liquid medium.[76] Acoustic radiation force, F, is proportional to pressure amplitude squared,[63] p^2. This force is used to balance (at its lower limit) or overcome Stokes' drag which depends on flow velocity, v, linearly (eqn (1)). Overall, then, it must be expected that the minimum required power input to the system be linearly related to the droplet velocity.

The flow rates at the oil and water inlets were altered over a series of experiments to investigate the relationship between minimum required power for droplet trapping and droplet volume. The alteration of these flow rates causes droplets of different sizes to be created,[77] though, clearly it also alters the flow rate against which the droplet must be retained. This latter effect is governed by the combined flow rate at the inlets, which was varied between 6 and 11 μL h^{-1}. Since flow rate is also a function of minimum trapping power; a linear approximating function derived for droplet velocity inside the expansion and minimum trapping power (extracted from the data shown in Fig. 5) was used to scale the experimental power values matching a flow rate 8 μL h^{-1} where applicable.

The minimum trapping power for various droplet volumes is displayed in Fig. 6(a). It can be seen (with reference to the data points shown as asterisks) that the trapping of larger droplets requires larger input powers, this means that when operating at these critical power levels, a droplet can be held, but when a second droplet comes into the channel and merges with the first, the resultant volume rise will ensure that the power is not sufficient to trap the combined volume, hence the droplet will move out of the expansion. The trap, merge and release sequence shown in Fig. 4 is thus assured at these powers.

The droplet volumes were calculated through image processing, for each data point taking into account a minimum of three images and averaged, the standard deviations are used for the error bars. The droplet volumes plotted are calculated before merging occurred, *i.e.* considering the volume of a single droplet in the trapping area.

For increasing droplet volume, the expansion chamber becomes increasingly blocked, leaving a smaller space for the oil to flow past. The trapped droplet therefore experiences more drag force exerted by the continuous phase flow. When the droplet volume is further increased, the entire channel

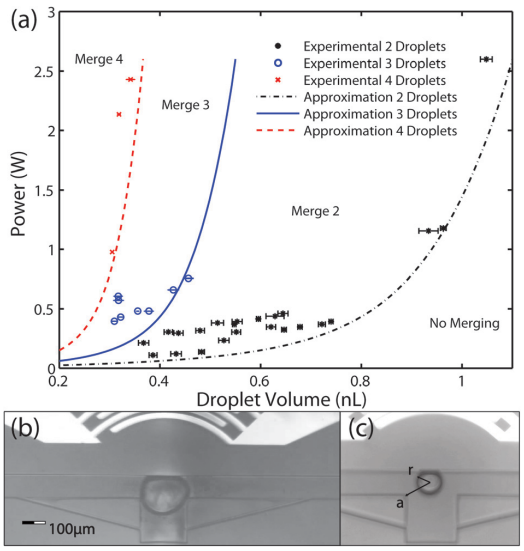

Fig. 6 (a) Minimum required trapping power as a function of droplet volume. Droplet size measurements were carried out through image processing considering a minimum of three images and averaged, standard deviations are shown as error bars. The graph is labeled to show regions where merging will not occur, as well as regions in which 2,3, and 4 droplets will merge. Data for two droplets merging is shown in asterisks (black). The dash-dot line (black) shows the analytically found drag force on the droplet in a constricted flow. To consider the merging of multiple droplets, the drag is scaled in the *x* direction, such that, for example for four droplet merging, the critical drag which must be overcome is that of 3 times the initial droplet volume. To support this, data points for the merging of both three (blue) and four (red) droplets are shown. (b) A 1.08 nL volume droplet that the current setup was unable to trap with maximum acoustic energy. It can be seen that the expansion chamber is completely filled by the droplet and there is no space for the continuous phase to flow. Haberman and Sayre's analytical drag formula[78] for a stationary sphere of radius r confined in a circular pipe of radius *a* (*a* & *r* calculated from experimental data as shown in (c)) was scaled and plotted as approximations for merging 2,3, and 4 consecutive droplets.

will become blocked and the current setup is unable to trap the droplet because there's insufficient space for the continuous phase to flow (see Fig. 6(b)). The presence of the trapped droplet in such a confined space means that Stokes drag which predicts linearity between radius and drag, no longer applies.

Haberman and Sayre[78] presented an analytical drag formula to calculate the drag force, $F_{d,conf}$ on a stationary sphere of radius r confined in a circular pipe of radius a. It is given, as a function of Stokes drag, by:

$$F_{d,conf} = \frac{\left(1-\frac{2}{3}R^2-0.20217R^5\right)F_d}{1-2.105R+2.0865R^3-1.7068R^5+0.72603R^6} \quad (3)$$

where R is the ratio of the confinement radii, $R = r/a$, and F_d is the unconfined drag on the particle – the Stokes' drag. Whilst this scenario is not exactly that of the system under examination here, it gives a better understanding of the drag acting on an object in an increasingly blocked channel.

In Fig. 6(a), this drag force (predicted to be scaling linearly with trapping power in eqn (2)) was normalized, scaled and plotted for experimental droplet volume values with matching a and r values gathered from the experiments as shown in Fig. 6(c). Again it is worth emphasizing that we cannot expect a highly accurate agreement against our data, as the droplets are trapped in a syringe driven rectangular cross-section flow as opposed to pressure driven axi-symmetric flow. However, a sharp increase in the analytical drag force can be observed as the flow is further restricted by increasing droplet size, which is of a similar nature to the increase in power required to trap the droplets. Stokes' drag by itself cannot account for confined flow which is why the minimum power needed to trap droplets of bigger volume grows asymptotically in the experimental results as well.

There is also the possibility of using excessive power to trap the first droplet. This can lead to the merging of more than two droplets. This system has been used for the merging of up to 4 consecutive droplets. Experimental results for merging of 3 and 4 consecutive droplets are also shown in Fig. 6(a). Time-lapse images for merging three droplets is shown in Fig. 7.

The power required to perform this multiple droplet merging is shown in Fig. 6(a) with circle (blue) and cross (red) data points, for 3 and 4 droplets respectively. Approximating functions for merging of 3 and 4 droplets are calculated by scaling down (x-axis) the original 2 droplet approximation curve by a factor of 2 and 3 respectively. Reported droplet volumes are for the first droplet only, however, the minimum trapping power is for trapping $n-1$ droplets where n is the

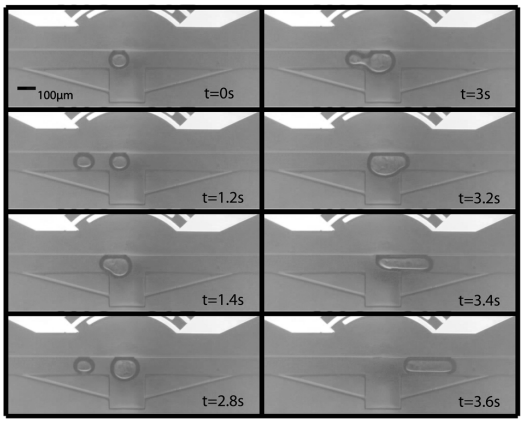

Fig. 7 Experimental results showing time lapse images of the 3-droplet merging experiment. The first droplet (0.4452 nL) is immobilized across the IDTs while the next droplet comes and merges with the stationary one (t = 1.4 s). The first two droplets stay trapped until the third droplet comes and merges with the lot (t = 3 s). As droplet volume is tripled, the system is unable to trap the droplet anymore therefore it is released from the trapping zone (t = 3.4 s).

View Article Online

Lab on a Chip Paper

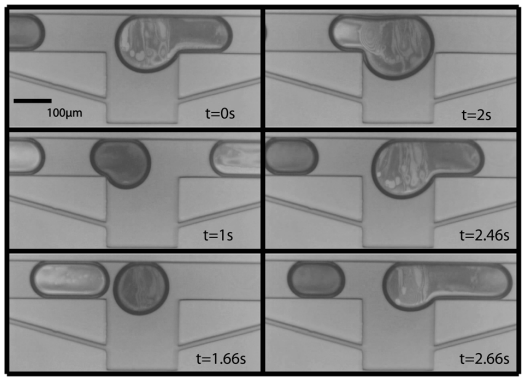

Fig. 8 Experimental results showing time lapse images of the droplet merging experiment with alternating droplets of water and black dye.

total number of droplets merged (*i.e.* 3 droplets are trapped for merging 4 droplets). This is why scaling down the approximation curve is straightforward; this way, regions of droplet volume and input power combinations emerge, in which no trapping occurs, or the merging of 2,3 or 4 droplets can be expected (Fig. 6(a)).

Finally, in order to demonstrate a possible application for the designed microfluidic chip, droplets of water and black dye were merged on demand. Time-lapse images of the experiment are shown in Fig. 8. Alternating droplets were achieved by use of 2 different T-junctions which joined oil, water and dye inlets, prior to the merging chamber (Fig. 1). The merging of these pure water and dye droplets, represents how samples and reagent droplets, for example, could readily be merged on demand, offering reduced reaction times and quantities of fluids used.

It should be noted that the volume of the smallest droplets trapped was limited to 0.3 nL (94.07 μm dia.) by the design of droplet generating T-junctions. Whilst, the maximum volume of droplets which could be trapped, 1.1 nL (167.36 μm dia.), was limited by constriction effects, and hence the geometry of the expansion chamber. The number of droplets trapped prior to release is dictated by a combination of the chamber geometry and the power used to excite the acoustic waves. Hence, it is reasonable to expect that it is possible to merge droplets of bigger or lesser volume by suitable designing of the expansion chamber, T-junction and FIDTs.

The throughput of the system was not optimized, however, it is worth noting that 2 droplets could be merged every 0.3 seconds, most of the time being spent in waiting for the second droplet to arrive. Future work includes improving the throughput of the system by increasing flow rates and optimizing the expansion chamber design.

6 Conclusions

It was experimentally shown that multiple droplets can readily be trapped and merged on demand using surface acoustic waves (SAWs). The minimum required trapping power for similar size droplets in varying flow rates were established with experimental results. Experimental results for the minimum trapping power as a function of droplet volume ranging from 0.3 to 1 nL were discussed for merging up to four consecutive droplets. To demonstrate a potential application, alternating water and black dye droplets were successfully merged on demand using the proposed microfluidic chip. SAW based droplet merging have the potential to replace existing technologies and serve as the next generation droplet merging technique because it offers power consumption, seamless integration and contamination free on-demand operation independent of droplet spacing.

Acknowledgements

This work was performed in part at the Melbourne Centre for Nanofabrication (MCN) in the Victorian Node of the Australian National Fabrication Facility (ANFF).

References

1 D. C. Duffy, J. C. McDonald, O. J. A. Schueller and G. M. Whitesides, *Anal. Chem.*, 1998, **70**, 4974–4984.
2 T. Thorsen, F. H. Roberts, F. H. Arnold and S. R. Quake, *Phys. Rev. Lett.*, 2001, **86**, 4163–4166.
3 S. L. Anna, N. Bontoux and H. A. Stone, *Appl. Phys. Lett.*, 2003, **82**, 364–366.
4 C. Cramer, P. Fischer and E. J. Windhab, *Chem. Eng. Sci.*, 2004, **59**, 3045–3058.
5 L. Schmid and T. Franke, *Lab Chip*, 2013, **13**, 1691–1694.
6 J. J. Agresti, E. Antipov, A. R. Abate, K. Ahn, A. C. Rowat, J.-C. Baret, M. Marquez, A. M. Klibanov, A. D. Griffiths and D. A. Weitz, *Proc. Natl. Acad. Sci. U. S. A.*, 2010, **107**, 4004–4009.
7 K. Ahn, C. Kerbage, T. P. Hunt, R. M. Westervelt, D. R. Link and D. A. Weitz, *Appl. Phys. Lett.*, 2006, **88**, 024104.
8 J.-C. Baret, O. J. Miller, V. Taly, M. Ryckelynck, A. El-Harrak, L. Frenz, C. Rick, M. L. Samuels, J. B. Hutchison, J. J. Agresti, D. R. Link, D. A. Weitz and A. D. Griffiths, *Lab Chip*, 2009, **9**, 1850–1858.
9 T. Franke, A. R. Abate, D. A. Weitz and A. Wixforth, *Lab Chip*, 2009, **9**, 2625–2627.
10 D. R. Link, E. Grasland-Mongrain, A. Duri, F. Sarrazin, Z. Cheng, G. Cristobal, M. Marquez and D. A. Weitz, *Angew. Chem., Int. Ed.*, 2006, **45**, 2556–2560.
11 K. Ahn, J. Agresti, H. Chong, M. Marquez and D. A. Weitz, *Appl. Phys. Lett.*, 2006, **88**, 264105.
12 C. Priest, S. Herminghaus and R. Seemann, *Appl. Phys. Lett.*, 2006, **89**, 134101–134101.
13 X. Niu, S. Gulati and J. Edel, *et al.*, *Lab Chip*, 2008, **8**, 1837–1841.
14 N. Bremond, A. R. Thiam and J. Bibette, *Phys. Rev. Lett.*, 2008, **100**, 024501.

15 T. S. Kaminski, S. Jakiela, M. A. Czekalska, W. Postek and P. Garstecki, *Lab Chip*, 2012, **12**, 3995–4002.
16 F. Scheiff, M. Mendorf, D. Agar, N. Reis and M. Mackley, *Lab Chip*, 2011, **11**, 1022–1029.
17 D. N. Adamson, D. Mustafi, J. X. J. Zhang, B. Zheng and R. F. Ismagilov, *Lab Chip*, 2006, **6**, 1178–1186.
18 D. R. Link, S. L. Anna, D. A. Weitz and H. A. Stone, *Phys. Rev. Lett.*, 2004, **92**, 054503.
19 A. C. Hatch, J. S. Fisher, A. R. Tovar, A. T. Hsieh, R. Lin, S. L. Pentoney, D. L. Yang and A. P. Lee, *Lab Chip*, 2011, **11**, 3838–3845.
20 Y.-C. Tan, J. S. Fisher, A. I. Lee, V. Cristini and A. P. Lee, *Lab Chip*, 2004, **4**, 292–298.
21 Y. Bai, X. He, D. Liu, S. N. Patil, D. Bratton, A. Huebner, F. Hollfelder, C. Abell and W. T. S. Huck, *Lab Chip*, 2010, **10**, 1281–1285.
22 P. Abbyad, R. Dangla, A. Alexandrou and C. N. Baroud, *Lab Chip*, 2011, **11**, 813–821.
23 C. H. Schmitz, A. C. Rowat, S. Köster and D. A. Weitz, *Lab Chip*, 2009, **9**, 44–49.
24 A. Huebner, D. Bratton, G. Whyte, M. Yang, A. J. deMello, C. Abell and F. Hollfelder, *Lab Chip*, 2009, **9**, 692–698.
25 M. Sun, S. S. Bithi and S. A. Vanapalli, *Lab Chip*, 2011, **11**, 3949–3952.
26 W. Wang, C. Yang and C. M. Li, *Lab Chip*, 2009, **9**, 1504–1506.
27 X. Niu, F. Gielen, J. B. Edel and A. J. deMello, *Nat. Chem.*, 2011, **3**, 437442.
28 F. Sarrazin, L. Prat, N. Di Miceli, G. Cristobal, D. Link and D. Weitz, *Chem. Eng. Sci.*, 2007, **62**, 1042–1048.
29 H. Song, D. Chen and R. Ismagilov, *Angew. Chem., Int. Ed.*, 2006, **45**, 7336–7356.
30 H. Song, J. D. Tice and R. F. Ismagilov, *Angew. Chem., Int. Ed.*, 2003, **42**, 768–772.
31 T. A. Franke and A. Wixforth, *ChemPhysChem*, 2008, **9**, 2140–2156.
32 S.-Y. Teh, R. Lin, L.-H. Hung and A. P. Lee, *Lab Chip*, 2008, **8**, 198–220.
33 G. M. Whitesides, *Nature*, 2006, **442**, 368–373.
34 J. S. Eow and M. Ghadiri, *Colloids Surf., A*, 2003, **219**, 253–279.
35 J. S. Eow, M. Ghadiri, A. O. Sharif and T. J. Williams, *Chem. Eng. J.*, 2001, **84**, 173–192.
36 J. S. Eow, M. Ghadiri and A. Sharif, *Colloids Surf., A*, 2003, **225**, 193–210.
37 P. Atten, L. Lundgaard and G. Berg, *J. Electrost.*, 2006, **64**, 550–554.
38 L.-H. Hung, K. M. Choi, W.-Y. Tseng, Y.-C. Tan, K. J. Shea and A. P. Lee, *Lab Chip*, 2006, **6**, 174–178.
39 Y.-C. Tan, Y. Ho and A. Lee, *Microfluid. Nanofluid.*, 2007, **3**, 495–499.
40 D. J. Collins, T. Alan, K. Helmerson and A. Neild, *Lab Chip*, 2013, **13**, 3225–3231.
41 P. Rogers and A. Neild, *Lab Chip*, 2011, **11**, 3710–3715.
42 K. Sritharan, C. J. Strobl, M. F. Schneider, A. Wixforth and Z. Guttenberg, *Appl. Phys. Lett.*, 2006, **88**, 054102.
43 T.-D. Luong, V.-N. Phan and N.-T. Nguyen, *Microfluid. Nanofluid.*, 2011, **10**, 619–625.
44 X. Ding, S.-C. S. Lin, M. I. Lapsley, S. Li, X. Guo, C. Y. Chan, I.-K. Chiang, L. Wang, J. P. McCoy and T. J. Huang, *Lab Chip*, 2012, **12**, 4228–4231.
45 D. J. Collins, T. Alan and A. Neild, *Lab Chip*, 2014, **14**, 1595–1603.
46 R. Walker, I. Gralinski, K. Keong Lay, T. Alan and A. Neild, *Appl. Phys. Lett.*, 2012, **101**, 163504.
47 R. Shilton, M. K. Tan, L. Y. Yeo and J. R. Friend, *J. Appl. Phys.*, 2008, **104**, 014910.
48 C. Devendran, I. Gralinski and A. Neild, *Microfluid. Nanofluid.*, 2014, 1–12.
49 P. Agrawal, P. S. Gandhi and A. Neild, *J. Appl. Phys.*, 2013, **114**, 114904.
50 P. Rogers, I. Gralinski, C. Galtry and A. Neild, *Microfluid. Nanofluid.*, 2013, **14**, 469–477.
51 P. Augustsson, J. Persson, S. Ekstrom, M. Ohlin and T. Laurell, *Lab Chip*, 2009, **9**, 810–818.
52 G. Destgeer, K. H. Lee, J. H. Jung, A. Alazzam and H. J. Sung, *Lab Chip*, 2013, **13**, 4210–4216.
53 X. Ding, S.-C. S. Lin, B. Kiraly, H. Yue, S. Li, I.-K. Chiang, J. Shi, S. J. Benkovic and T. J. Huang, *Proc. Natl. Acad. Sci. U. S. A.*, 2012, **109**, 11105–11109.
54 J. Nam, Y. Lee and S. Shin, *Microfluid. Nanofluid.*, 2011, **11**, 317–326.
55 J. Shi, X. Mao, D. Ahmed, A. Colletti and T. J. Huang, *Lab Chip*, 2008, **8**, 221–223.
56 J. Shi, D. Ahmed, X. Mao, S.-C. S. Lin, A. Lawit and T. J. Huang, *Lab Chip*, 2009, **9**, 2890–2895.
57 J. Shi, H. Huang, Z. Stratton, Y. Huang and T. J. Huang, *Lab Chip*, 2009, **9**, 3354–3359.
58 X. Ding, P. Li, S.-C. S. Lin, Z. S. Stratton, N. Nama, F. Guo, D. Slotcavage, X. Mao, J. Shi, F. Costanzo and T. J. Huang, *Lab Chip*, 2013, **13**, 3626–3649.
59 S.-C. S. Lin, X. Mao and T. J. Huang, *Lab Chip*, 2012, **12**, 2766–2770.
60 R. M. White and F. W. Voltmer, *Appl. Phys. Lett.*, 1965, **7**, 314–316.
61 L. Rayleigh, *Proc. London Math. Soc.*, 1885, **s1–17**, 4–11.
62 K. Yosioka, *Acustica*, 1955, **5**, 167–173.
63 L. P. Gor'kov, *Sov. Phys. Dokl.*, 1962, **6**, 773–775.
64 V. Skowronek, R. W. Rambach, L. Schmid, K. Haase and T. Franke, *Anal. Chem.*, 2013, **85**, 9955–9959.
65 J. Lee and K. K. Shung, *J. Acoust. Soc. Am.*, 2006, **120**, 1084–1094.
66 A. Ashkin, *Proc. Natl. Acad. Sci. U. S. A.*, 1997, **94**, 4853–4860.
67 D. G. Grier, *Nature*, 2003, **424**, 810–816.
68 J. Lee, K. Ha and K. K. Shung, *J. Acoust. Soc. Am.*, 2005, **117**, 3273–3280.
69 J. Lee, C. Lee, H. H. Kim, A. Jakob, R. Lemor, S.-Y. Teh, A. Lee and K. K. Shung, *Biotechnol. Bioeng.*, 2011, **108**, 1643–1650.
70 J. Lee, S.-Y. Teh, A. Lee, H. H. Kim, C. Lee and K. K. Shung, *Appl. Phys. Lett.*, 2009, **95**, 073701.

71 K. Svoboda and S. M. Block, *Annu. Rev. Biophys. Biomol. Struct.*, 1994, **23**, 247–285.
72 J. Green, G. Kino and B. Khuri-Yakub, *1980 Ultrasonics Symposium*, 1980, pp. 69–73.
73 M. K. Tan, J. R. Friend and L. Y. Yeo, *Phys. Rev. Lett.*, 2009, **103**, 024501.
74 L. Fisher, E. Mitchell and N. Parker, *J. Food Sci.*, 1985, **50**, 1201–1202.
75 K. Franke, M. Ross-Messemer, A. Menck, R. Hoeller, H. Schmidt and M. Weilmacht, *IEEE Trans. Ultrason., Ferroelectr., Freq. Control*, 2003, **50**, 77–80.
76 L. L. Beranek, *Acoustics*, McGraw-Hill, New York, 1954.
77 P. Garstecki, M. J. Fuerstman, H. A. Stone and G. M. Whitesides, *Lab Chip*, 2006, **6**, 437–446.
78 W. Haberman and R. Sayre, *David Taylor Model Basin Reports*, 1958.

Chapter 5

Microfluidic Plug Steering using Surface Acoustic Waves

5.1 Overview

This chapter presents a microfluidic device that can steer plugs into one of the two outlets of the chip using surface acoustic wave (SAW) induced interface deformation. Sorting microfluidic droplets is another key requirement in the design of LOC devices. Many studies demand droplets to be sorted into different outlets thereby getting rid of unwanted droplets or collecting wanted droplets into one specific channel for further analysis or manipulation. Directing droplets at a Y-junction has previously been achieved using dielectrophoresis, electrophoresis and SAW. The proposed device detailed in this chapter takes droplet sorting a step further by offering enhanced control over the sorting process. This allows the user to either sort an entire plug into one of the outlets or to split the plug at the Y-junction evenly or unevenly by adjusting the applied SAW power.

The proposed microfluidic device consists of two sets of SAW generating electrodes implemented at opposing sides of a Y-junction channel with integrated by-pass channels. When a set of electrodes are actuated, they generate SAWs which impinge on the interface of a plug where an acoustic contrast is present. This leads to the deformation of the interface away from the travelling SAWs which steers the plugs into the desired branches of the Y-junction outlets. In the absence of SAWs, however, the plugs can be split into two equal volume daughter droplets. Furthermore, if the applied SAW power is relatively low, a plug could be partially split into two unequal daughter droplets. Plug steering as a whole and partial splitting depends highly on plug volume, velocity and input SAW power which have all been thoroughly characterised within the presented work.

In this chapter; a review of droplet steering methods, fabrication and working principle of the proposed device are presented. This is followed by thorough characterisation of the system via detailed analysis of experimental results and discussion. The presented plug steering technique can easily be integrated to existing LOC devices where it could be used to either steer plugs or split them in a controlled manner. The splitting could be followed by further manipulation or analysis of the split droplets depending on the specific studies' requirements.

5.2 Publication

The following publication has been published and reprinted from [18].

Monash University

Declaration for Thesis Chapter 5
Declaration by candidate

In the case of Chapter 5, the nature and extent of my contribution to the work was the following:

Nature of contribution	**Extent of contribution**
Design and fabrication of devices, experimentation, development, result analysis, interpretation and writing.	90%

The following co-authors contributed to the work:

Name	**Nature of contribution**	**Extent of contribution**
Dr. Tuncay Alan	Project Supervision, editing	N/A
Assoc. Prof. Adrian Neild	Project Supervision, editing	N/A

The undersigned hereby certify that the above declaration correctly reflects the nature and extent of the candidate's and co-authors' contributions to this work.

Candidate's Signature: 

Candidate's Name: Muhsincan Sesen

Date: 5th August 2016

Main Supervisor's Signature: 

Main Supervisors's Name: Assoc. Prof. Adrian Neild

Date: 5th August 2016

Lab on a Chip

PAPER

View Article Online
View Journal

Cite this: DOI: 10.1039/c5lc00468c

Microfluidic plug steering using surface acoustic waves†

Muhsincan Sesen, Tuncay Alan and Adrian Neild*

Received 24th April 2015,
Accepted 5th June 2015

DOI: 10.1039/c5lc00468c

www.rsc.org/loc

Digital microfluidic systems, in which isolated droplets are dispersed in a carrier medium, offer a method to study biological assays and chemical reactions highly efficiently. However, it's challenging to manipulate these droplets in closed microchannel devices. Here, we present a method to selectively steer plugs (droplets with diameters larger than the channel's width) at a specially designed Y-junction within a microfluidic chip. The method makes use of surface acoustic waves (SAWs) impinging on a multiphase interface in which an acoustic contrast is present. As a result, the liquid–liquid interface is subjected to acoustic radiation forces. These forces are exploited to steer plugs into selected branches of the Y-junction. Furthermore, the input power can be finely tuned to split a plug into two uneven plugs. The steering of plugs as a whole, based on plug volume and velocity is thoroughly characterized. The results indicate that there is a threshold plug volume after which the steering requires elevated electrical energy input. This plug steering method can easily be integrated to existing lab-on-a-chip devices and it offers a robust and active plug manipulation technique in closed microchannels.

1 Introduction

Digital microfluidics, the compartmentalization of small volumes of one phase within a second immiscible phase, offers the potential of conducting chemical reactions and biological analysis in multiple assays. Hence, offering reduced analysis costs, faster reactions and high throughput analysis capabilities with high sensitivity.[1] However, governing fluid behavior at the microscale is a challenging task[2] and has led to the investigation of several forcing mechanisms; for example, electric,[3–5] magnetic,[6–8] centrifugal[9] and acoustic forces[10–14] have been used to manipulate flows, droplets, particles and cells at the microscale.

A desire to control fluid behavior in digital microfluidic systems has led to the development of special microchannel structures[15–18] to manipulate droplets in a passive manner relying on hydrodynamic and capillary phenomena. In addition, active manipulation of droplets has been studied. Electric fields is one of the mechanisms that have been utilized to perform such tasks.[19–22] For example, dielectrophoresis (DEP) has been used to direct droplets into trapping chambers[23] and induce droplet coalescence by destabilizing the oil/water interface.[22,24] A second actuation mechanism used to gain control over droplet behavior is acoustic vibration. The vibration can be induced in a number of ways, including the use of a resonating piezoelectric disk causing control of the size of bubble produced in a flow-focusing junction[25] or by use of surface acoustic waves (SAW).[26]

Surface acoustic waves are generated by patterned electrodes on a piezoelectric substrate[27] and are easily integrated to a microfluidic chip. They have been used for particle concentration,[28,29] trajectory control[30,31] and sorting,[32,33] for atomization,[34,35] for sessile droplet displacement[36] and for manipulating cells.[37–39] In two phase microfluidic systems, SAW has been used for mixing,[40] control of droplet size,[41] individual droplet production,[42] droplet merging[43] and sorting droplets at single[44] and multiple Y-junctions.[45] For sorting droplets; Franke *et al.*[44] designed a system such that a single branch had a lower hydrodynamic resistance making that the preferred pathway by default and ultrasonic forces were utilized to redirect the droplets into the non-preferred, higher resistance path.

In this paper, we report steering of plugs in Y-junctions of equal hydrodynamic resistance using acoustically generated forces. Here, we use the term plug, as opposed to a droplet, to refer to a fluid body which is large enough to be in contact with all four walls of a closed microfluidic channel. In the case of a droplet in a channel the nature of the acoustic forces generated on it are similar to those for a solid particle. The acoustic radiation force is determined by integrating second order time averaged terms over the surface of the (solid or fluid) sphere. In the case of a plug, however, the ultrasonic

Department of Mechanical and Aerospace Engineering, Monash University, Clayton, VIC 3800, Australia. E-mail: adrian.neild@monash.edu; Tel: +61 3 990 54655

† Electronic supplementary information (ESI) available. See DOI: 10.1039/c5lc00468c

interaction is restricted to the interface between the two immiscible fluids, in a straight channel this is the head and tail of the plug, around a junction an additional surface is created at the opening of the second channel. As such, in order to steer a plug, the liquid/liquid interface, at which there is an acoustic impedance mismatch, must be displaced.

Hertz and Mende were the first to observe the deformation of liquid–liquid interface where the acoustic properties of the liquids were different.[46] More recently, Issenmann *et al.* further characterized acoustically induced interface deformation[47] and a similar effect was applied to mix different density fluids by acoustically resonating the entire system to deform and destabilize the liquid–liquid interface.[48] Furthermore, acoustic induced interface deformation has been used to create picolitre droplets.[42]

In this work, we direct focused surface acoustic waves at the oil/water interface, inducing a net acoustic radiation force sufficient to obstruct the progress of a plug into a selected branch of the Y-junction. This method allows an incoming plug to be steered into the desired branch at the Y-junction. Moreover, an incoming plug could be controllably split into two daughter plugs of uneven volume by adjusting the input power.

2 Experimental methods

The microfluidic chip designed for steering plugs is shown in Fig. 1a. Water-in-oil plugs are generated *via* the use of a T-junction geometry[49] just after the inlets (an oil and a water phase), upstream from the Y junction. After formation, plugs travel downstream along a 100 μm wide and 50 μm high rectangular cross-section microchannel, until they reach the Y-junction which is positioned at the center of the chip for easy optical access (Fig. 1b). The three channels that meet to form the Y-junction are of the same dimensions. Downstream of the junction, connecting channels pass between the two emerging branches. In contrast to changing the direction of a droplet at a Y-junction,[19,20,44] steering a plug will alter the fluid flow profiles throughout each outlet channel. These connecting channels are designed to assist with the equalization of pressure in the two branches. Focused electrode pairs deposited onto a piezoelectric substrate (inter-digital transducers) were aligned so that the focal area coincides with the neck of the Y-junction.

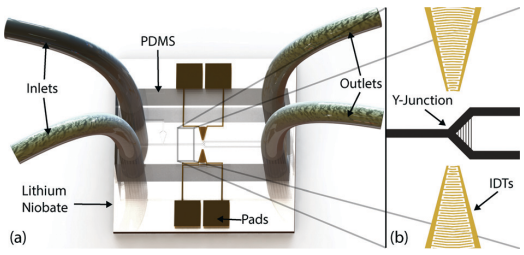

Fig. 1 (a) PDMS microfluidic channels bonded onto a piezoelectric substrate with patterned electrodes, the two inlets (an oil and a water phase) are connected by a T-junction (not visible) at which plugs are formed upstream of the Y-junction, and (b) the Y-junction is seen with connecting channels between the two downstream branches, the two sets of electrodes focused at the neck of the junction are also shown.

Fluorinated oil (FC-40) stabilized with 2% (w/w) surfactant (Pico-Surf™1, Dolomite) (viscosity, μ = 3.4 cP, interfacial tension $\gamma \approx 5$ mN m^{-1} (ref. 50)) was used as the continuous phase while the dispersed phase was DI water. Syringe pumps (NE-1000, New Era Pump Systems, Inc.) were used to regulate fluid flow as desired; the syringes were connected to the device using PTFE tubing. A 3D-printed platform was used to clamp the device as well as to interface with the electrodes on the piezoelectric substrate. A microscope (Olympus BX43, Tokyo, Japan) equipped with an eyepiece camera (5MP, Dino-Lite AM7023B, New Taipei City, Taiwan) was used for image acquisition. The videos were analyzed using "Droplet morphometry and velocimetry" (DMV) software developed by Basu.[51] DMV is a video processing software that makes use of edge detection and droplet tracking to extract information about the droplets such as shape, velocity, size, *etc.* In the presented work, DMV analysis was carried out using the same settings over a range of videos to obtain plug velocity and size information.

A power signal generator (F20, PowerSAW) (BelektroniG, Bruenig & Guhr Elektronik) was used to generate SAWs on the piezoelectric substrate by applying an AC signal to the inter-digital transducers. The PowerSAW determines the scattering parameters during operation which are used to accurately calculate the actual power (accounting for any losses in the cabling) that a device is using to induce the SAWs.

Focused inter-digital transducers (FIDTs) with a pitch of 60 μm were operated at 64 MHz in this study. FIDTs consist of curved electrodes and they have been used widely in the literature to focus the ultrasonic power along a narrow region.[32,37,42,43,52–55] This narrow region was designed to be of a similar size to the width of the working section which coincides with the neck of the Y-junction.

In order to fabricate the FIDTs; lithium niobate, $LiNbO_3$ (LN), substrates of 500 μm thickness (single side polished, 128° Y-cut, X-propagating) were patterned and a 200 nm thick aluminium layer was deposited following a 10 nm chromium layer for adhesion. The substrate was then diced into the desired dimensions. Similar for the microchannels, polydimethylsiloxane (PDMS) (SYLGARD® 184, Dow Corning) (10 : 1) was cast onto a silicon master mold patterned by standard lithography followed by deep reactive ion etching to a depth of 50 μm and silanization. Both the LN substrate and PDMS surfaces were subjected to air plasma (Harrick Plasma PDC-32G) for surface activation and subsequent covalent bonding using a custom built alignment system operated under a stereo microscope (Olympus, SZX16, Tokyo, Japan).

3 Operating principle

When an AC signal is applied at a frequency matched to the pitch of the electrodes, SAWs are generated on the surface of

an LN substrate due to piezoelectric coupling between an electrical field and mechanical displacement. Typically, SAWs are generated in the MHz scale frequencies and have nm-scale displacement amplitudes. SAWs propagate along the piezoelectric substrate, once in the presence of a microfluidic channel, the energy is coupled into the fluid, leading to various phenomena such as acoustic streaming,[56] pressure gradients[57] and acoustic radiation force.[58,59] SAWs have been used in a multitude of studies addressing tasks including particle manipulation,[30,33] droplet manipulation[43,44] and interface deformation.[41,42] When an acoustic wave meets an interface, where there is an acoustic impedance mismatch, a net radiation force results. Specifically between two fluids, the acoustic radiation pressure, $\bar{P}$, acting on the interface is given by:[60]

$$\overline{P} = E_i\left\{1 - \frac{c_1}{c_2} + R_c^2\left(1 + \frac{c_1}{c_2}\right)\right\} \quad (1)$$

where E_i is the energy density of the incident wave, R_c is the acoustic reflection coefficient and c is the speed of sound in the fluids.

A secondary pressure is applied on such an interface due to acoustic streaming. When the acoustic waves couple into a medium, they exert a body force on the fluid which causes a steady state swirling pattern. Such acoustic streaming may develop in both of the working fluids which may contribute to the force already acting on the interface.[47] However, given that the available body of fluid for acoustic streaming is no more than a wavelength on each direction, its effects will be very small and we will assume they are negligible for the remainder of this study.

By use of these forces generated at the interface between two immiscible liquids, this work aims to direct a plug to exit a Y-junction along a selected branch. As a consequence of the motion of the plug through the junction, the flows in the attached channels are affected. In order to understand this process, we analyze the system whilst a plug is being steered (Fig. 2).

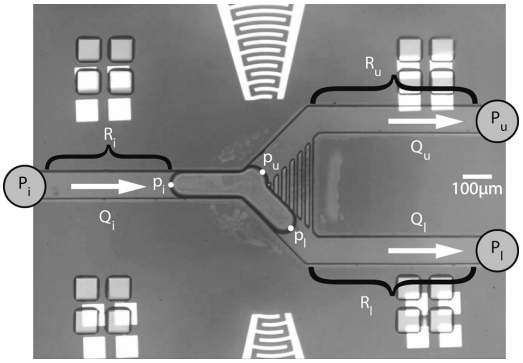

Fig. 2 Diagram for analyzing the pressure balance while a plug is being steered.

Microfluidic networks can be considered analogous to a resistor network in an electrical circuit to simplify analysis.[61] Considering capillary and Reynolds numbers are small; we can analyze a plug that is being steered using the following set of equations (Fig. 2):[62]

$$P_i - R_iQ_i + 2\gamma H_i = p_i \quad (2)$$

$$P_u + R_uQ_u + 2\gamma H_u + P_{ARP} = p_u \quad (3)$$

$$P_l + R_lQ_l + 2\gamma H_l = p_l \quad (4)$$

where P and p are local and external pressures respectively with subscripts for inlet (i), upper (u) and lower (l) channel (the descriptions being with reference to Fig. 2); Q denotes flow rates, γ is the interfacial tension between the two mediums and H represents the mean curvature of the interface. P_{ARP} is the pressure originating from acoustic radiation acting on the interface (referred to as acoustic radiation pressure), it is applied, in the equation, by the upper electrodes to steer the plug into the lower channel, and R stands for the microfluidic analogy of ohmic resistance, or hydrodynamic resistance. Keeping in mind that the capillary pressure will be the same for the steering channels because their dimensions are equal (*i.e.* $\gamma H_u = \gamma H_l$); we subtract eqn (4) from eqn (3) to get:

$$P_{ARP} = \Delta p - \Delta P - \Delta M \quad (5)$$

where Δp and ΔP are local and external pressure differences (*i.e.* $\Delta p = p_u - p_l$) and ΔM is the difference of pressure drops in the upper and lower channels (*i.e.* $\Delta M = R_uQ_u - R_lQ_l$). The local pressure difference between the two interfaces (Δp) can further be simplified considering a single-phase microfluidic system, in which case, the pressure drop in a microfluidic channel of rectangular section is known.[63] Substituting this into eqn (5), we get:

$$P_{ARP} = AU_mL\mu - \Delta P - \Delta M \quad (6)$$

where A is a constant depending on the channel geometry, U_m is the mean flow velocity, L is length and μ is the viscosity of the fluid. This is the governing equation which indicates how much acoustic radiation pressure will be needed to steer a plug under a set of given circumstances which will be analyzed.

3.1 Fluid pumped through the inlets

Depending on the way that we control flow through the junction, further simplifications can be made. Firstly if the flow is pumped through the inlets, then both outlets are at an equal pressure (open to atmosphere) (*i.e.* $\Delta P = 0$). Furthermore, in such a system, once the head of a large plug has passed the entrance to all the connecting channels, there won't be any flow in the upper channel, hence $Q_u = 0$ and

View Article Online
Paper Lab on a Chip

consequently $Q_l = Q_i$. Applying these factors in the governing eqn (6), we obtain:

$$P_{ARP} = AU_m L\mu + R_l Q_i \quad (7)$$

This suggests that the acoustic radiation pressure required to impede the progress of a plug is equal to the pressure drop from the top channel interface to the bottom channel interface of the plug (first term in eqn (7)) and an additional hydrodynamic resistance term (second term in eqn (7)). If an order of magnitude analysis is performed on the terms that contribute to the acoustic radiation pressure requirement, we find that the hydrodynamic resistance term is an order of magnitude higher than the pressure drop term when fluid is being pumped through the system. This implies that the necessary acoustic power depends highly on the hydrodynamic resistance in the steered channel as well as the inlet flow rate.

3.2 Fluid withdrawn from outlet channels

3.2.1 Connecting channels are not blocked. Alternatively, if the flow is drawn through the system, the previous assumptions do not hold. It is this flow regime that we investigate the system predominantly, as in a more complex digital microfluidic system, we must expect to have more complex flow regimes than results from simply pumping a constant volumetric flow rate through a single junction.

To draw the fluid, the two syringes attached to the outlets will attempt to maintain equal flow rates in the upper and lower channel, hence $2Q_u = 2Q_l = Q_i$. Even when a plug is being steered, before the connecting channels are blocked, flow will be equal in both outlet channels as dictated by the syringe pumps. This is because of the fact that the continuous medium is able to pass into the upper branch from the lower branch through the connecting channels. In such a case, it can be expected that the working outlet pressures of the syringes are reasonably close (*i.e.* $\Delta P \approx 0$). Moreover, we further assume that the hydrodynamic resistances in the outlets have a static and a dynamic term, for continuous medium and the plugs in the outlet, respectively:[64]

$$R = \bar{R} + nR_p \quad (8)$$

where $\bar{R}$ is the average hydrodynamic resistance of a channel without any plugs and n is the number of plugs currently in the channel and R_p is the hydrodynamic resistance of a plug, assuming the plugs are the same. Applying all the above assumptions and substituting eqn (8) to the governing eqn (6) for the system when the connecting channels are not blocked by the plug and the syringes are equally withdrawing from the outlets, we get:

$$P_{ARP} = AU_m L\mu + (nR_p)Q_i \quad (9)$$

It should be noted here that for every plug that is steered into the desired channel, there will be an additional $R_p Q_i$ pressure requirement where R_p is the hydrodynamic resistance of that plug. An order of magnitude study on these governing terms reveal that these terms are of the same order, implying that they are equally important factors for steering plugs through a Y-junction.

3.2.2 Connecting channels are blocked (by the plug). Once the head of the plug reaches the end of the connecting channels, then fluid flow ceases to exist in the upper channel until the tail of the plug reaches the neck of the junction. In this stage, a very short time in our experiments, the pressure in the syringe connected to the upper channel decreases rapidly as the constant suction of the syringe expands any air in the syringe or results in compliance within the tubes or PDMS. In this regime we can expect a rapid rise in the required P_{ARP} as the length of the plug increases beyond the length of channel over which connecting channels are present.

4 Results and discussion

It is well known that a long plug will split into two equal sized plugs upon entering a two way junction with equal hydrodynamic resistances.[63] Fig. 3a shows a plug that is split into two at the Y-junction without any acoustic energy applied. This is explained by the equal amount of pressure encountered by the interfaces of the plug (*i.e.* $p_u \approx p_d$). The multiple exposure image shows the symmetric advancement of the interface into the outlet channels (Fig. 3b).

In contrast; by exciting surface acoustic waves, the progression of an interface into either of the branches can be halted and stabilized at the junction as a result of the net acoustic radiation pressure (ARP) induced on the interface itself. This is demonstrated in (Fig. 4a) for the case in which fluid is pumped through the channel with both outlets at atmospheric pressure. As explained in section 3.1, this flow scenario enables variation in the flow rates in each exit channel enabling an expectation that longer plugs can be steered. Indeed it can be seen that actuating the top electrode blocks the upper channel (Fig. 4a) for the full duration of the time

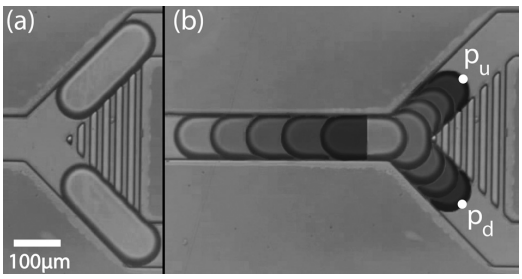

Fig. 3 (a) A plug is split in half in the absence of acoustic actuation and (b) the interfaces equally extend into the outlet channels (multiple exposure image with similar shades at each time frame).

View Article Online

Lab on a Chip Paper

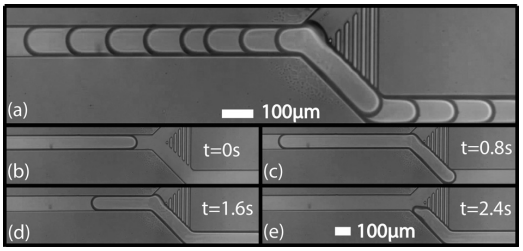

Fig. 4 (a) Multiple exposure image shows the upper interface is halted and stable due to the net acoustic radiation pressure induced on the sound discontinuity interface (upper set of electrodes are actuated) and (b)–(e) shows time-lapse images of a plug being steered into the lower channel.

required for the plug to completely pass through the junction. Of course, meanwhile the leading interface progresses along the lower channel (Fig. 4c). As a result; a plug with a relatively large volume, here 7.33 nL, can be steered intact, into the desired outlet.

Steering of these large plugs is only possible when both the outlets are open to atmosphere and the fluids are pumped from the inlet ports. For practical purposes, the analysis carried out in the rest of this work focuses on a different case where fluid is withdrawn at equal flow rates from each outlet using syringes mounted on a double syringe pump. This method is likely to be more applicable to situations in which additional manipulations such as merging[43] or additional steering are required further downstream of the Y-junction so a pressure balance across the branches can't be assumed.

The suction induces fluid flow in both outlet channels at all times and therefore restricts the maximum volume of the plug that can be steered. When both outlets are open to the atmosphere, a scenario involving absence of flow in one of the channels is possible. However when suction is present, this is not the case. The connecting channels between the two branches are designed to allow the carrier medium to flow from the branch into which the plug is steered to the other branch allowing an equal flow condition in both branches to be maintained until the connecting channels are blocked.

The effect of the connecting channels can be observed by analyzing a series of multiple exposure images. Initially, under the influence of the acoustic waves, the interface is observed to be held in a stable location (Fig. 5(a)) up until the head of the plug blocks the last available connecting channel. At this point, the stability of the interface is quickly lost. The syringe pump connected to the upper channel seeks to extract fluid continuously and as a result the interface is drawn, against the resistance of the acoustic forces, into the lower branch (Fig. 5(b)).

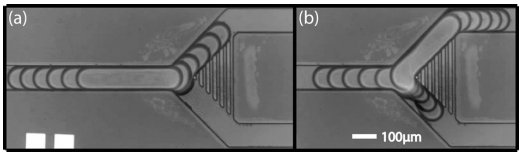

Fig. 5 (a) Multiple exposure images showing interface deformation before and (b) after the connecting channels are blocked while a plug is being steered into the upper channel. Ultimately the plug splits into two parts.

The time-lapse images of a plug during successful steering are shown in Fig. 6. As the plug reaches the Y-junction, it preferentially follows the upper channel due to the additional acoustic pressure applied to the interface *via* the impinging SAWs from below (Fig. 6b). It can be observed that the plug does not bulge into the bottom channel until it totally blocks the connecting channels (Fig. 6c). When the connecting channels are free, oil passes from the upper branch to the lower one such that a constant flow is maintained in both outlets and allowing, with the assistance of the acoustic radiation pressure, a stable interface at the entrance to the lower channel. However, when the plug blocks the connecting channels, the pressure starts to decrease in the lower channel (as a result of the absence of flow) and the interface at the junction of this lower channel starts to advance (Fig. 6d). The plug progresses in the lower channel and develops a finger until an opening, "tunnel", forms as the tail end of the plug reaches the junction (Fig. 6e) allowing oil flow into the lower channel. Below a certain finger length, interfacial tension can draw the plug back into the upper channel and to its minimum energy state (Fig. 6f) leading to successful steering. If the finger extends further into the channel, the plug ultimately splits, this limits the maximum volume of a plug that could be steered under these conditions.

The break-up of a plug encountering a Y-junction without connecting channels has previously been studied in the absence of surface acoustic waves by Ménétrier-Deremble and Tabeling.[62] They analyzed various Y-junctions for plug break-up and concluded that there's a critical finger length

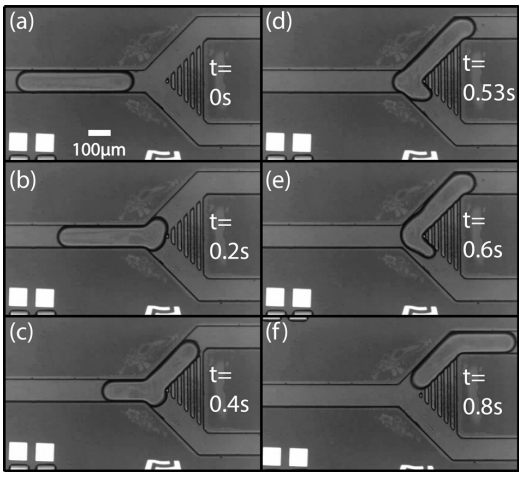

Fig. 6 (a)–(f) Timelapse images of a plug during steering when the lower electrodes are actuated. (d), (e) The plug develops a finger into the bottom channel and (f) the finger retracts due to interfacial tension.

beyond which the plug can't retract and prevent break up into two separate plugs (one in each channel). Indeed, in the system presented here, if the plug was longer than the one shown, the tail of the droplet would be further upstream in Fig. 6d, delaying the possibility of a tunnel forming, and as such the interface would progress further into the lower channel eventually causing the plug to split.

Moreover, if we analyze plug steering at various acoustic powers; we can see that the development of the finger (formed by the movement of the interface into the undesired channel) is postponed as we switch from low to high acoustic energy (Fig. 7). Higher acoustic energy induces a higher ARP on the interface and thus compensates for the decreasing pressure at the upper channel whereas lower ARP is unable to restrain the interface sufficiently and the plug develops a longer finger into the upper channel which eventually leads to the break-up of the plug (in both the low and medium power cases shown).

We further use this to our advantage by manipulating the applied electrical input power to control how much the plugs split. In Fig. 8, the volume ratio (MAX(V_1, V_2)/(V_1 + V_2)), where V is the volume of the daughter plugs, is shown with respect to the applied input power. It can be seen that for plugs of 2.35 nL mean volume (relative standard deviation (RSD) = %20.2) and 980 μm s^{-1} mean velocity (RSD = %21.6), the splitting ratio increases as the applied power increases. This is because of the elevated net acoustic radiation pressure applied on the interface. It's able to hold the interface for a longer period of time allowing the size of the steered daughter plugs to increase up to a point where the plug is completely steered into the desired branch. With this; an incoming plug could be split in half, split into two uneven plugs controllably or steered into one of the channels as a whole on demand. This offers great potential beyond the plug steering method. It should be noted here that the proposed system was designed for steering plugs as a whole; splitting plugs with control was a by-product which we will seek to improve in the future to offer more accuracy, currently the split plug volume variance at a specified power level is at most 15%. This is due to the fact that the plug can stretch a lot before it splits therefore even the slightest hydrodynamic imbalance in the outlet channels results in discrepancies in the split plug volume.

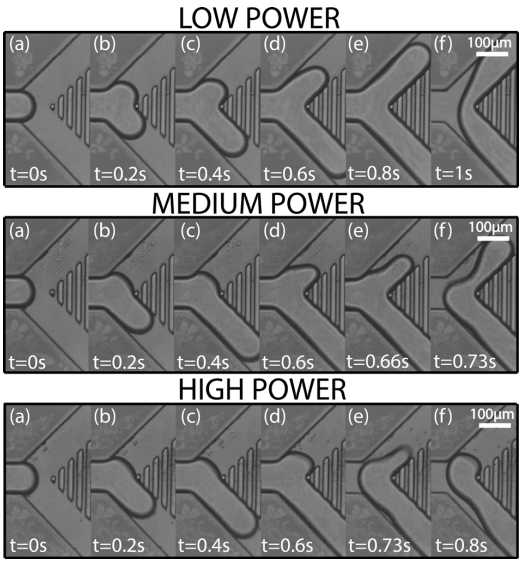

Fig. 7 (a)–(f) Timelapse images of the interface deformation at low (140 mW), medium (225 mW) and high (285 mW) power values for plugs of similar volume and velocity. Note that the actuation is applied from the upper electrodes and the images are not time synchronized.

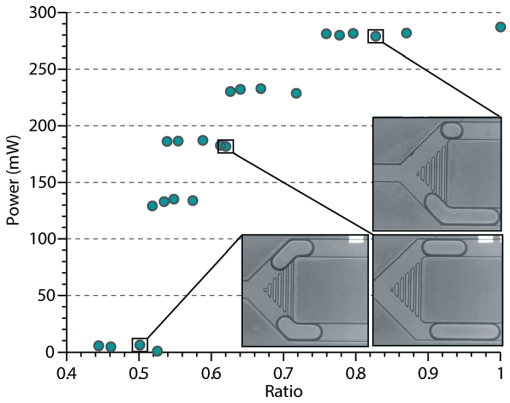

Fig. 8 Plot showing the volume ratio (MAX(V_1, V_2)/(V_1 + V_2)) of two daughter plugs at a given power level. The insets show the split daughter plugs at different ratios.

Thus far, we have examined the nature of the control which can be gained by SAW on the behavior of the plug interfaces at the junction and the various resultant outcomes in terms of steering or plug break-up. We will now examine the key parameters governing this process, namely the plug volume, velocity and the applied electrical power. We have gathered data over a range of plug sizes and velocities by altering the flow conditions imposed by the three syringe pumps (one on the oil inlet, and one on each of the two outlets). The reported plug velocity and volume values are measured using the DMV video analysis software,[51] whereas the power input and $S11$ values were extracted from the signal generator, PowerSAW.

In order to characterize how these parameters influence the steering process, we first plot the maximum plug volume that can be steered by different electrical power inputs (Fig. 9a) for a subset of data exhibiting relatively low plug velocity variance (mean velocity of 1007 μm s^{-1} and relative standard deviation (RSD) of %17.7), hence restricting the effect of this variable to a minimum. Applying a linear fit to this data; we get an approximating function for correlating plug volume and required power input with an R-squared value of 96.8. This fitted line is later used to remove the effect of plug volume from our data set in Fig. 9b.

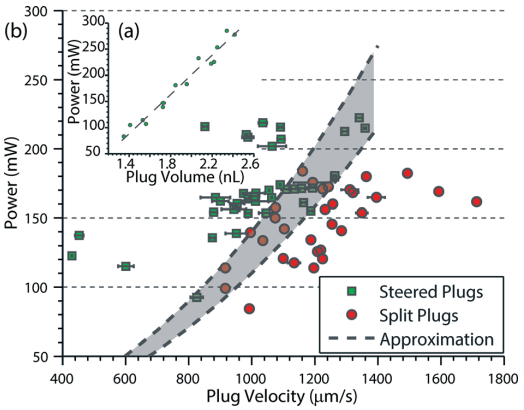

Fig. 9 (a) Maximum plug volume with a mean velocity of 1007 μm s^{-1} that can be steered by the applied electrical power input. (b) The successful steering (square markers) and splitting (circle markers) of a plug at the given power input and plug velocity for droplets ranging from 1.5 nL to 2 nL. The data points were normalized with respect to plug volume (1.69 nL) using the linear interpolation function obtained from inset (a).

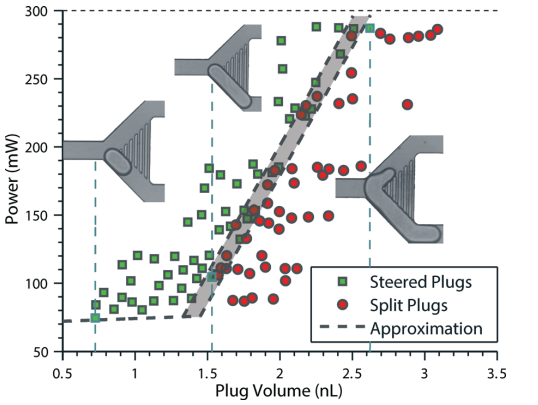

Fig. 10 The power required to steer a plug with a mean velocity of 988 μm s^{-1} and associated volume. Square markers identify plugs that were successfully steered as a whole whereas the circle markers are for plugs that split. The insets provide visuals for different plug volumes corresponding to the highlighted data points and dashed lines.

For each data point in Fig. 9b, the velocity is plotted against the power, the power being first normalized based on the plug volume using the linear fit function obtained from Fig. 9a. Across the data set, two outcomes can occur, steering or splitting of the plugs; the former are displayed as green square markers, whereas the latter are depicted using red circular markers. The error bars shown are standard deviations of the measured velocities calculated by the DMV software.[51]

It can be seen that three regions emerge from the scatter plot; one in which steering successfully takes place, one where the plugs split and the intersection of these regions is the transition region where steering is not always successful. This is attributed to the slight hydrodynamic resistance variance in the outlet channels. Clearly as the velocity of a plug approaching the junction increases, the acoustic energy required to stabilize its interface and steer it also increases. From the previous analysis, if equal hydrodynamic resistance in both channels is assumed, the required acoustic radiation pressure increases proportional to the mean flow velocity (*i.e.* $P_{ARP} \propto U_m$) (eqn (9)). The input electrical energy (P_e), on the other hand, is proportional to the acoustic radiation pressure induced in the working fluids, squared[43] (*i.e.* $P_e \propto P_{ARP}^2$) which leads to a square relationship between electrical power input and the plug velocity. For this reason, the boundaries of the transition region between steering and splitting (Fig. 9b) have been marked by using two approximating functions of the form $P_e = A_i U_m^2$ where A_i is a constant value selected to identify the upper and lower bounds of the transition region.

The final set of data, Fig. 10 shows the required power as a function of plug volume. Again to remove the effect of the third variable, in this case the velocity of the plug, the power has been normalized, here by using the fitted curves in Fig. 9 (it can be seen in Fig. 10 that the data tends to sit in different power bands, each band is a different power tested, the height of each band gives an idea of the modest change this normalization step makes). Specifically, the slope of these curves was used to perform a linear interpolation for the power input values relative to a band of plug velocity values (mean = 988 μm s^{-1}, RSD = %26.8). The results are plotted in Fig. 10 where, again, the green square markers identify plugs that were steered as a whole and the red circular markers are for plugs that split. The insets provide images for various plug volumes in the dataset so that the length of the plugs can be visually compared with the length of the channel over which the connecting channels are present.

At low volumes all the plugs steer even at low power inputs, however once the volume is increased such that the plug is long enough (≈1.5 nL) to block all the connecting channels, an intact plug can no longer be steered without substantially increasing the power. This clearly demonstrates the role the connecting channels play, and ties in with the description of the pressure characteristics in the channels given above. For larger plug volumes, the interface at the entrance to the undesired channel becomes harder to stabilize due to the suction of the syringe pump attached to that channel, thus necessitating a significant increase in power.

A transition region where some plugs are successfully steered and some are split is also shown in Fig. 10. This is attributed to the hydrodynamic inequalities in the outlet channels. The largest plug (≈2.62 nL) that was successfully steered (see inset of Fig. 10) was limited by the design of the connecting channels, however, having established the functionality of the connecting channels, it is clear that it is possible to steer plugs of larger volume by increasing the number of connecting channels after the Y-junction. The smallest plug that was steered, on the other hand, was simply limited

by the droplet generating T-junction geometry which could easily be modified to produce smaller plugs or droplets.

5 Conclusion

We present a novel microfluidic lab on a chip device that is able to steer plugs of 0.75 nL to 2.62 nL volume into the desired branch of a specially designed Y-junction. Focused surface acoustic waves act on the interface of water-in-oil plugs which results in a net acoustic radiation pressure applied at the interface. This pressure deforms the interface and forces plugs to steer into the selected branches of the Y-junction. We thoroughly characterize the system and establish operating regions for the successful steering of plugs with various volume and velocities. In addition, the splitting of the plugs could be modulated to produce daughter plugs of desired volume; this offers additional versatility to our plug steering method. The proposed design could be useful in droplet microfluidic systems where active sorting of plugs is required. Surface acoustic wave generating IDTs are easily integrated onto existing lab on a chip devices and can be coupled with other droplet microfluidic manipulation methods like merging, mixing and dilution.

References

1 A. Theberge, F. Courtois, Y. Schaerli, M. Fischlechner, C. Abell, F. Hollfelder and W. Huck, *Angew. Chem., Int. Ed.*, 2010, **49**, 5846–5868.
2 G. M. Whitesides, *Nature*, 2006, **442**, 368–373.
3 F. F. Becker, X.-B. Wang, Y. Huang, R. Pethig, J. Vykoukal and P. Gascoyne, *Proc. Natl. Acad. Sci. U. S. A.*, 1995, **92**, 860–864.
4 N. M. Toriello, E. S. Douglas and R. A. Mathies, *Anal. Chem.*, 2005, **77**, 6935–6941.
5 H.-S. Moon, K. Kwon, S.-I. Kim, H. Han, J. Sohn, S. Lee and H.-I. Jung, *Lab Chip*, 2011, **11**, 1118–1125.
6 T. P. Forbes and S. P. Forry, *Lab Chip*, 2012, **12**, 1471–1479.
7 A. H. C. Ng, K. Choi, R. P. Luoma, J. M. Robinson and A. R. Wheeler, *Anal. Chem.*, 2012, **84**, 8805–8812.
8 A. Chen, T. Byvank, W.-J. Chang, A. Bharde, G. Vieira, B. L. Miller, J. J. Chalmers, R. Bashir and R. Sooryakumar, *Lab Chip*, 2013, **13**, 1172–1181.
9 M. Madou, J. Zoval, G. Jia, H. Kido, J. Kim and N. Kim, *Annu. Rev. Biomed. Eng.*, 2006, **8**, 601–628.
10 P. Rogers and A. Neild, *Lab Chip*, 2011, **11**, 3710–3715.
11 P. Rogers, I. Gralinski, C. Galtry and A. Neild, *Microfluid. Nanofluid.*, 2013, **14**, 469–477.
12 C. Devendran, I. Gralinski and A. Neild, *Microfluid. Nanofluid.*, 2014, **17**, 879–890.
13 R. Walker, I. Gralinski, K. Keong Lay, T. Alan and A. Neild, *Appl. Phys. Lett.*, 2012, **101**, 163504.
14 P. Agrawal, P. S. Gandhi and A. Neild, *J. Appl. Phys.*, 2013, **114**, 114904.
15 X. Niu, F. Gielen, J. B. Edel and A. J. deMello, *Nat. Chem.*, 2011, **3**, 437–442.
16 X. Niu, S. Gulati and J. Edel, *et al.*, *Lab Chip*, 2008, **8**, 1837–1841.
17 P. Abbyad, R. Dangla, A. Alexandrou and C. N. Baroud, *Lab Chip*, 2011, **11**, 813–821.
18 A. Huebner, D. Bratton, G. Whyte, M. Yang, A. J. deMello, C. Abell and F. Hollfelder, *Lab Chip*, 2009, **9**, 692–698.
19 K. Ahn, C. Kerbage, T. P. Hunt, R. M. Westervelt, D. R. Link and D. A. Weitz, *Appl. Phys. Lett.*, 2006, **88**, 024104.
20 J. J. Agresti, E. Antipov, A. R. Abate, K. Ahn, A. C. Rowat, J.-C. Baret, M. Marquez, A. M. Klibanov, A. D. Griffiths and D. A. Weitz, *Proc. Natl. Acad. Sci. U. S. A.*, 2010, **107**, 4004–4009.
21 D. R. Link, E. Grasland-Mongrain, A. Duri, F. Sarrazin, Z. Cheng, G. Cristobal, M. Marquez and D. A. Weitz, *Angew. Chem., Int. Ed.*, 2006, **45**, 2556–2560.
22 C. Priest, S. Herminghaus and R. Seemann, *Appl. Phys. Lett.*, 2006, **89**, 134101.
23 W. Wang, C. Yang and C. M. Li, *Lab Chip*, 2009, **9**, 1504–1506.
24 K. Ahn, J. Agresti, H. Chong, M. Marquez and D. A. Weitz, *Appl. Phys. Lett.*, 2006, **88**, 264105.
25 Z. Z. Chong, S. B. Tor, N. H. Loh, T. N. Wong, A. M. Ganan-Calvo, S. H. Tan and N.-T. Nguyen, *Lab Chip*, 2015, **15**, 996–999.
26 X. Ding, P. Li, S.-C. S. Lin, Z. S. Stratton, N. Nama, F. Guo, D. Slotcavage, X. Mao, J. Shi, F. Costanzo and T. J. Huang, *Lab Chip*, 2013, **13**, 3626–3649.
27 R. M. White and F. W. Voltmer, *Appl. Phys. Lett.*, 1965, **7**, 314–316.
28 P. R. Rogers, J. R. Friend and L. Y. Yeo, *Lab Chip*, 2010, **10**, 2979–2985.
29 D. J. Collins, T. Alan and A. Neild, *Appl. Phys. Lett.*, 2014, **105**, 033509.
30 X. Ding, S.-C. S. Lin, M. I. Lapsley, S. Li, X. Guo, C. Y. Chan, I.-K. Chiang, L. Wang, J. P. McCoy and T. J. Huang, *Lab Chip*, 2012, **12**, 4228–4231.
31 X. Ding, Z. Peng, S.-C. S. Lin, M. Geri, S. Li, P. Li, Y. Chen, M. Dao, S. Suresh and T. J. Huang, *Proc. Natl. Acad. Sci. U. S. A.*, 2014, **111**, 12992–12997.
32 G. Destgeer, K. H. Lee, J. H. Jung, A. Alazzam and H. J. Sung, *Lab Chip*, 2013, **13**, 4210–4216.
33 D. J. Collins, T. Alan and A. Neild, *Lab Chip*, 2014, **14**, 1595–1603.
34 A. Qi, L. Y. Yeo and J. R. Friend, *Phys. Fluids*, 2008, **20**, 074103 (1994–present).
35 S. R. Heron, R. Wilson, S. A. Shaffer, D. R. Goodlett and J. M. Cooper, *Anal. Chem.*, 2010, **82**, 3985–3989.
36 P. Brunet, M. Baudoin, O. B. Matar and F. Zoueshtiagh, *Phys. Rev. E: Stat., Nonlinear, Soft Matter Phys.*, 2010, **81**, 036315.
37 N. Sivanantha, C. Ma, D. J. Collins, M. Sesen, J. Brenker, R. L. Coppel, A. Neild and T. Alan, *Appl. Phys. Lett.*, 2014, **105**, 103704.
38 T. Franke, S. Braunmuller, L. Schmid, A. Wixforth and D. A. Weitz, *Lab Chip*, 2010, **10**, 789–794.
39 F. Guo, P. Li, J. B. French, Z. Mao, H. Zhao, S. Li, N. Nama, J. R. Fick, S. J. Benkovic and T. J. Huang, *Proc. Natl. Acad. Sci. U. S. A.*, 2015, **112**, 43–48.

40 Q. Zeng, F. Guo, L. Yao, H. Zhu, L. Zheng, Z. Guo, W. Liu, Y. Chen, S. Guo and X. Zhao, *Sens. Actuators, B*, 2011, **160**, 1552–1556.
41 L. Schmid and T. Franke, *Lab Chip*, 2013, **13**, 1691–1694.
42 D. J. Collins, T. Alan, K. Helmerson and A. Neild, *Lab Chip*, 2013, **13**, 3225–3231.
43 M. Sesen, T. Alan and A. Neild, *Lab Chip*, 2014, **14**, 3325–3333.
44 T. Franke, A. R. Abate, D. A. Weitz and A. Wixforth, *Lab Chip*, 2009, **9**, 2625–2627.
45 S. Li, X. Ding, F. Guo, Y. Chen, M. I. Lapsley, S.-C. S. Lin, L. Wang, J. P. McCoy, C. E. Cameron and T. J. Huang, *Anal. Chem.*, 2013, **85**, 5468–5474.
46 G. Hertz and H. Mende, *Z. Phys.*, 1939, **114**, 354–367.
47 B. Issenmann, A. Nicolas, R. Wunenburger, S. Manneville and J.-P. Delville, *EPL*, 2008, **83**, 34002.
48 L. Johansson, S. Johansson, F. Nikolajeff and S. Thorslund, *Lab Chip*, 2009, **9**, 297–304.
49 T. Thorsen, F. H. Roberts, F. H. Arnold and S. R. Quake, *Phys. Rev. Lett.*, 2001, **86**, 4163–4166.
50 M. Rhee, Y. K. Light, S. Yilmaz, P. D. Adams, D. Saxena, R. J. Meagher and A. K. Singh, *Lab Chip*, 2014, **14**, 4533–4539.
51 A. S. Basu, *Lab Chip*, 2013, **13**, 1892–1901.
52 R. Shilton, M. K. Tan, L. Y. Yeo and J. R. Friend, *J. Appl. Phys.*, 2008, **104**, 014910.
53 M. K. Tan, J. R. Friend and L. Y. Yeo, *Phys. Rev. Lett.*, 2009, **103**, 024501.
54 G. Destgeer, B. H. Ha, J. H. Jung and H. J. Sung, *Lab Chip*, 2014, **14**, 4665–4672.
55 G. Destgeer, S. Im, B. Hang Ha, J. Ho Jung, M. Ahmad Ansari and H. Jin Sung, *Appl. Phys. Lett.*, 2014, **104**, 023506.
56 W. Nyborg, *Phys. Acoust.*, 1965, **2**, 265.
57 J. Shi, X. Mao, D. Ahmed, A. Colletti and T. J. Huang, *Lab Chip*, 2008, **8**, 221–223.
58 L. V. King, Proceedings of the Royal Society of London, *Proc. R. Ir. Acad., Sect. A*, 1934, **147**, 212–240.
59 K. Yosioka, *Acustica*, 1955, **5**, 167–173.
60 F. E. Borgnis, *Rev. Mod. Phys.*, 1953, **25**, 653–664.
61 J. Kirshner and S. Katz, *Design Theory of Fluidic Components*, Academic Press, New York, 1975.
62 L. Ménétrier-Deremble and P. Tabeling, *Phys. Rev. E: Stat., Nonlinear, Soft Matter Phys.*, 2006, **74**, 035303.
63 D. N. Adamson, D. Mustafi, J. X. J. Zhang, B. Zheng and R. F. Ismagilov, *Lab Chip*, 2006, **6**, 1178–1186.
64 M. Schindler and A. Ajdari, *Phys. Rev. Lett.*, 2008, **100**, 044501.

Chapter 6

Towards an Ordered Library of Droplets: Plug Sensing, Splitting and Merging using Surface Acoustic Waves

6.1 Overview

The previous systems are further improved in this chapter and an automated microfluidic system capable of sensing, splitting, merging and mixing droplets is presented. The sensing is achieved by using capacitive electrodes which can communicate with a computer via a microchip and a microcontroller board. The processed signal is used to accurately time the arrival of a plug at a T-junction by-pass channel where it could be split by actuating SAW generating inter-digital transducers (IDTs) to induce acoustic streaming. Once the plug is split, it could be trapped in a hydrodynamic merging chamber until other plugs are split. Once more daughter droplets reach the merging chamber and coalesce beyond a certain volume, they exit the merging chamber and go through a serpentine channel which facilitates chaotic mixing of the merged droplet.

Previous work on droplet splitting utilises passive methods which do not offer any control over the splitting except for the predetermined specifications; with the presented technique, the users can control the final split volume as well as its content which can be used to perform a combinatorial study.

In this chapter; an extensive review of droplet sensing and splitting methods as well as high throughput screening, fabrication and working principle of the proposed device are presented. This is followed by thorough characterisation of the system via detailed analysis of experimental results and discussion. The proposed automated droplet manipulation can easily be scaled or integrated to existing LOC devices, it offers a robust and contamination-free plug splitting technique in closed microchannels that can be used with screening studies in an attempt to find the desired chemical reaction.

6.2 Publication

The following manuscript is in preparation and expected to be submitted to *Lab on a Chip*. It has been formatted according to *Royal Society of Chemistry* guidelines.

Monash University

Declaration for Thesis Chapter 6
Declaration by candidate

In the case of Chapter 6, the nature and extent of my contribution to the work was the following:

Nature of contribution	**Extent of contribution**
Design and fabrication of devices, experimentation, development, result analysis, interpretation and writing.	70%

The following co-authors contributed to the work:

Name	**Nature of contribution**	**Extent of contribution**
Citsabehsan Devendran	Numerical analysis, writing	10%
Sean Malikides	Sensor integration, experimentation, writing	10%
Dr. Tuncay Alan	Project Supervision, editing	N/A
Assoc. Prof. Adrian Neild	Project Supervision, editing	N/A

The undersigned hereby certify that the above declaration correctly reflects the nature and extent of the candidate's and co-authors' contributions to this work.

Candidate's Signature: 

Candidate's Name: Muhsincan Sesen

Date: 5th August 2016

Main Supervisor's Signature: 

Main Supervisors's Name: Assoc. Prof. Adrian Neild

Date: 5th August 2016

CREATED USING THE RSC LaTeX PCCP ARTICLE TEMPLATE – SEE www.rsc.org/electronicfiles FOR DETAILS

ARTICLE TYPE www. rsc.org/xxxxxx | XXXXXXXX

Towards an ordered library of droplets: Plug sensing, splitting and merging using surface acoustic waves †

Muhsincan Sesen,[a] Citsabehsan Devendran,[a] Sean Malikides,[a] Tuncay Alan,[a] and Adrian Neild,*[a]

Received Xth XXXXXXXXXX 20XX, Accepted Xth XXXXXXXXX 20XX

First published on the web Xth XXXXXXXXXX 200X

DOI: 10.1039/b000000x

Exhaustive analytical studies can be carried out in rapid succession within microfluidic devices when aqueous droplets are dispersed in a carrier fluid. Droplet microfluidics offers chemical and physical isolation of droplets whereby, every single droplet can be identified as individual reaction chamber. Mono-disperse droplet formation and further manipulation capabilities allows a multitude of studies to be carried out with these systems. Here we present an on-demand method of generating required libraries of droplets with distinct and adjustable volumes. The droplets are first sensed by a capacitive sensor so that they can be split on-demand at a T-junction using surface acoustic waves (SAWs). SAWs couple into a fluid medium at a Rayleigh angle inducing acoustic streaming that drives the carrier fluid in the by-pass channel. The by-pass loop is designed to have higher resistance ensuring the droplets are unaffected without actuation, however, when actuated, the incoming droplet in the main channel is drawn into the by-pass channel arising from the resultant pressure gradient. Careful consideration of various parameters enable good control and flexibility in splitting the incoming droplets precisely. A range of parameters determine the final split daughter droplet volume and are thoroughly characterized by experiments and simulations. Furthermore, it is demonstrated that the split droplets are trapped and merged with a second split droplet to produce a combinatorial library. The proposed system enables ease of integration with existing lab-on-a-chip systems as well as offering a robust and contamination-free droplet manipulation technique in closed microchannels leading to potential implementation in screening studies.

1 Introduction

High throughput screening (HTS) has been a widely used method for early drug screening studies carried out by pharmaceutical companies. HTS is an empirical method which exhaustively tests disease-carrying targets (i.e cells and proteins) against a library of compounds yielding millions of combinations in the hunt for a positive match. HTS has recently played a key role in the discovery of drugs to combat diabetes, cancer and HIV[1]. Typically, HTS reactions are conducted in microtiter plates containing a matrix of wells; reagents are loaded onto the plates by pipettes integrated to robotic arms; the analysis (i.e mixing, dilution, detection) necessitates the utilization of bulky and expensive equipment. Miniaturization of these wells, driven by the need for higher throughput (reduced reaction times) and lower reagent costs (reduced volumes), has reached limits imposed by the accuracy of robotic dispensing and evaporation in such open systems[2,3].

Lab on a chip (LOC) devices, specifically digital microfluidic devices, where droplets are dispersed in a carrier medium, could potentially revolutionize HTS technology[3–5] since they offer ultra miniaturization with increased throughputs, lower costs and single-cell analysis capabilities without any moving parts. Moreover, they are not prone to issues related to evaporation and are compatible with sub-nanoliter volumes[6]. Microfluidic HTS (μHTS) also offer higher precision compared to standard microplate based techniques as droplet operations are rapidly characterized and controlled with minimal errors[3].

Although droplet based microfluidics offers many advantages over standard microplate based techniques, there still exists a number of shortcomings associated with this paradigm shift. While liquids in open systems are handled by automated dispensing pumps, mixed by large shakers and diluted by solutions prepared in advance, the manipulation of droplets in microfluidic systems poses a great challenge given the fact that microfluidic systems are enclosed, planar and driven by continuous flow at higher throughputs. A key challenge, that is yet to be resolved, is the ordered formation of an m by n matrix of droplets. Creating a more accurate replica of the multi-well plate within closed microfluidic systems lies at the heart of this long-awaited paradigm shift towards μHTS.

The formation of a 1 by n vector of droplets has been accomplished by using a pre-loaded droplet to form a concentration gradient amongst daughter droplets[7] and by using robotic setups to reposition the fluid inlet of the device so that

† Electronic Supplementary Information (ESI) available: [details of any supplementary information available should be included here]. See DOI: 10.1039/b000000x/

[a]*Department of Mechanical and Aerospace Engineering, Monash University, Clayton, VIC 3800, Australia. E-mail: adrian.neild@monash.edu; Tel: +61 3 990 54655*

plugs of desired chemical content could be siphoned in a programmable manner[8,9], referred to as a Serial Sample Loading (SSL) system[8] within the manuscript. A vector of droplets were also realized on parallel channels wihtin a multi-layered microfluidic device[10] as well as using a PEEK cross to collect different droplets streams into a single container[11].

Nevertheless, creating an m by n matrix of droplets remains a major challenge. Theberge *et al.*[11] proposed to merge reagent droplets created by an SSL system with various sample droplets dispersed in a container to form such a matrix in an unordered manner. Zec *et al.*[8] reports the formation of an ordered droplet matrix by forming the initial vector using an in-house built SSL system and crossing them with droplets from multiple secondary inlets alternated by valves via pneumatic PDMS deformation.

To this end, a method to extract a droplet from a plug into a secondary channel on demand using surface acoustic waves (SAWs) is proposed. Plugs generated by an SSL system are detected with a capacitive sensor and SAWs are programmed to be excited as required (e.g every 5 plugs) leading to droplet extraction of a known volume. This method would allow splitting of multiple incoming droplets of different constituents that can later be hydrodynamically merged in the secondary channel to form a new droplet composing of a mixture of two or more constituents with specified concentrations. This can then be extended by replicating and integrating the design multiple times in a single chip, resulting in a droplet matrix of desired individual content.

This approach is mainly based on two major techniques; the sensing and manipulation of droplets in microfluidic channels. In regards to droplet sensing within closed microfluidic channels, two primary methods exist; optical and electrical detection. Optical methods include droplet detection based on fluorescence intensity[12,13], light intensity[14], droplet-light coupling leading to whispering gallery mode resonances[15] and photodiode sensing[16,17]. While optical detection can achieve high throughputs, it usually requires expensive and bulky equipment to operate. Electrical detection, on the other hand, can be achieved with electrodes integrated on a chip. Some examples of electrical detection are microwave sensing[18], multiplexed electrical sensing[19], conductive sensing[20] and capacitive sensing[21–24]. Resistive and conductive methods offer superior sensitivity but require contact with the droplets in which case cross-contamination can be an issue. In contrast, capacitive sensors are fabricated with the use of a passivation layer, therefore, eradicating issues associated with cross-contamination at the expense of sensitivity.

In the proposed design, methods from Elbuken *et al.*'s capacitive sensor[22] were adopted due to their robustness, ease of integration and readily available, affordable components. The fabrication techniques were slightly altered to improve compatibility with existing SAW inducing inter-digital transducer (IDT) fabrication methods.

The second major technique used in this paper is the manipulation of droplets and plugs (active and passive). Passive techniques exploit hydrodynamic forces and are usually able to yield faster throughputs whilst active techniques work with a number of different forcing mechanisms and can offer programmability enabling on demand actuation. In the former context; droplet generation[25,26], trapping[27–31], splitting[32,33], dilution[7], merging[34,35] and mixing[36] have successfully been demonstrated.

On the other hand, active methods such as electric forces have been used for trapping and merging droplets in microfluidic chambers[37,38], for sorting droplets[12,39,40] and inducing electrocoalescence of adjacent droplets[41,42]. Mechanical forces (PDMS membrane deformation) have been used to generate, trap and fuse droplets[43,44]. Bulk acoustic waves (BAWs) have been used to manipulate[45], trap and sort droplets (CITE VAN) whereas SAWs have been used to generate[46], merge[47] and sort droplets[48,49]. Furthermore; plug steering, splitting[50] and break-up[51] has been demonstrated with SAWs.

Despite the implementation of acoustics in digital microfluidics are relatively recent and therefore limited, it's been extensively used in the broader field of microfluidics[52,53]. For example, BAWs find numerous applications in particle and/or cell manipulation[54–57], separation[58–60], trapping[61–63] and washing[64] as well as microfluidic mixing[65–67]. SAWs have also been used for manipulating cells[68–70], microfluidic pumping[71]; particle concentration[72–74], trajectory control[75,76] and sorting[77–79].

Here, we present a microfluidic platform capable of splitting a plug on-demand for further manipulation and observation. The system utilizes acoustic forces, is well characterized and modular; therefore, allowing ease of modification to suit system requirements. Moreover, it is capable of generating an ordered droplet matrix while making use of readily available and affordable components without the need for moving parts or a microscope.

The proposed system initially detects an incoming plug with a capacitive sensor; thereafter the IDTs are programmed to excite SAWs, along a secondary channel, which couple into the continuous phase and induce acoustic streaming to augment the flow in the secondary channel. This results in a pressure drop in the secondary channel that draws part of the main plug in. Depending on the duration of the applied SAWs, various size droplets can be extracted from the main plug. The split droplet travels into the secondary channel and gets trapped in a passive merging chamber adapted from Niu *et al.*'s[35] previous work. The trapped droplet remains in the merging chamber until a second split droplet comes into contact and coalescence takes place.

In this paper, detailed experimental and numerical analysis on the underlying physics of droplet splitting are presented

considering the effect of SAW excitation duration and amplitude. Finally, the influence of the initial plug size along with geometrical limitations and possible improvements are discussed. The proposed system can easily be adopted and optimized for numerous biological and chemical studies.

2 Working Principle

Surface acoustic waves (SAWs) are generated by applying an alternating current (AC) on micro-fabricated electrodes patterned on a piezoelectric substrate. These electrode pairs are designed to be equidistant and are known as inter-digital transducers (IDTs). When the IDTs are interfaced with a specific frequency AC signal, they electromechanically couple with the piezoelectric substrate, resulting in a mechanical displacement emanating from one set of finger pair, which in turn is reinforced by a neighboring pair, resulting in maximized displacements known as traveling SAWs (TSAWs). SAWs are mechanical (Rayleigh type) surface waves exhibiting amplitudes of a few nanometers oscillating at MHz frequencies. They are energy efficient, bio-compatible[80] and easily integrable with microfluidic systems; additionally they offer contact-free and portable manipulation.

A set of focused IDTs (FIDTs) with a wavelength of 30 µm were utilized in this study. FIDTs are a specific type of IDTs which concentrates the acoustic energy along a narrow band such as the 50 µm wide by-pass channel used in this study. The FIDTs, patterned onto lithium niobate, $LiNbO_3$ (LN) substrate were excited with an AC signal of 122 MHz frequency resulting in TSAWs which coupled into the continuous medium inducing acoustic streaming.

A streaming flow in the direction of SAW propagation arises when SAWs encounter a fluid body, refract with a Rayleigh angle and attenuate due to viscous dissipation. The Rayleigh angle is given by $\sigma_R = sin^{-1} c_l/c_s$ where c_l and c_s are the speed of sound in the liquid medium and the substrate, respectively. The exponential decay of the SAWs leads to a strong gradient formed in the liquid which results in steady streaming, called acoustic streaming. Acoustic streaming has been studied extensively in the field of non-linear acoustics[81–83]. Acoustic streaming induced by SAWs lead to widespread usage in microfluidics such as mixing[84], micropumping[71,85], droplet translation[86] and sorting[48].

In the context of this study, two important aspects of acoustic streaming will be considered. Firstly; when SAWs couple into the fluid medium, they generate pressure waves that rapidly decay as the SAWs attenuate. This leads to a significant pressure gradient along the direction of propagation which drives a steady fluid flow from high pressure to low pressure zones (denoted P_1 and P_2 in figure 1, respectively). Secondly, it is without doubt that this high pressure point, P_1, needs to be fed with a liquid medium in order to satisfy continuity and sustain the steady streaming. Inevitably, this feed is supplied from the main channel in the proposed design (Fig. 1) and draws fluid from the main channel at the entrance of the by-pass loop. This is the underlying mechanism used to split plugs within this study.

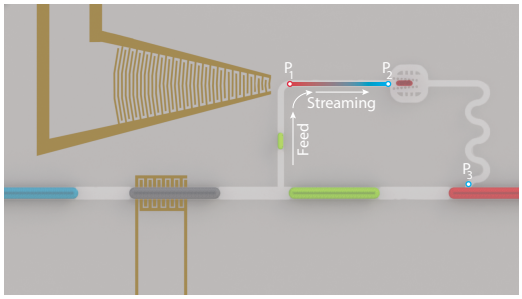

Fig. 1 Working principle

When a plug interface is present at the T-junction and the IDTs are actuated, the feed draws the interface further into the by-pass channel, eventually splitting a controlled volume from the main plug. The extent of splitting depends on a number of parameters such as the duration and amplitude of the applied electrical pulse, plug velocity, outlet pressure (P_3 in figure 1), plug volume and position at the onset of actuation. The effects of these parameters will be analyzed and discussed in section 4 where accurate control of final split volume is demonstrated.

Understanding these parameters enable good control and flexibility that render the proposed method highly integrable and applicable in numerous different microfluidics based systems. For example, a volume dependent study could be carried out by looking at how samples and reagents react given a set of varying initial volumes. Furthermore, a range of sample-reagent combinations could be mixed and analysed in the search for an optimum combination.

3 Methods

3.1 Experimental Methods

3.1.1 Fabrication

The proposed chip is comprised of the capacitive sensor, the IDTs and fluid confining channels. The fabrication techniques used are highly standard and widely used in typical SAW based microfluidic devices[47,50].

Both the sensor and the IDTs are fabricated in the same manner; a masking layer of photoresist was patterned on lithium niobate, $LiNbO_3$ (LN), substrate of 500 µm thickness (single side polished, 128°Y-cut, X-propagating) using stan-

dard lithography techniques. This is followed by, a thin adhesion layer of chromium (10 nm) and 200 nm of aluminium deposition via physical vapor deposition and an additional 250 nm thick layer of silicon dioxide, SiO_2 as a passivation layer. This final layer not only enhances the bond between the LN wafer and polydimethylsiloxane (PDMS) but also shields the electrodes from shorting as well as droplets to prevent cross-contamination. The capacitive electrodes for sensing plugs were adapted from the designs tested and optimized for a fringing field capacitive pH sensor[87].

The channel structure, however, was fabricated using a deep reactive ion etched (DRIE) silicon mold and PDMS. PDMS surface was activated by exposure to air plasma (Harrick Plasma PDC-32G) and bonded to LN chips irreversibly.

3.1.2 Setup

The fabricated microfluidic chip was mounted onto a 3D printed holder (Fig. 2) and positioned beneath a microscope (Olympus BX43, Tokyo, Japan). The holder houses a peltier cooler that regulates the temperature of the chip ensuring uniformity across experiments. Contact pads located on one side of holder are interfaced with an amplifier (AR 25A250A, Amplifier Research) which modulates the output signals from a programmable RF-Synthesizer (HAMEG 8135, HAMEG Instruments GmbH, Germany) controlled by a PC (Fig. 2). The pads on the other side, however, were connected to a capacitive-to-digital converter microchip, AD7746, which has built-in excitation sources and filtering/amplifying circuits[88]. The AD7746 provides two individual measurement channels and the measurement range is reported as ± 4 pF with a precision of 4 fF[22]. The microchip signals were detected with a programmable microcontroller (Arduino Uno R2) and relayed to a PC via USB. A diagram of the experimental setup is shown in figure 2.

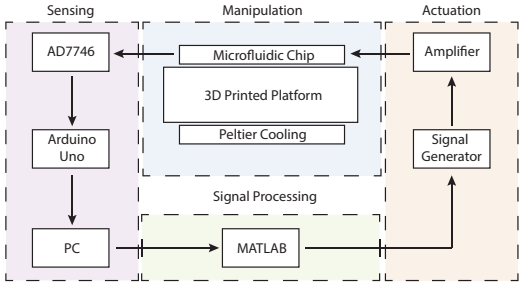

Fig. 2 Schematic diagram of the microfluidic system showing the sensing, signal processing, actuation and manipulation cycle.

An in-house built MATLAB GUI was employed to communicate with the capacitive sensors and the RF-Synthesizer (Fig. 2) allowing users to input and alter the required parameters; 'Threshold (T)', 'Droplet Skip (DS)', 'Delay Time (DT)', 'Pulse Time (PT)'and 'Power (P)'. The GUI is programmed such that if the capacitance reading surpasses the defined capacitance T; an RF pulse is triggered every DS number of droplets, after DT has elapsed, for the duration of PT, with power P to generate SAWs. It should be noted that all these parameters can be updated in real-time during experiments. Furthermore, the working code could be easily modified to accommodate more controls or parameters to carry out a specific study.

Microfluidic inlet ports were connected to 100 µL gastight glass syringes (Hamilton Company) through polytetrafluoroethylene (PTFE) tubing. The syringes were driven by Legato 270 syringe pumps (KD Scientific, Inc.). The dispersed phase used was Milli-Q water whilst an engineered fluid (3M™ Novec™ 7500) stabilized by 2% surfactant (PicoSurf™ 1, Sphere Fluidics, UK) was used as the carrier fluid throughout the experiments. An additional 2% surfactant (Pico-Break™, Sphere Fluidics, UK) was introduced to the continuous phase to facilitate droplet merging. This carrier fluid with both surfactants was only used in the showcase study.

The videos and images were recorded by a parfocal microscope camera (5MP, Dino-Lite AM7023B, New Taipei City, Taiwan). In order to carry out the analysis, the videos were processed using "Droplet morphometry and velocimetry"(DMV) software[89]. DMV is a post-processing tool that identifies and tracks droplets/plugs to report properties such as area, velocity, location, etc. Herein, DMV was used to gather size and velocity information about the droplets/plugs using the same settings across the range of recorded videos.

3.2 Numerical Methods

Numerical simulations were developed to understand the underlying physics of the proposed system. A good numerical model representing the physical system allows further investigation into relevant parameters and limitations of the system. In this work, the use of SAWs are proposed to induce acoustic streaming within the top by-pass channel as a result of a pressure gradient generated by the incident traveling surface acoustic wave (TSAW). This pressure gradient is responsible for driving the flow in the by-pass loop, which in turn draws fluid from the main channel in accordance with conservation of mass and therefore, the underlying mechanism responsible for droplet splitting. To illustrate this effect a simplified 2D model capturing the salient features has been developed using COMSOL Multiphysics® 5.0.

To meaningfully represent the system at hand, a laminar two-phase flow, level set module was utilized. The two phases used in the numerical simulations were assigned the corre-

sponding properties of oil (Fluid 1) and water (Fluid 2) as used experimentally. The plugs, exhibiting similar volume as experiments, were generated upstream using a fluid pinch off at a flow focusing junction. The generated plugs then traverse a closed microfluidic channel network integrated with a by-pass loop consistent with experimental designs (Fig. 3).

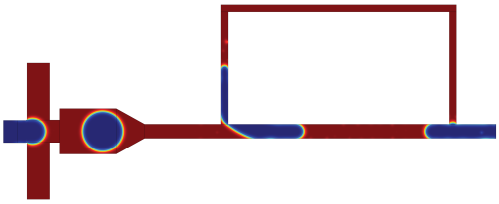

Fig. 3 Numerical model results of a two phase volume fraction plot. Red denotes the oil phase (Fluid 1) whereas the blue regions represent the water phase (Fluid 2).

The oil and water inlets were imposed with corresponding input flow rate boundary conditions required to produce stable droplets. At the exit, downstream, the outlet was set to a zero pressure, no viscous stress boundary condition. It should be noted, experimentally the droplets were produced using a T-junction and not a flow focusing junction. However, the droplet generation method is irrelevant as it does not affect the splitting mechanism at hand. To represent the pressure gradient induced by the SAW, a volume force domain condition was imposed on the upper by-pass channel (i.e horizontal section).

The developed model was used to investigate various parameters such as the duration of the applied volume force (i.e. PT in experiments) and its magnitude analogous to P in experiments. In addition, the effects of the onset of actuation and the existence of a plug blocking the second T-junction are investigated in order to gain insight into the effect it has on the pressure distribution within the by-pass loop, hence, the resultant split droplet size.

The resulting extracted droplet volumes were evaluated using a surface integration function built within COMSOL Multiphysics 5.0. The surface integration of the water phase (i.e. Fluid 2) results in an area that provides information of the extracted droplet volume produced. These results are later compared to the corresponding experimental results obtained from DMV software.

4 Results & Discussion

Extensive experimental and numerical analysis considering the proposed microfluidic platform with a simple by-pass loop (i.e without hydrodynamic merging and mixing) has been conducted to characterize the final split daughter droplet volume. The results of this study will be detailed and discussed in this section.

Firstly, it is noteworthy to mention the important role of the by-pass loop geometry in this study. Although split plugs can be directed to a secondary outlet with a regulated outlet pressure, offering enhanced accuracy, this system implements a closed loop geometry to ensure potential assembly of multiple loops on a single microfluidic chip enabling combinatorial studies as well as rendering this technique modular and easily integrable to existing lab-on-a-chip (LOC) devices.

In the case of a closed loop geometry, the behavior of an incoming plug as it passes through the T-junction depends on the relative hydrodynamic resistances of each branch. When carefully designed, the plugs do not split at the junction without external actuation (Fig. 4).

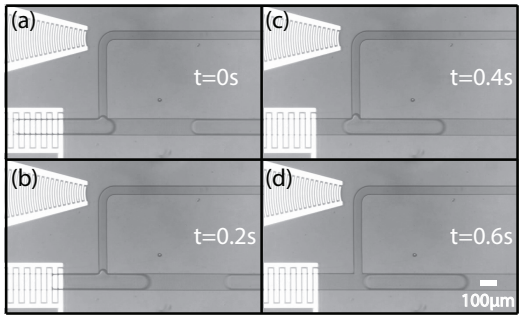

Fig. 4 Timelapse images of plug crossing the by-pass junction without splitting in the absence of actuation.

On the other hand; when SAWs are directed at the horizontal section of the by-pass channel (Fig. 5(a)), acoustic streaming boosts fluid flow creating a suction effect within the by-pass channel that draws the plug in for the duration of the applied pulse (450 ms in this case) (Fig. 5(b)-(c)). Once the SAW actuation is terminated, the plug interface that has protruded into the by-pass channel stays dormant until the main plug ends (Fig. 5(d)-(e)). The interface thins at the edge of the T-junction as it's sheared by the oil phase, thus, splitting the plug into two (Fig. 5(f)).

One key parameter that influence the final droplet volume is the duration of the applied SAW pulse. In an effort to understand how pulse duration affects the outcome, a set of experiments have been conducted keeping the initial plug volume, applied SAW power and system flow rate constant, whilst the

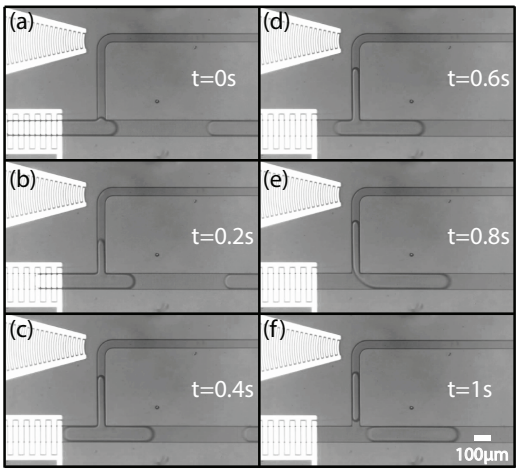

Fig. 5 Timelapse images of plug splitting where SAWs are applied (a) after the plug just passes the T-junction at t=0 s. (b)-(c) The plug is withdrawn to the by-pass channel during the period of actuation (450 ms in this case). (d)-(e) The interface retains its final position after actuation has stopped until the main plug finishes its journey. (f) The plug splits as the interface thins and eventually ruptures at the corner of the T-junction.

pulse duration was gradually increased. The results from this experimental set are plotted in figure 6. Mother plugs of 3.66 nL volume were successfully split to yield daughter droplets volumes ranging from as low as 250 pL up to 1.5 nL.

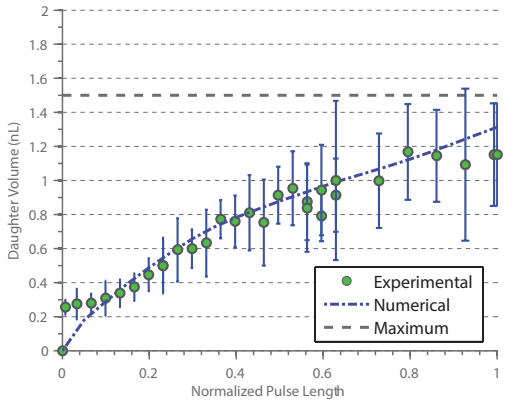

Fig. 6 Experimental and numerical results showing the effects of pulse duration on the daughter droplet volume. There's a maximum expected volume (denoted by dashed line) due to geometrical limitations.

Given the fact that the flow rate was constant during the experiments; it's straightforward to expect a linear increase in the final droplet volume as the pulse duration is incremented. Although this linear trend can be observed in the middle section ($\approx$ 0.2-0.6 Pulse Length), it levels out at the extrema. The short pulse leveling is attributed to the pull-back effect whereas its counterpart is due to geometrical maximum volume limitations. These two phenomena will be discussed in detail.

Firstly; in spite of the fact that the interface was observed to be stable after the SAW actuation has stopped (Fig. 5(d)-(e)), it would occasionally pull-back a little bit, negatively influencing the final daughter droplet volume. The reason for this phenomenon was identified to be the presence of another mother plug at the by-pass channel outlet (P_3 in fig. 1) via numerical simulations.

It is well known that if we consider a plug in a microfluidic channel, a Laplace pressure discontinuity exists across the oil-water interface[90] given by $\Delta P_L = \sigma(w^{-1} + h^{-1})$ where w and h are the width and height of the microfluidic channel, and σ is the interfacial tension between the two phases. Due to this discontinuity; outlet pressure (P_3 in fig. 1) rapidly increases as a mother plug crosses the outlet T-junction. If a stable interface exists at the splitting junction at that moment, it will succumb to the altered pressure distribution, resulting in a small withdrawal of the interface. This pull-back effect is responsible for the non-linearity of the short pulse region mentioned earlier. Resulting from this prolonged duration of interface stability requirement when shorter pulses are applied; the pull-back effect impacts the final droplet volume more at shorter pulses.

The saturation of the daughter droplet volume at higher pulse lengths, however, is explained by the maximum volume condition imposed by geometrical limitations of the proposed system. Due to the nature of SAWs and the high pressure region at the onset of acoustic streaming (P_1 in fig. 1), a plug interface can only be drawn up to that region. Once there, it will experience acoustic radiation forces that repel the interface as well as the inherently undesirable high pressure region for the interface. These factors lead to the limitation of the daughter droplet volume to a specific maximum volume calculated geometrically and plotted in figure 6 with dashed lines.

The results discussed above relating to figure 6 were further verified by running a 2D numerical simulation of the proposed system. Similarly; the initial plug size, velocity and actuation amplitude were held constant while a parametric sweep of the duration of actuation was studied. The results are plotted in figure 6 with a dash-dot line. Due to the nature of the developed numerical model, the time scale are not directly comparable to experiments. To make a valid comparison with experimental results, the pulse lengths have been normalized by the minimum and maximum time values.

The results from the numerical simulation closely match the

experimental findings with the exception of the saturation towards the maximum pulse length which appears to be less pronounced. This is attributed to the fundamental difference between experiments and simulation where the effect of SAWs were simplified to a volume force that acts on the upper section of the by-pass channel. Even though it captures the effect of high pressure on convergence explained earlier, it does not simulate the effect of acoustic radiation forces experienced by the droplet interface.

A second key parameter that governs the final droplet volume is the intensity of the applied acoustic energy. As the SAW power is increased, the plug interface is drawn into the by-pass channel at a higher rate. In order to understand how the electrical input amplitude impacts the final droplet volume, another set of experiments were undertaken where, the flow rate, initial plug volume and pulse length were kept constant while the applied voltage is incremented. The results from these experiments are plotted in figure 7.

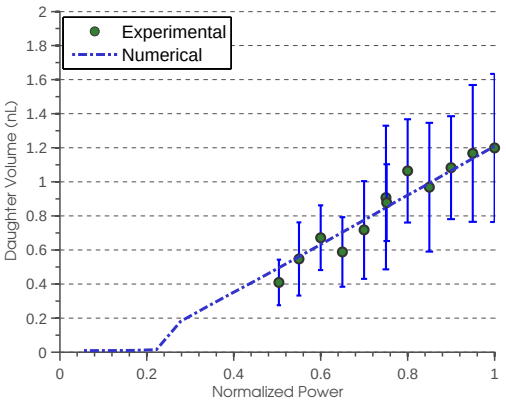

Fig. 7 Experimental and numerical results showing the effects of input voltage on the daughter droplet volume.

Prior to discussing the results from figure 7, it is imperative to understand what is meant by normalized voltage and how it impacts the system. Experimentally, the applied peak-to-peak voltage was measured from the signal generator and normalized by the maximum voltage applied. On the other hand, the normalized power from the numerical simulations is based on normalizing the artificially applied volume force.

An order of magnitude study was carried out to relate these two parameters. Starting with applied voltage; the input power, P_i, scales with voltage squared, V^2. Similarly, it was previously demonstrated[91] that this input SAW power is proportional to the square of the particle oscillation velocity observed at the surface of the piezoelectric substrate, ξ^2. It is these oscillations that give rise to pressure waves inside the fluid medium and it is widely known that the two correlate linearly (i.e $\xi \propto P$)[92]. The effect of these pressure waves have been simulated as an external volume force applied on the upper section of the by-pass channel. Overall, it is important to verify that the experimental and the numerical values are of the same order of magnitude in order to make a valid comparison:

$$V^2 \propto P_i \propto \xi^2 \propto P^2 \tag{1}$$

The effect of the applied voltage on the observed daughter droplet volume is not as straightforward; Nyborg[83] has formulated the equations that govern the streaming field arising from non-linear effects of the incident acoustic waves. By looking at the experimental results in figure 7; a locally linear, increasing and saturating trend similar to the results in figure 6 are observed. As the intensity of the acoustic energy increases; the acoustic streaming field follows suit, resulting in a more pronounced suction and draws the plug interface into the by-pass channel at a higher rate leading to larger daughter droplets at fixed pulse lengths. The saturation towards the maximum are explained by acoustic radiation forces and the high pressure region as discussed earlier.

The pulse length used in experiments and numerical simulations were matched by correlating the data presented in figure 6. The applied body force on the upper section of the channel was gradually increased whilst all the other parameters were held constant. The final split daughter droplet volume was measured and plotted in figure 7 indicated with a dashed line. Likewise in numerical simulations; as the volume force was increased, the streaming induced flow in the upper channel was enhanced, resulting in quicker suction of the plug into the by-pass channel thereby leading to an increase in the final split volume. Here, the pressure gradient enforced in the upper section of the by-pass channel drives fluid flow according to Hagen-Poiseuille law imposing a linear increase in flow velocity with respect to the pressure gradient.

As demonstrated, the proposed microfluidic platform is modular and robust therefore it's a strong candidate for handling a vast number of workflows when combined with previous methods such as droplet merging[47,93], steering[50], hydrodynamic trapping[27,28,94] or mixing[36]. Crucially, it can be utilized to optimize chemical reactions and sample-reagent studies by virtue of combinatorial analysis. The authors envisage that this platform, alongside other systems[8–11], will be the pioneers of a new era, closed channel microfluidic high throughput screening (μHTS).

A hydrodynamic merging section adapted from Niu *et al.*'s[93] previous work has been integrated into the proposed platform as a showcase study to further demonstrate the versatility and compatability of this system. In this study, once a plug is split into the by-pass channel (Fig. 8(a)), it starts traveling towards the hydrodynamic merging chamber located

downstream. In the meantime, another plug is split by a second SAW actuation (Fig. 8(b)). Once the first droplet reaches the merging chamber, it gets trapped until the second droplet arrives (Fig. 8(c)). As this happens, a thin oil film prevents coalescence at the droplet-droplet interface[95,96] (Fig. 8(d)). This liquid film drains out over a short period of time and intermolecular forces take over to rupture the interface leading to fusion of the trapped droplets (Fig. 8(e)). The merging chamber is designed to contain a maximum volume of plug, above which, the larger merged plug exits the chamber (Fig. 8(f)). The fused droplet travels further into the by-pass channel and goes through a serpentine mixer[36] to facilitate mixing (Fig. 1).

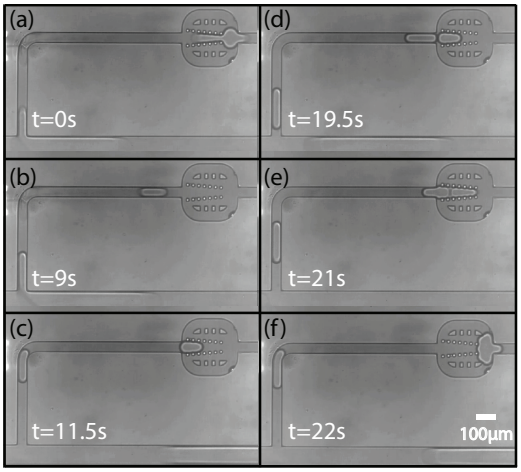

Fig. 8 Sequential images showing plug splitting and merging. (a) The first plug is split by SAW actuation and it travels along the by-pass channel. (b) A second plug is split while the first one travels to the merging chamber and (c) gets trapped there. (d) The second droplet travels in the by-pass channel until it interfaces with the trapped one. (e) The droplets stay in contact while liquid film drains at the interface and coalescence takes place. (f) Once merged, the droplet exits the trapping chamber and travels to the serpentine mixing region.

The potential application of a combinatorial study is clearly demonstrated with the proposed microfluidic platform where hydrodynamic merging and mixing are integrated respectively to the by-pass channel. Utilizing this proposed system, plugs of various content could be split on demand using SAW actuation and merged within the merging chamber in order to study the reactions between two of more samples.

5 Conclusion

In the presented work, a microfluidic platform capable of sensing, splitting and merging plugs was presented. Plugs are first sensed by a capacitive sensor allowing programmability and timely application of SAWs. SAWs directed at a by-pass loop were shown to drive fluid flow leading to plug splitting at the by-pass junction. It was shown that the final daughter droplet volume is finely controlled via two different approaches, adjusting the pulse length or the SAW power. . The authors favor the former method simply because it is straightforward, intuitive and locally linear. The effects of both parameters were further backed by numerical simulations.

Moreover, consecutive split droplets of different content were trapped in a hydrodynamic merging chamber for coalescence followed by serpentine channel mixing. The proposed platform is modular, easily integrable and robust, thereby offering a multitude of studies to be conducted with slight alterations. It is also demonstrated that an ordered droplet library can be formed when an SSL system is integrated as the plug generation method. The proposed design holds tremendous potential for implementation of µHTS systems. Furthermore, the splitting by-pass channel design could be replicated as many times as required on the same microfluidic chip allowing kinetics studies to be parallelized.

References

1 R. Macarron, M. N. Banks, D. Bojanic, D. J. Burns, D. A. Cirovic, T. Garyantes, D. V. S. Green, R. P. Hertzberg, W. P. Janzen, J. W. Paslay, U. Schopfer and G. S. Sittampalam, *Nat Rev Drug Discov*, 2011, **10**, 188–195.

2 M. Berg, K. Undisz, R. Thiericke, P. Zimmermann, T. Moore and C. Posten, *Journal of Biomolecular Screening*, 2001, **6**, 47–56.

3 W. Janzen, in *Molecular Biomethods Handbook*, ed. J. Walker and R. Rapley, Humana Press, 2008, pp. 1097–1118.

4 S. A. Sundberg, *Current Opinion in Biotechnology*, 2000, **11**, 47 – 53.

5 E. Brouzes, M. Medkova, N. Savenelli, D. Marran, M. Twardowski, J. B. Hutchison, J. M. Rothberg, D. R. Link, N. Perrimon and M. L. Samuels, *Proceedings of the National Academy of Sciences*, 2009, **106**, 14195–14200.

6 R. P. Hertzberg and A. J. Pope, *Current Opinion in Chemical Biology*, 2000, **4**, 445 – 451.

7 X. Niu, F. Gielen, J. B. Edel and A. J. deMello, *Nature Chemistry*, 2011, **3**, 437–442.

8 H. Zec, T. D. Rane and T.-H. Wang, *Lab on a Chip*, 2012, **12**, 3055.

9 F. Gielen, L. van Vliet, B. T. Koprowski, S. R. A. Devenish, M. Fischlechner, J. B. Edel, X. Niu, A. J. deMello and F. Hollfelder, *Analytical Chemistry*, 2013, **85**, 4761–4769.

10 D.-K. Kang, X. Gong, S. Cho, J. young Kim, J. B. Edel, S.-I. Chang, J. Choo and A. J. deMello, *Analytical Chemistry*, 2015, **87**, 10770–10778.

11 A. B. Theberge, E. Mayot, A. E. Harrak, F. Kleinschmidt, W. T. S. Huck and A. D. Griffiths, *Lab on a Chip*, 2012, **12**, 1320.

12 J.-C. Baret, O. J. Miller, V. Taly, M. Ryckelynck, A. El-Harrak, L. Frenz, C. Rick, M. L. Samuels, J. B. Hutchison, J. J. Agresti, D. R. Link, D. A. Weitz and A. D. Griffiths, *Lab Chip*, 2009, **9**, 1850–1858.

13 M. Srisa-Art, A. J. deMello and J. B. Edel, *Chemical Communications*, 2009, 6548.

14 S. Jakiela, S. Makulska, P. M. Korczyk and P. Garstecki, *Lab on a Chip*, 2011, **11**, 3603.

15 A. I. E. Abed and V. Taly, *Optical Materials*, 2013, **36**, 64–68.
16 N.-T. Nguyen, S. Lassemono and F. A. Chollet, *Sensors and Actuators B: Chemical*, 2006, **117**, 431–436.
17 M. R. de Saint Vincent, S. Cassagnere, J. Plantard and J.-P. Delville, *Microfluidics and Nanofluidics*, 2012, **13**, 261–271.
18 G. Yesiloz, M. S. Boybay and C. L. Ren, *Lab Chip*, 2015, **15**, 4008–4019.
19 M. C. Cole and P. J. Kenis, *Sensors and Actuators B: Chemical*, 2009, **136**, 350–358.
20 E. Moiseeva, A. Fletcher and C. Harnett, *Sensors and Actuators B: Chemical*, 2011, **155**, 408–414.
21 X. Niu, M. Zhang, S. Peng, W. Wen and P. Sheng, *Biomicrofluidics*, 2007, **1**, 044101.
22 C. Elbuken, T. Glawdel, D. Chan and C. L. Ren, *Sensors and Actuators A: Physical*, 2011, **171**, 55–62.
23 J. Li, Y. Wang, E. Dong and H. Chen, *Lab on a Chip*, 2014, **14**, 860.
24 P. K. Isgor, M. Marcali, M. Keser and C. Elbuken, *Sensors and Actuators B: Chemical*, 2015, **210**, 669–675.
25 T. Thorsen, R. W. Roberts, F. H. Arnold and S. R. Quake, *Phys. Rev. Lett.*, 2001, **86**, 4163–4166.
26 S. L. Anna, N. Bontoux and H. A. Stone, *Applied Physics Letters*, 2003, **82**, 364–366.
27 C. H. Schmitz, A. C. Rowat, S. Köster and D. A. Weitz, *Lab on a Chip*, 2009, **9**, 44–49.
28 A. Huebner, D. Bratton, G. Whyte, M. Yang, A. J. deMello, C. Abell and F. Hollfelder, *Lab on a Chip*, 2009, **9**, 692–698.
29 Y. Bai, X. He, D. Liu, S. N. Patil, D. Bratton, A. Huebner, F. Hollfelder, C. Abell and W. T. S. Huck, *Lab Chip*, 2010, **10**, 1281–1285.
30 P. Abbyad, R. Dangla, A. Alexandrou and C. N. Baroud, *Lab on a Chip*, 2011, **11**, 813–821.
31 J. Tullis, C. L. Park and P. Abbyad, *Lab on a Chip*, 2014, **14**, 3285.
32 D. R. Link, S. L. Anna, D. A. Weitz and H. A. Stone, *Phys. Rev. Lett.*, 2004, **92**, 054503.
33 T. S. Kaminski, S. Jakiela, M. A. Czekalska, W. Postek and P. Garstecki, *Lab Chip*, 2012, **12**, 3995–4002.
34 N. Bremond, A. R. Thiam and J. Bibette, *Phys. Rev. Lett.*, 2008, **100**, 024501.
35 X. Niu, S. Gulati, J. B. Edel and A. J. deMello, *Lab on a Chip*, 2008, **8**, 1837.
36 H. Song, J. D. Tice and R. F. Ismagilov, *Angewandte Chemie International Edition*, 2003, **42**, 768–772.
37 W. Wang, C. Yang and C. M. Li, *Lab Chip*, 2009, **9**, 1504–1506.
38 W. Wang, C. Yang, X. Q. Cui, Q. L. Bao and C. M. Li, *Microfluidics and Nanofluidics*, 2010, **9**, 1175–1183.
39 D. R. Link, E. Grasland-Mongrain, A. Duri, F. Sarrazin, Z. Cheng, G. Cristobal, M. Marquez and D. A. Weitz, *Angewandte Chemie International Edition*, 2006, **45**, 2556–2560.
40 K. Ahn, C. Kerbage, T. P. Hunt, R. M. Westervelt, D. R. Link and D. A. Weitz, *Applied Physics Letters*, 2006, **88**, 024104–3.
41 C. Priest, S. Herminghaus and R. Seemann, *Applied Physics Letters*, 2006, **89**, 134101–134101.
42 K. Ahn, J. Agresti, H. Chong, M. Marquez and D. A. Weitz, *Applied Physics Letters*, 2006, **88**, 264105–3.
43 D. H. Yoon, A. Jamshaid, J. Ito, A. Nakahara, D. Tanaka, T. Akitsu, T. Sekiguchi and S. Shoji, *Lab on a Chip*, 2014, **14**, 3050.
44 S. H. Jin, H.-H. Jeong, B. Lee, S. S. Lee and C.-S. Lee, *Lab Chip*, 2015, **15**, 3677–3686.
45 I. Leibacher, P. Reichert and J. Dual, *Lab Chip*, 2015, **15**, 2896–2905.
46 D. J. Collins, T. Alan, K. Helmerson and A. Neild, *Lab Chip*, 2013, **13**, 3225–3231.
47 M. Sesen, T. Alan and A. Neild, *Lab Chip*, 2014, **14**, 3325–3333.
48 T. Franke, A. R. Abate, D. A. Weitz and A. Wixforth, *Lab Chip*, 2009, **9**, 2625–2627.
49 S. Li, X. Ding, F. Guo, Y. Chen, M. I. Lapsley, S.-C. S. Lin, L. Wang, J. P. McCoy, C. E. Cameron and T. J. Huang, *Analytical Chemistry*, 2013, **85**, 5468–5474.
50 M. Sesen, T. Alan and A. Neild, *Lab Chip*, 2015, **15**, 3030–3038.
51 L. Schmid and T. Franke, *Lab on a chip*, 2013, **13**, 1691–1694.
52 T. M. Squires and S. R. Quake, *Reviews of Modern Physics*, 2005, **77**, 977–1026.
53 H. Bruus, J. Dual, J. Hawkes, M. Hill, T. Laurell, J. Nilsson, S. Radel, S. Sadhal and M. Wiklund, *Lab on a Chip*, 2011, **11**, 3579.
54 A. Haake, A. Neild, G. Radziwill and J. Dual, *Biotechnol. Bioeng.*, 2005, **92**, 8–14.
55 R. Walker, I. Gralinski, K. K. Lay, T. Alan and A. Neild, *Appl. Phys. Lett.*, 2012, **101**, 163504.
56 P. Glynne-Jones, C. E. M. Demore, C. Ye, Y. Qiu, S. Cochran and M. Hill, *IEEE Transactions on Ultrasonics Ferroelectrics and Frequency Control*, 2012, **59**, 1258–1266.
57 C. Devendran, D. R. Billson, D. A. Hutchins and A. Neild, *Sensors and Actuators B: Chemical*, 2016, **224**, 529–538.
58 T. Laurell, F. Petersson and A. Nilsson, *Chem. Soc. Rev.*, 2007, **36**, 492–506.
59 H. V. Phan, M. Şeşen, T. Alan and A. Neild, *Appl. Phys. Lett.*, 2014, **105**, 193507.
60 C. Devendran, I. Gralinski and A. Neild, *Microfluidics and Nanofluidics*, 2014, **17**, 879–890.
61 M. Evander, L. Johansson, T. Lilliehorn, J. Piskur, M. Lindvall, S. Johansson, M. Almqvist, T. Laurell and J. Nilsson, *Analytical Chemistry*, 2007, **79**, 2984–2991.
62 P. Rogers and A. Neild, *Lab on a Chip*, 2011, **11**, 3710.
63 P. Rogers, I. Gralinski, C. Galtry and A. Neild, *Microfluidics and Nanofluidics*, 2013, **14**, 469–477.
64 J. J. Hawkes, R. W. Barber, D. R. Emerson and W. T. Coakley, *Lab on a Chip*, 2004, **4**, 446.
65 G. G. Yaralioglu, I. O. Wygant, T. C. Marentis and B. T. Khuri-Yakub, *Analytical Chemistry*, 2004, **76**, 3694–3698.
66 P.-H. Huang, Y. Xie, D. Ahmed, J. Rufo, N. Nama, Y. Chen, C. Y. Chan and T. J. Huang, *Lab on a Chip*, 2013, **13**, 3847.
67 H. V. Phan, M. B. Coşkun, M. Şeşen, G. Pandraud, A. Neild and T. Alan, *Lab Chip*, 2015, **15**, 4206–4216.
68 N. Sivanantha, C. Ma, D. J. Collins, M. Sesen, J. Brenker, R. L. Coppel, A. Neild and T. Alan, *Applied Physics Letters*, 2014, **105**, 103704–5.
69 T. Franke, S. Braunmuller, L. Schmid, A. Wixforth and D. A. Weitz, *Lab Chip*, 2010, **10**, 789–794.
70 F. Guo, P. Li, J. B. French, Z. Mao, H. Zhao, S. Li, N. Nama, J. R. Fick, S. J. Benkovic and T. J. Huang, *Proceedings of the National Academy of Sciences*, 2015, **112**, 43–48.
71 M. Cecchini, S. Girardo, D. Pisignano, R. Cingolani and F. Beltram, *Appl. Phys. Lett.*, 2008, **92**, 104103.
72 C. D. Wood, S. D. Evans, J. E. Cunningham, R. ORorke, C. Walti and A. G. Davies, *Appl. Phys. Lett.*, 2008, **92**, 044104.
73 D. J. Collins, T. Alan and A. Neild, *Applied Physics Letters*, 2014, **105**, 033509–4.
74 D. J. Collins, B. Morahan, J. Garcia-Bustos, C. Doerig, M. Plebanski and A. Neild, *Nature Communications*, 2015, **6**, 8686.
75 X. Ding, S.-C. S. Lin, M. I. Lapsley, S. Li, X. Guo, C. Y. Chan, I.-K. Chiang, L. Wang, J. P. McCoy and T. J. Huang, *Lab Chip*, 2012, **12**, 4228–4231.
76 X. Ding, Z. Peng, S.-C. S. Lin, M. Geri, S. Li, P. Li, Y. Chen, M. Dao, S. Suresh and T. J. Huang, *Proceedings of the National Academy of Sciences*, 2014, **111**, 12992–12997.
77 G. Destgeer, K. H. Lee, J. H. Jung, A. Alazzam and H. J. Sung, *Lab Chip*, 2013, **13**, 4210–4216.
78 D. J. Collins, T. Alan and A. Neild, *Lab Chip*, 2014, **14**, 1595–1603.

79 C. Devendran, N. R. Gunasekara, D. J. Collins and A. Neild, *RSC Advances*, 2016, **6**, 5856–5864.

80 S.-C. S. Lin, X. Mao and T. J. Huang, *Lab Chip*, 2012, **12**, 2766–2770.

81 L. Rayleigh, *Philosophical Transactions of the Royal Society of London*, 1884, 1–21.

82 C. Eckart, *Physical Review*, 1948, **73**, 68.

83 W. Nyborg, *Physical acoustics*, 1965, **2**, 265.

84 A. Wixforth, *Journal of the Association for Laboratory Automation*, 2006, **11**, 399–405.

85 Z. v. Guttenberg, A. Rathgeber, S. Keller, J. Rädler, A. Wixforth, M. Kostur, M. Schindler and P. Talkner, *Physical Review E*, 2004, **70**, 056311.

86 C. J. Strobl, Z. Von Guttenberg and A. Wixforth, *Ultrasonics, Ferroelectrics, and Frequency Control, IEEE Transactions on*, 2004, **51**, 1432–1436.

87 M. S. Arefin, M. B. Coskun, T. Alan, J.-M. Redoute, A. Neild and M. R. Yuce, *Appl. Phys. Lett.*, 2014, **104**, 223503.

88 A. Devices, *Analog Devices AD7746: 24-bit, 2 Channel Capacitance to Digital Converter*, Analog devices technical report, 2010.

89 A. S. Basu, *Lab Chip*, 2013, **13**, 1892–1901.

90 L. Ménétrier-Deremble and P. Tabeling, *Phys. Rev. E*, 2006, **74**, 035303.

91 K. Franke, M. Ross-Messemer, A. Menck, R. Hoeller, H. Schmidt and M. Weilmacht, *Ultrasonics, Ferroelectrics and Frequency Control, IEEE Transactions on*, 2003, **50**, 77–80.

92 L. L. Beranek, *Acoustics*, McGraw-Hill, New York, 1954.

93 X. Niu, S. Gulati, J. Edel *et al.*, *Lab Chip*, 2008, **8**, 1837–1841.

94 H. Boukellal, Š. Selimović, Y. Jia, G. Cristobal and S. Fraden, *Lab on a Chip*, 2009, **9**, 331–338.

95 E. Klaseboer, J. P. Chevaillier, C. Gourdon and O. Masbernat, *Journal of colloid and interface science*, 2000, **229**, 274–285.

96 S. Feng, L. Yi, L. Zhao-Miao, C. Ren-Tuo and W. Gui-Ren, *Chinese Journal of Analytical Chemistry*, 2015, **43**, 1942–1954.

Chapter 7

Conclusions and Future Work

This chapter will discuss the conclusions of the work presented in this thesis. This will be followed by detailed discussion of the outcomes of this research. To conclude, recommendation of future work is presented.

7.1 Conclusions

This thesis describes three pioneering droplet microfluidic platforms capable of performing droplet manipulation techniques of utmost significance. All three systems achieve droplet actuation by using surface acoustic waves (SAWs) in their own unique way yet in a highly integrable manner, boasting compatibility amongst each other as well as with existing lab-on-chip (LOC) devices. These systems offer enhanced flexible control over droplet behaviour so that almost any specific study could be performed with ease.

The first platform developed, as discussed in chapter 4, enables active merging of up to four consecutive droplets using SAWs.. Acoustic tweezers type trapping of a droplet within an expansion chamber leads to collision with the successor droplet and consequent coalescence. The merged volume exits the expansion chamber due to a sharp increase in the drag force experienced by the droplet, explained by increased volume and confined geometry. The onset of coalesced droplet exit from the expansion chamber can be controlled to ensure a predetermined number of droplets have merged by varying parameters such as the initial droplet volume, velocity and the applied electrical energy. The parameter space is extensively characterised and regions where merging of two, three and four consecutive droplets take place have been established by detailed experimental results and analysis.

The second microfluidic platform designed and tested that is presented in this thesis, is detailed in chapter 5 where steering of plugs is achieved. This platform makes use of SAWs impinging on a fluid discontinuity to deform and deflect plugs into one of the two outlets. This method, allows controlled plug sorting at a Y-junction using two sets of SAW generating electrodes positioned on each side of the Y-junction. Moreover, as the SAW power is decreased, the steering potential diminishes; instead, plugs are split into two. It was also shown that this splitting can be controlled, offering flexibility to the design in hand. The steering and the splitting processes depend on the initial plug volume,

velocity and applied acoustic energy. The system is thoroughly characterised and capable of steering plugs as large as 7 nanolitres.

The final microfluidic platform studied as part of this thesis is described in chapter 6. This programmable, automated platform is able to electrically sense an incoming plug and split a controlled volume into a by-pass loop using SAWs. SAWs directed at one section of the by-pass loop were shown to induce acoustic streaming which boosts fluid flow in the by-pass loop leading to suction of a plug into the loop; consequently splitting a part of it. The final split volume is accurately controlled by adjusting the duration of the applied SAW as well as its amplitude. The system was thoroughly characterised by experimental and numerical simulations providing further insight into the splitting process. Moreover, a showcase study was carried out where a hydrodynamic merging chamber was integrated to the by-pass loop in order to merge the split droplets. This exemplified the possibility of carrying out a combinatorial study using the presented platform.

All three platforms developed and discussed in this thesis are designed in such a way that they are easily scalable and integrable to existing LOC platforms allowing a multitude of studies to be carried out with control. Depending on specific study requirements, these methods could be assembled in series or integrated with other methods on a single microfluidic chip with ease.

7.2 Outcomes

The key outcomes of the study presented in this thesis are applicability of SAWs in droplet microfluidic systems, observation and analysis of novel mechanisms, modular design in microfluidic systems and droplet microfluidic high throughput screening (μHTS) capabilities.

Although SAWs have been widely used in microfluidics, notably for particle and cell manipulation, atomisation, mixing and pumping, the applications of SAW in droplet microfluidic systems are underwhelming. In this sense, the thesis explores unique ways of manipulating droplets in closed microfluidic channels greatly contributing to the existing knowledge. SAW actuation holds numerous advantages over its counterparts; SAWs are biocompatible, easy to operate and integrate with microfluidic systems and they offer portable and contamination free manipulation while exhibiting superior energy efficiency without the need for moving parts. These make SAW actuation a strong candidate for use in droplet microfluidic systems.

A second important outcome of the presented thesis stems from the novel mechanisms explored throughout the study. Droplets with diameters larger than the wavelength were shown to be trapped in high acoustic pressure zones generated by SAWs. This was of a direct result of the properties of fluids used in the study. It was shown that this mechanism could be used to merge consecutive droplets on demand.

Moreover, the concept-to-prototype process was expedited owing to the modular and integrable nature of the presented methods. Commonly, microfluidic devices are designed to perform a single task or a workflow that is highly specific to the study it's designed for therefore it's hard for other researchers to implement those methods for another study. By designing these systems without imposing any inlet or outlet conditions such as biasing,

these systems are rendered compatible with existing methods. This allows researchers to scale and implement these methods into their workflows in an easier and quicker manner.

Furthermore, the work presented in this thesis exhibits novel, highly applicable mechanisms/systems to address challenges present in miniaturization of laboratory scale systems, specifically high throughput screening (HTS). The highly anticipated paradigm shift that will improve HTS significantly was addressed. HTS studies are expected to be carried out in droplet microfluidic devices; decreasing the amount of fluids used and allowing higher throughput studies to be performed on chips with improved sensitivities. However, droplet microfluidic systems are enclosed and driven by continuous pumps, rendering it difficult to create combinatorial libraries. The microfluidic platform developed in chapter 6 addresses this issue and exemplifies how such a combinatorial library could be realised with droplet microfluidic systems using SAWs.

7.3 Future Work

Future work involves further improvement of the microfluidic platform presented in chapter 6 where pressure driven pumps or a fixed volume droplet generator (see fig. 2.11) will be used to decrease plug volume variability to enhance final volume accuracy. Further characterisation of the device will also be performed analysing effects of initial plug volume and the onset of actuation. The integration of outlet pressure regulating channels will decrease and possibly eliminate the observed pull-back effects as suggested by numerical simulations.

Furthermore, single cell studies will be undertaken in an attempt to achieve %100 single cells per droplet distribution (see fig. 2.3). It is of utmost importance to increase the efficiency of single cell studies in order to achieve faster and more relДçable results and this can be made possible by using SAWs. This could be accomplished by sorting the droplets into waste and collect outlets using the system discussed in chapter 5, for example. For this reason, the possibility of sensing the cells inside droplets will be further investigated.

Additionally, heating in SAW microfluidic systems will be investigated further in order to understand the governing mechanisms so that device optimisation for minimising waste heat could be achieved. Such a study will prove to be extremely useful for SAW microfluidic devices designed to handle cells and other biological samples.

Bibliography

[1] C. Holtze, A. C. Rowat, J. J. Agresti, J. B. Hutchison, F. E. Angile, C. H. J. Schmitz, S. Koster, H. Duan, K. J. Humphry, R. A. Scanga, J. S. Johnson, D. Pisignano, and D. A. Weitz. Biocompatible surfactants for water-in-fluorocarbon emulsions. *Lab Chip*, 8:1632–1639, 2008.

[2] Adam R. Abate, Chia-Hung Chen, Jeremy J. Agresti, and David A. Weitz. Beating poisson encapsulation statistics using close-packed ordering. *Lab Chip*, 9:2628–2631, 2009.

[3] Jon F. Edd, Dino Di Carlo, Katherine J. Humphry, Sarah Koster, Daniel Irimia, David A. Weitz, and Mehmet Toner. Controlled encapsulation of single-cells into monodisperse picolitre drops. *Lab Chip*, 8:1262–1264, 2008.

[4] Charles N. Baroud, Francois Gallaire, and Remi Dangla. Dynamics of microfluidic droplets. *Lab Chip*, 10:2032–2045, 2010.

[5] David J. Collins, Tuncay Alan, Kristian Helmerson, and Adrian Neild. Surface acoustic waves for on-demand production of picoliter droplets and particle encapsulation. *Lab Chip*, 13:3225–3231, 2013.

[6] Volkert van Steijn, Piotr M Korczyk, Ladislav Derzsi, Adam R Abate, David A Weitz, and Piotr Garstecki. Block-and-break generation of microdroplets with fixed volume. *Biomicrofluidics*, 7(2):024108, 2013.

[7] Shaojiang Zeng, Bowei Li, Xiao'ou Su, Jianhua Qin, and Bingcheng Lin. Microvalve-actuated precise control of individual droplets in microfluidic devices. *Lab Chip*, 9(10):1340–1343, 2009.

[8] Lothar Schmid and Thomas Franke. SAW-controlled drop size for flow focusing. *Lab Chip*, 13(9):1691–1694, 2013.

[9] Nam-Trung Nguyen, Teck-Hui Ting, Yit-Fatt Yap, Teck-Neng Wong, John Chee-Kiong Chai, Wee-Liat Ong, Junlong Zhou, Say-Hwa Tan, and Levent Yobas. Thermally mediated droplet formation in microchannels. *Applied Physics Letters*, 91(8):084102, 2007.

[10] Si Hyung Jin, Heon-Ho Jeong, Byungjin Lee, Sung Sik Lee, and Chang-Soo Lee. A programmable microfluidic static droplet array for droplet generation transportation, fusion, storage, and retrieval. *Lab Chip*, 15(18):3677–3686, 2015.

[11] Slawomir Jakiela, Sylwia Makulska, Piotr M. Korczyk, and Piotr Garstecki. Speed of flow of individual droplets in microfluidic channels as a function of the capillary number volume of droplets and contrast of viscosities. *Lab Chip*, 11(21):3603, 2011.

[12] Nam-Trung Nguyen, Sumantri Lassemono, and Franck Alexis Chollet. Optical detection for droplet size control in microfluidic droplet-based analysis systems. *Sensors and Actuators B: Chemical*, 117(2):431–436, oct 2006.

[13] Matthieu Robert de Saint Vincent, Sebastien Cassagnere, Joel Plantard, and Jean-Pierre Delville. Real-time droplet caliper for digital microfluidics. *Microfluidics and Nanofluidics*, 13(2):261–271, mar 2012.

[14] Jeremy J. Agresti, Eugene Antipov, Adam R. Abate, Keunho Ahn, Amy C. Rowat, Jean-Christophe Baret, Manuel Marquez, Alexander M. Klibanov, Andrew D. Griffiths, and David A. Weitz. Ultrahigh-throughput screening in drop-based microfluidics for directed evolution. *Proceedings of the National Academy of Sciences*, 107(9):4004–4009, 2010.

[15] Keunho Ahn, Charles Kerbage, Tom P. Hunt, R. M. Westervelt, Darren R. Link, and D. A. Weitz. Dielectrophoretic manipulation of drops for high-speed microfluidic sorting devices. *Applied Physics Letters*, 88(2):024104 –024104–3, 2006.

[16] Hongbo Zhou and Shuhuai Yao. Electrostatic charging and control of droplets in microfluidic devices. *Lab Chip*, 13:962–969, 2013.

[17] Thomas Franke, Adam R. Abate, David A. Weitz, and Achim Wixforth. Surface acoustic wave (SAW) directed droplet flow in microfluidics for PDMS devices. *Lab Chip*, 9:2625–2627, 2009.

[18] Muhsincan Sesen, Tuncay Alan, and Adrian Neild. Microfluidic plug steering using surface acoustic waves. *Lab Chip*, 15:3030–3038, 2015.

[19] Shen Feng, Li Yi, Liu Zhao-Miao, Cao Ren-Tuo, and Wang Gui-Ren. Advances in micro-droplets coalescence using microfluidics. *Chinese Journal of Analytical Chemistry*, 43(12):1942–1954, 2015.

[20] C. Priest, S. Herminghaus, and R. Seemann. Controlled electrocoalescence in microfluidics: Targeting a single lamella. *Applied Physics Letters*, 89(13):134101–134101, 2006.

[21] Keunho Ahn, Jeremy Agresti, Henry Chong, Manuel Marquez, and D. A. Weitz. Electrocoalescence of drops synchronized by size-dependent flow in microfluidic channels. *Applied Physics Letters*, 88(26):264105 –264105–3, 2006.

[22] X. Niu, S. Gulati, J.B. Edel, et al. Pillar-induced droplet merging in microfluidic circuits. *Lab Chip*, 8(11):1837–1841, 2008.

[23] Nicolas Bremond, Abdou R. Thiam, and Jérôme Bibette. Decompressing emulsion droplets favors coalescence. *Phys. Rev. Lett.*, 100:024501, 2008.

[24] Sanghyun Lee, Hojin Kim, Dong-Joon Won, Jaehyung Lee, and Joonwon Kim. On-demand, parallel droplet merging method with non-contact droplet pairing in droplet-based microfluidics. *Microfluidics and Nanofluidics*, 20(1):1–9, 2016.

[25] Jonathan Tullis, Chong L Park, and Paul Abbyad. Selective fusion of anchored droplets via changes in surfactant concentration. *Lab Chip*, 14(17):3285–3289, 2014.

[26] Muhsincan Sesen, Tuncay Alan, and Adrian Neild. Microfluidic on-demand droplet merging using surface acoustic waves. *Lab Chip*, 14:3325–3333, 2014.

[27] D. R. Link, S. L. Anna, D. A. Weitz, and H. A. Stone. Geometrically mediated breakup of drops in microfluidic devices. *Phys. Rev. Lett.*, 92:054503, 2004.

[28] David N. Adamson, Debarshi Mustafi, John X. J. Zhang, Bo Zheng, and Rustem F. Ismagilov. Production of arrays of chemically distinct nanolitre plugs via repeated splitting in microfluidic devices. *Lab Chip*, 6:1178–1186, 2006.

[29] Ansgar Huebner, Dan Bratton, Graeme Whyte, Min Yang, Andrew J. deMello, Chris Abell, and Florian Hollfelder. Static microdroplet arrays: a microfluidic device for droplet trapping, incubation and release for enzymatic and cell-based assays. *Lab Chip*, 9(5):692–698, 2009.

[30] Christian HJ Schmitz, Amy C Rowat, Sarah Köster, and David A Weitz. Dropspots: a picoliter array in a microfluidic device. *Lab Chip*, 9(1):44–49, 2009.

[31] Paul Abbyad, Rémi Dangla, Antigoni Alexandrou, and Charles N Baroud. Rails and anchors: guiding and trapping droplet microreactors in two dimensions. *Lab Chip*, 11(5):813–821, 2011.

[32] Wei Wang, Chun Yang, and Chang Ming Li. On-demand microfluidic droplet trapping and fusion for on-chip static droplet assays. *Lab Chip*, 9:1504–1506, 2009.

[33] Noo Li Jeon, Stephan K. W. Dertinger, Daniel T. Chiu, Insung S. Choi, Abraham D. Stroock, and George M. Whitesides. Generation of solution and surface gradients using microfluidic systems. *Langmuir*, 16(22):8311–8316, 2000.

[34] Dong-Ku Kang, Xiuqing Gong, Soongwon Cho, Jin-young Kim, Joshua B Edel, Soo-Ik Chang, Jaebum Choo, and Andrew J deMello. 3D droplet microfluidic systems for high-throughput biological experimentation. *Analytical Chemistry*, 87(21):10770–10778, 2015.

[35] Meng Sun, Swastika S. Bithi, and Siva A. Vanapalli. Microfluidic static droplet arrays with tuneable gradients in material composition. *Lab Chip*, 11:3949–3952, 2011.

[36] Xize Niu, Fabric Gielen, Joshua B. Edel, and Andrew J. deMello. A microdroplet dilutor for high-throughput screening. *Nat Chem*, 3(6):437–442, 2011.

[37] Helen Song, Michelle R. Bringer, J.D. Tice, Cory J. Gerdts, and Rustem F. Ismagilov. Experimental test of scaling of mixing by chaotic advection in droplets moving through microfluidic channels. *Applied Physics Letters*, 83(22):4664–4666, 2003.

[38] Albert Liau, Rohit Karnik, Arun Majumdar, and Jamie H. Doudna Cate. Mixing crowded biological solutions in milliseconds. *Analytical Chemistry*, 77(23):7618–7625, 2005.

[39] Hoang Van Phan, M. Bulut Coskun, Muhsincan Sesen, Gregory Pandraud, Adrian Neild, and Tuncay Alan. Vibrating membrane with discontinuities for rapid and efficient microfluidic mixing. *Lab Chip*, 15:4206–4216, 2015.

[40] Hoang V. Phan, Muhsincan Sesen, Tuncay Alan, and Adrian Neild. Single line particle focusing using a vibrating bubble. *Applied Physics Letters*, 105(19), 2014.

[41] Ninnuja Sivanantha, Charles Ma, David J. Collins, Muhsincan Sesen, Jason Brenker, Ross L. Coppel, Adrian Neild, and Tuncay Alan. Characterization of adhesive properties of red blood cells using surface acoustic wave induced flows for rapid diagnostics. *Applied Physics Letters*, 105(10):103704–5, 2014.

[42] H.T.G. van Lintel, F.C.M. van De Pol, and S. Bouwstra. A piezoelectric micropump based on micromachining of silicon. *Sensors and Actuators*, 15(2):153 – 167, 1988.

[43] S. Masuda, M. Washizu, and T. Nanba. Novel method of cell fusion in field constriction area in fluid integration circuit. *Industry Applications, IEEE Transactions on*, 25(4):732–737, Jul 1989.

[44] D. Jed Harrison, Andreas Manz, Zhonghui Fan, Hans Luedi, and H. Michael Widmer. Capillary electrophoresis and sample injection systems integrated on a planar glass chip. *Analytical Chemistry*, 64(17):1926–1932, 1992.

[45] G. M. Whitesides. The origins and the future of microfluidics. *Nature*, 442(7101):368–373, 2006.

[46] Eric K Sackmann, Anna L Fulton, and David J Beebe. The present and future role of microfluidics in biomedical research. *Nature*, 507(7491):181–189, 2014.

[47] Piia von Lode. Point-of-care immunotesting: Approaching the analytical performance of central laboratory methods. *Clinical Biochemistry*, 38(7):591 – 606, 2005.

[48] Lisa R Volpatti and Ali K Yetisen. Commercialization of microfluidic devices. *Trends in biotechnology*, 32(7):347–350, 2014.

[49] Elisabeth Verpoorte. Microfluidic chips for clinical and forensic analysis. *Electrophoresis*, 23(5):677–712, 2002.

[50] David E. Bruns, Edward R. Ashwood, and Carl A. Burtis. *Fundamentals of Molecular Diagnostics*. Evolve, 2007.

[51] Ken-ichi Ohno, Kaoru Tachikawa, and Andreas Manz. Microfluidics: Applications for analytical purposes in chemistry and biochemistry. *Electrophoresis*, 29(22):4443–4453, 2008.

[52] Georgette B. Salieb-Beugelaar, Giuseppina Simone, Arun Arora, Anja Philippi, and Andreas Manz. Latest developments in microfluidic cell biology and analysis systems. *Analytical Chemistry*, 82(12):4848–4864, 2010. PMID: 20462184.

[53] Leanne Marle and Gillian M. Greenway. Microfluidic devices for environmental monitoring. *TrAC Trends in Analytical Chemistry*, 24(9):795 – 802, 2005.

[54] Shi Cheng and Zhigang Wu. Microfluidic electronics. *Lab Chip*, 12:2782–2791, 2012.

[55] Suresh Neethirajan, Isao Kobayashi, Mitsutoshi Nakajima, Dan Wu, Saravanan Nandagopal, and Francis Lin. Microfluidics for food, agriculture and biosystems industries. *Lab Chip*, 11:1574–1586, 2011.

[56] Alberto Escarpa. Lights and shadows on food microfluidics. *Lab Chip*, 14:3213–3224, 2014.

[57] C. Zhang, K. Khoshmanesh, A. Mitchell, and K. Kalantar-zadeh. Dielectrophoresis for manipulation of micro/nano particles in microfluidic systems. *Analytical and Bioanalytical Chemistry*, 396(1):401–420, 2010.

[58] Khashayar Khoshmanesh, Saeid Nahavandi, Sara Baratchi, Arnan Mitchell, and Kourosh Kalantar-zadeh. Dielectrophoretic platforms for bio-microfluidic systems. *Biosensors and Bioelectronics*, 26(5):1800 – 1814, 2011.

[59] James Friend and Leslie Y. Yeo. Microscale acoustofluidics: Microfluidics driven via acoustics and ultrasonics. *Rev. Mod. Phys.*, 83:647–704, Jun 2011.

[60] Lotien Richard Huang, Edward C. Cox, Robert H. Austin, and James C. Sturm. Continuous particle separation through deterministic lateral displacement. *Science*, 304(5673):987–990, 2004.

[61] Nicole Pamme. Magnetism and microfluidics. *Lab Chip*, 6:24–38, 2006.

[62] Robert Gorkin, Jiwoon Park, Jonathan Siegrist, Mary Amasia, Beom Seok Lee, Jong-Myeon Park, Jintae Kim, Hanshin Kim, Marc Madou, and Yoon-Kyoung Cho. Centrifugal microfluidics for biomedical applications. *Lab Chip*, 10:1758–1773, 2010.

[63] J. de Jong, R. G. H. Lammertink, and M. Wessling. Membranes and microfluidics: a review. *Lab Chip*, 6:1125–1139, 2006.

[64] Bo Zheng, Cory J Gerdts, and Rustem F Ismagilov. Using nanoliter plugs in microfluidics to facilitate and understand protein crystallization. *Current Opinion in Structural Biology*, 15:548–55, 2005.

[65] Jung-Uk Shim, Galder Cristobal, Darren R Link, Todd Thorsen, and Seth Fraden. Using microfluidics to decouple nucleation and growth of protein crystals. *Crystal Growth & Design*, 7:2192–2194, 2007.

[66] Saurabh Vyawahare, Andrew D. Griffiths, and Christoph A. Merten. Miniaturization and parallelization of biological and chemical assays in microfluidic devices. *Chemistry & Biology*, 17(10):1052–1065, 2010.

[67] Ashleigh B. Theberge, Fabienne Courtois, Yolanda Schaerli, Martin Fischlechner, Chris Abell, Florian Hollfelder, and Wilhelm T. S. Huck. Microdroplets in microfluidics: An evolving platform for discoveries in chemistry and biology. *Angewandte Chemie International Edition*, 49(34):5846–5868, 2010.

[68] Ali Abou-Hassan, Olivier Sandre, and Valérie Cabuil. Microfluidics in inorganic chemistry. *Angewandte Chemie International Edition*, 49(36):6268–6286, 2010.

[69] Steven A Sundberg. High-throughput and ultra-high-throughput screening: solution- and cell-based approaches. *Current Opinion in Biotechnology*, 11(1):47 – 53, 2000.

[70] WilliamP. Janzen. High throughput screening. In JohnM. Walker and Ralph Rapley, editors, *Molecular Biomethods Handbook*, pages 1097–1118. Humana Press, 2008.

[71] Eric Brouzes, Martina Medkova, Neal Savenelli, Dave Marran, Mariusz Twardowski, J. Brian Hutchison, Jonathan M. Rothberg, Darren R. Link, Norbert Perrimon, and Michael L. Samuels. Droplet microfluidic technology for single-cell high-throughput screening. *Proceedings of the National Academy of Sciences*, 106(34):14195–14200, 2009.

[72] P. Szymański, M. Markowicz, and E. Mikiciuk-Olasik. Adaptation of high-throughput screening in drug discovery–toxicological screening tests. *International Journal of Molecular Sciences*, 13(1):427–452, 2011.

[73] Michael Berg, Katrin Undisz, Ralf Thiericke, Peter Zimmermann, Thomas Moore, and Clemens Posten. Evaluation of liquid handling conditions in microplates. *Journal of Biomolecular Screening*, 6(1):47–56, 2001.

[74] Robert P Hertzberg and Andrew J Pope. High-throughput screening: new technology for the 21st century. *Current Opinion in Chemical Biology*, 4(4):445 – 451, 2000.

[75] Aisha Qi, James R. Friend, Leslie Y. Yeo, David A. V. Morton, Michelle P. McIntosh, and Leone Spiccia. Miniature inhalation therapy platform using surface acoustic wave microfluidic atomization. *Lab Chip*, 9:2184–2193, 2009.

[76] Jinjie Shi, Daniel Ahmed, Xiaole Mao, Sz-Chin Steven Lin, Aitan Lawit, and Tony Jun Huang. Acoustic tweezers: patterning cells and microparticles using standing surface acoustic waves (SSAW). *Lab Chip*, 9:2890–2895, 2009.

[77] Haiyan Li, JamesR. Friend, and LeslieY. Yeo. Surface acoustic wave concentration of particle and bioparticle suspensions. *Biomedical Microdevices*, 9(5):647–656, 2007.

[78] Ralf Seemann, Martin Brinkmann, Thomas Pfohl, and Stephan Herminghaus. Droplet based microfluidics. *Reports on Progress in Physics*, 75(1):016601, 2012.

[79] Helen Song, , and Rustem F. Ismagilov. Millisecond kinetics on a microfluidic chip using nanoliters of reagents. *Journal of the American Chemical Society*, 125(47):14613–14619, 2003. PMID: 14624612.

[80] Brian M Paegel, Robert G Blazej, and Richard A Mathies. Microfluidic devices for DNA sequencing: sample preparation and electrophoretic analysis. *Current Opinion in Biotechnology*, 14(1):42 – 50, 2003.

[81] Rajesh R. Naik, Sarah J. Stringer, Gunjan Agarwal, Sharon E. Jones, and Morley O. Stone. Biomimetic synthesis and patterning of silver nanoparticles. *Nat Mater*, 1(3):169–172, November 2002.

[82] Daniel Figeys and Devanand Pinto. Lab-on-a-chip: a revolution in biological and medical sciences. *Analytical Chemistry*, 72(9):330–A, 2000.

[83] Marc Madou, Jim Zoval, Guangyao Jia, Horacio Kido, Jitae Kim, and Nahui Kim. Lab on a CD. *Annual Review of Biomedical Engineering*, 8(1):601–628, 2006.

[84] Luc Gervais, Nico de Rooij, and Emmanuel Delamarche. Microfluidic chips for point-of-care immunodiagnostics. *Advanced Materials*, 23(24):H151–H176, 2011.

[85] Curtis D. Chin, Vincent Linder, and Samuel K. Sia. Commercialization of microfluidic point-of-care diagnostic devices. *Lab Chip*, 12:2118–2134, 2012.

[86] Ali Kemal Yetisen, Muhammad Safwan Akram, and Christopher R. Lowe. Paper-based microfluidic point-of-care diagnostic devices. *Lab Chip*, 13:2210–2251, 2013.

[87] Philip S. Waggoner and Harold G. Craighead. Micro- and nanomechanical sensors for environmental, chemical, and biological detection. *Lab Chip*, 7:1238–1255, 2007.

[88] Nam-Trung Nguyen and Steven T Wereley. *Fundamentals and applications of microfluidics*. Artech House, 2002.

[89] Todd M. Squires and Stephen R. Quake. Microfluidics: Fluid physics at the nanoliter scale. *Rev. Mod. Phys.*, 77:977–1026, Oct 2005.

[90] Wei Wang, Chun Yang, XiaoQiang Cui, QiaoLiang Bao, and ChangMing Li. Droplet microfluidic preparation of au nanoparticles-coated chitosan microbeads for flow-through surface-enhanced raman scattering detection. *Microfluidics and Nanofluidics*, 9(6):1175–1183, 2010.

[91] David C. Duffy, Heather L. Gillis, Joe Lin, Norman F. Sheppard, and Gregory J. Kellogg. Microfabricated Centrifugal Microfluidic Systems: Characterization and Multiple Enzymatic Assays. *Analytical Chemistry*, 71(20):4669–4678, oct 1999.

[92] Jens Ducree, Stefan Haeberle, Sascha Lutz, Sarah Pausch, Felix von Stetten, and Roland Zengerle. The centrifugal microfluidic Bio-Disk platform. *J. Micromech. Microeng.*, 17(7):S103–S115, jun 2007.

[93] Suzanne Hugo, Kevin Land, Marc Madou, and Horacio Kido. A centrifugal microfluidic platform for point-of-care diagnostic applications. *SAJS*, 110(1/2):1–7, 2014.

[94] Thomas P. Forbes and Samuel P. Forry. Microfluidic magnetophoretic separations of immunomagnetically labeled rare mammalian cells. *Lab Chip*, 12:1471–1479, 2012.

[95] Aaron Chen, Tom Byvank, Woo-Jin Chang, Atul Bharde, Greg Vieira, Brandon L. Miller, Jeffrey J. Chalmers, Rashid Bashir, and Ratnasingham Sooryakumar. On-chip magnetic separation and encapsulation of cells in droplets. *Lab Chip*, 13:1172–1181, 2013.

[96] Frank M White and Isla Corfield. *Viscous fluid flow*, volume 3. McGraw-Hill New York, 2006.

[97] George Karniadakis, Ali Beskok, and Narayan Aluru. *Microflows and nanoflows: fundamentals and simulation*, volume 29. Springer Science & Business Media, 2006.

[98] Dong Hyun Yoon, Afshan Jamshaid, Junichi Ito, Asahi Nakahara, Daiki Tanaka, Takashiro Akitsu, Tetsushi Sekiguchi, and Shuichi Shoji. Active microdroplet merging by hydrodynamic flow control using a pneumatic actuator-assisted pillar structure. *Lab Chip*, 14(16):3050, 2014.

[99] David J. Collins, Tuncay Alan, and Adrian Neild. The particle valve: On-demand particle trapping, filtering, and release from a microfabricated polydimethylsiloxane membrane using surface acoustic waves. *Applied Physics Letters*, 105(3):033509–4, 2014.

[100] Ali Koşar, Chandan Mishra, and Yoav Peles. Laminar flow across a bank of low aspect ratio micro pin fins. *Journal of Fluids Engineering*, 127(3):419–430, March 2005.

[101] Rosaria Ferrigno, Abraham D Stroock, Thomas D Clark, Michael Mayer, and George M Whitesides. Membraneless vanadium redox fuel cell using laminar flow. *Journal of the American Chemical Society*, 124(44):12930–12931, 2002.

[102] Zhiqiang Li, Ying Zhang, Philip R. LeDuc, and Kelvin B. Gregory. Microbial electricity generation via microfluidic flow control. *Biotechnology and Bioengineering*, 108(9):2061–2069, 2011.

[103] Fatma Zeynep Temel and Serhat Yesilyurt. Simulation-based analysis of micro-robots swimming at the center and near the wall of circular mini-channels. *Microfluidics and Nanofluidics*, 14(1):287–298, 2012.

[104] Isao Kobayashi, Kunihiko Uemura, and Mitsutoshi Nakajima. Formulation of monodisperse emulsions using submicron-channel arrays. *Colloids and Surfaces A: Physicochemical and Engineering Aspects*, 296(1):285–289, 2007.

[105] Lih Feng Cheow, Levent Yobas, and Dim-Lee Kwong. Digital microfluidics: droplet based logic gates. *Applied Physics Letters*, 90(5):054107, 2007.

[106] Michael J Fuerstman, Piotr Garstecki, and George M Whitesides. Coding/decoding and reversibility of droplet trains in microfluidic networks. *Science*, 315(5813):828–832, 2007.

[107] Manu Prakash and Neil Gershenfeld. Microfluidic bubble logic. *Science*, 315(5813):832–835, 2007.

[108] Songzi Kou, Han Na Lee, Danny van Noort, K. M. K. Swamy, So Hyun Kim, Jung Hyun Soh, Kang-Mu Lee, Seong-Won Nam, Juyoung Yoon, and Sungsu Park. Fluorescent molecular logic gates using microfluidic devices. *Angewandte Chemie*, 120(5):886–890, 2008.

[109] Mira T Guo, Assaf Rotem, John A Heyman, and David A Weitz. Droplet microfluidics for high-throughput biological assays. *Lab Chip*, 12(12):2146–2155, 2012.

[110] Haakan N Joensson and Helene Andersson Svahn. Droplet microfluidics - a tool for single-cell analysis. *Angewandte Chemie International Edition*, 51(49):12176–12192, 2012.

[111] JM Kirshner and S Katz. *Design Theory of Fluidic Components*. Academic Press, New York, 1975.

[112] Michael J. Fuerstman, Pascal Deschatelets, Ravi Kane, Alexander Schwartz, Paul J. A. Kenis, John M. Deutch, and George M. Whitesides. Solving mazes using microfluidic networks. *Langmuir*, 19(11):4714–4722, 2003.

[113] William BJ Zimmerman. *Microfluidics: history, theory and applications*, volume 466. Springer Science & Business Media, 2006.

[114] Brian J Kirby. *Micro-and nanoscale fluid mechanics: transport in microfluidic devices*. Cambridge University Press, 2010.

[115] RJ Cornish. Flow in a pipe of rectangular cross-section. *Proceedings of the Royal Society of London. Series A, Containing Papers of a Mathematical and Physical Character*, pages 691–700, 1928.

[116] Kwang W Oh, Kangsun Lee, Byungwook Ahn, and Edward P Furlani. Design of pressure-driven microfluidic networks using electric circuit analogy. *Lab Chip*, 12(3):515–545, 2012.

[117] Laure Ménétrier-Deremble and Patrick Tabeling. Droplet breakup in microfluidic junctions of arbitrary angles. *Physical Review E*, 74:035303, Sep 2006.

[118] Michael Schindler and Armand Ajdari. Droplet traffic in microfluidic networks: A simple model for understanding and designing. *Physical Review Letters*, 100(4):044501, 2008.

[119] DA Sessoms, Malika Belloul, Wilfried Engl, M Roche, L Courbin, and P Panizza. Droplet motion in microfluidic networks: Hydrodynamic interactions and pressure-drop measurements. *Physical Review E*, 80(1):016317, 2009.

[120] G. Hertz and H. Mende. Der schallstrahlungsdruck in flüssigkeiten. *Zeitschrift für Physik*, 114(5-6):354–367, 1939.

[121] B. Issenmann, A. Nicolas, R. Wunenburger, S. Manneville, and J.-P. Delville. Deformation of acoustically transparent fluid interfaces by the acoustic radiation pressure. *EPL (Europhysics Letters)*, 83(3):34002, 2008.

[122] Priscilla R. Rogers, James R. Friend, and Leslie Y. Yeo. Exploitation of surface acoustic waves to drive size-dependent microparticle concentration within a droplet. *Lab Chip*, 10(21):2979–2985, 2010.

[123] Darren R. Link, Erwan Grasland-Mongrain, Agnes Duri, Flavie Sarrazin, Zhengdong Cheng, Galder Cristobal, Manuel Marquez, and David A. Weitz. Electric control of droplets in microfluidic devices. *Angewandte Chemie International Edition*, 45(16):2556–2560, 2006.

[124] Orlin D Velev and Ketan H Bhatt. On-chip micromanipulation and assembly of colloidal particles by electric fields. *Soft Matter*, 2(9):738–750, 2006.

[125] Sung-Yong Park, Ting-Hsiang Wu, Yue Chen, Michael A Teitell, and Pei-Yu Chiou. High-speed droplet generation on demand driven by pulse laser-induced cavitation. *Lab Chip*, 11(6):1010–1012, 2011.

[126] Jie Xu and Daniel Attinger. Drop on demand in a microfluidic chip. *Journal of Micromechanics and Microengineering*, 18(6):065020, 2008.

[127] Todd Thorsen, F. H Roberts, Frances H. Arnold, and Stephen R. Quake. Dynamic pattern formation in a vesicle-generating microfluidic device. *Physical Review Letters*, 86:4163–4166, 2001.

[128] Piotr Garstecki, Michael J. Fuerstman, Howard A. Stone, and George M. Whitesides. Formation of droplets and bubbles in a microfluidic t-junction-scaling and mechanism of break-up. *Lab Chip*, 6:437–446, 2006.

[129] Amit Gupta, S. M. Sohel Murshed, and Ranganathan Kumar. Droplet formation and stability of flows in a microfluidic t-junction. *Applied Physics Letters*, 94(16), 2009.

[130] Haihu Liu and Yonghao Zhang. Droplet formation in a t-shaped microfluidic junction. *Journal of applied physics*, 106(3):034906, 2009.

[131] Volkert van Steijn, Chris R. Kleijn, and Michiel T. Kreutzer. Predictive model for the size of bubbles and droplets created in microfluidic t-junctions. *Lab Chip*, 10:2513–2518, 2010.

[132] M De Menech, P Garstecki, F Jousse, and HA Stone. Transition from squeezing to dripping in a microfluidic T-shaped junction. *journal of Fluid Mechanics*, 595:141–161, 2008.

[133] Gordon F Christopher, N Nadia Noharuddin, Joshua A Taylor, and Shelley L Anna. Experimental observations of the squeezing-to-dripping transition in t-shaped microfluidic junctions. *Physical Review E*, 78(3):036317, 2008.

[134] Aaron M Streets and Yanyi Huang. Chip in a lab: Microfluidics for next generation life science research. *Biomicrofluidics*, 7(1):011302, 2013.

[135] JK Nunes, SSH Tsai, J Wan, and HA Stone. Dripping and jetting in microfluidic multiphase flows applied to particle and fibre synthesis. *Journal of Physics D: Applied Physics*, 46(11):114002, 2013.

[136] Shelley L. Anna, Nathalie Bontoux, and Howard A. Stone. Formation of dispersions using "flow focusing" in microchannels. *Applied Physics Letters*, 82(3):364–366, 2003.

[137] Remi Dreyfus, Patrick Tabeling, and Herve Willaime. Ordered and disordered patterns in two-phase flows in microchannels. *Phys. Rev. Lett.*, 90:144505, 2003.

[138] Carsten Cramer, Peter Fischer, and Erich J. Windhab. Drop formation in a co-flowing ambient fluid. *Chemical Engineering Science*, 59(15):3045 – 3058, 2004.

[139] Ho Cheung Shum, Daeyeon Lee, Insun Yoon, Tom Kodger, and David A Weitz. Double emulsion templated monodisperse phospholipid vesicles. *Langmuir*, 24(15):7651–7653, 2008.

[140] Mark B Romanowsky, Adam R Abate, Assaf Rotem, Christian Holtze, and David A Weitz. High throughput production of single core double emulsions in a parallelized microfluidic device. *Lab Chip*, 12(4):802–807, 2012.

[141] Jean-Christophe Baret, Oliver J. Miller, Valerie Taly, Michael Ryckelynck, Abdeslam El-Harrak, Lucas Frenz, Christian Rick, Michael L. Samuels, J. Brian Hutchison, Jeremy J. Agresti, Darren R. Link, David A. Weitz, and Andrew D. Griffiths. Fluorescence-activated droplet sorting (FADS): efficient microfluidic cell sorting based on enzymatic activity. *Lab Chip*, 9:1850–1858, 2009.

[142] Monpichar Srisa-Art, Andrew J. deMello, and Joshua B. Edel. High-throughput confinement and detection of single DNA molecules in aqueous microdroplets. *Chemical Communications*, page 6548, 2009.

[143] Matthew C. Cole and Paul J.A. Kenis. Multiplexed electrical sensor arrays in microfluidic networks. *Sensors and Actuators B: Chemical*, 136(2):350–358, mar 2009.

[144] E.V. Moiseeva, A.A. Fletcher, and C.K. Harnett. Thin-film electrode based droplet detection for microfluidic systems. *Sensors and Actuators B: Chemical*, 155(1):408–414, 2011.

[145] Gurkan Yesiloz, Muhammed Said Boybay, and Carolyn L. Ren. Label-free high-throughput detection and content sensing of individual droplets in microfluidic systems. *Lab Chip*, 15(20):4008–4019, 2015.

[146] Xize Niu, Mengying Zhang, Suili Peng, Weijia Wen, and Ping Sheng. Real-time detection control, and sorting of microfluidic droplets. *Biomicrofluidics*, 1(4):044101, 2007.

[147] Caglar Elbuken, Tomasz Glawdel, Danny Chan, and Carolyn L. Ren. Detection of microdroplet size and speed using capacitive sensors. *Sensors and Actuators A: Physical*, 171(2):55–62, nov 2011.

[148] Jiang Li, Yixuan Wang, Enkai Dong, and Haosheng Chen. USB-driven microfluidic chips on printed circuit boards. *Lab Chip*, 14(5):860, 2014.

[149] Pelin Kubra Isgor, Merve Marcali, Mert Keser, and Caglar Elbuken. Microfluidic droplet content detection using integrated capacitive sensors. *Sensors and Actuators B: Chemical*, 210:669–675, apr 2015.

[150] Md Shamsul Arefin, M. Bulut Coskun, Tuncay Alan, Jean-Michel Redoute, Adrian Neild, and Mehmet Rasit Yuce. A microfabricated fringing field capacitive pH sensor with an integrated readout circuit. *Applied Physics Letters*, 104(22):223503, jun 2014.

[151] Anne Y Fu, Hou-Pu Chou, Charles Spence, Frances H Arnold, and Stephen R Quake. An integrated microfabricated cell sorter. *Analytical Chemistry*, 74(11):2451–2457, 2002.

[152] Chun-Guang Yang, Zhang-Run Xu, and Jian-Hua Wang. Manipulation of droplets in microfluidic systems. *TrAC Trends in Analytical Chemistry*, 29(2):141 – 157, 2010.

[153] Shia-Yen Teh, Robert Lin, Lung-Hsin Hung, and Abraham P. Lee. Droplet microfluidics. *Lab Chip*, 8:198–220, 2008.

[154] E Klaseboer, J Ph Chevaillier, C Gourdon, and Olivier Masbernat. Film drainage between colliding drops at constant approach velocity: experiments and modeling. *Journal of Colloid and Interface Science*, 229(1):274–285, 2000.

[155] Howard A Stone, Abraham D Stroock, and Armand Ajdari. Engineering flows in small devices: microfluidics toward a lab-on-a-chip. *Annu. Rev. Fluid Mech.*, 36:381–411, 2004.

[156] M. Mousavichoubeh, M. Ghadiri, and M. Shariaty-Niassar. Electro-coalescence of an aqueous droplet at an oil-water interface. *Chemical Engineering and Processing: Process Intensification*, 50(3):338 – 344, 2011.

[157] John S. Eow and Mojtaba Ghadiri. Drop-drop coalescence in an electric field: the effects of applied electric field and electrode geometry. *Colloids and Surfaces A: Physicochemical and Engineering Aspects*, 219(1-3):253 – 279, 2003.

[158] John S. Eow, Mojtaba Ghadiri, Adel O. Sharif, and Trevor J. Williams. Electrostatic enhancement of coalescence of water droplets in oil: a review of the current understanding. *Chemical Engineering Journal*, 84(3):173 – 192, 2001.

[159] Max Chabert, Kevin D. Dorfman, and Jean-Louis Viovy. Droplet fusion by alternating current (AC) field electrocoalescence in microchannels. *Electrophoresis*, 26(19):3706–3715, 2005.

[160] John S Eow, Mojtaba Ghadiri, and Adel Sharif. Experimental studies of deformation and break-up of aqueous drops in high electric fields. *Colloids and Surfaces A: Physicochemical and Engineering Aspects*, 225(1-3):193 – 210, 2003.

[161] P. Atten, L. Lundgaard, and G. Berg. A simplified model of electrocoalescence of two close water droplets in oil. *Journal of Electrostatics*, 64(7-9):550 – 554, 2006.

[162] Jiu-Sheng Chen and Jia-Huan Jiang. Droplet microfluidic technology: Mirodroplets formation and manipulation. *Chinese Journal of Analytical Chemistry*, 40(8):1293 – 1300, 2012.

[163] Lung-Hsin Hung, Kyung M. Choi, Wei-Yu Tseng, Yung-Chieh Tan, Kenneth J. Shea, and Abraham Phillip Lee. Alternating droplet generation and controlled dynamic droplet fusion in microfluidic device for cds nanoparticle synthesis. *Lab Chip*, 6:174–178, 2006.

[164] Yung-Chieh Tan, YaoLi Ho, and AbrahamPhillip Lee. Droplet coalescence by geometrically mediated flow in microfluidic channels. *Microfluidics and Nanofluidics*, 3(4):495–499, 2007.

[165] Yung-Chieh Tan, Jeffrey S. Fisher, Alan I. Lee, Vittorio Cristini, and Abraham Phillip Lee. Design of microfluidic channel geometries for the control of droplet volume, chemical concentration, and sorting. *Lab Chip*, 4:292–298, 2004.

[166] Andrew C. Hatch, Jeffrey S. Fisher, Armando R. Tovar, Albert T. Hsieh, Robert Lin, Stephen L. Pentoney, David L. Yang, and Abraham P. Lee. 1-million droplet array with wide-field fluorescence imaging for digital PCR. *Lab Chip*, 11:3838–3845, 2011.

[167] Frederik Scheiff, Matthias Mendorf, David Agar, Nuno Reis, and Malcolm Mackley. The separation of immiscible liquid slugs within plastic microchannels using a metallic hydrophilic sidestream. *Lab Chip*, 11:1022–1029, 2011.

[168] Yunpeng Bai, Ximin He, Dingsheng Liu, Santoshkumar N. Patil, Dan Bratton, Ansgar Huebner, Florian Hollfelder, Chris Abell, and Wilhelm T. S. Huck. A double droplet trap system for studying mass transport across a droplet-droplet interface. *Lab Chip*, 10:1281–1285, 2010.

[169] Ashleigh B. Theberge, Estelle Mayot, Abdeslam El Harrak, Felix Kleinschmidt, Wilhelm T. S. Huck, and Andrew D. Griffiths. Microfluidic platform for combinatorial synthesis in picolitre droplets. *Lab Chip*, 12:1320–1326, 2012.

[170] X. Niu and Andrew J. deMello. Building droplet-based microfluidic systems for biological analysis. *Biochemical Society Transactions*, 40(4):615–623, 2012.

[171] K Handique and M A Burns. Mathematical modeling of drop mixing in a slit-type microchannel. *Journal of Micromechanics and Microengineering*, 11(5):548, 2001.

[172] H. Song, D.L. Chen, and R.F. Ismagilov. Reactions in droplets in microfluidic channels. *Angewandte Chemie International Edition*, 45(44):7336–7356, 2006.

[173] Po Ki Yuen. Smartbuild–a truly plug-n-play modular microfluidic system. *Lab on a Chip*, 8(8):1374–1378, 2008.

[174] Helena Zec, Tushar D. Rane, and Tza-Huei Wang. Microfluidic platform for on-demand generation of spatially indexed combinatorial droplets. *Lab Chip*, 12(17):3055, 2012.

[175] Albert G Mulley Jr. Shock-wave lithotripsy. *New England Journal of Medicine*, 314(13):845–847, 1986.

[176] LH Thompson and LK Doraiswamy. Sonochemistry: science and engineering. *Industrial & Engineering Chemistry Research*, 38(4):1215–1249, 1999.

[177] OS Salawu. Detection of structural damage through changes in frequency: a review. *Engineering Structures*, 19(9):718–723, 1997.

[178] Sz-Chin Steven Lin, Xiaole Mao, and Tony Jun Huang. Surface acoustic wave (SAW) acoustophoresis: now and beyond. *Lab Chip*, 12:2766–2770, 2012.

[179] Albrecht Haake, Adrian Neild, Gerald Radziwill, and Jurg Dual. Positioning displacement, and localization of cells using ultrasonic forces. *Biotechnology and Bioengineering*, 92(1):8–14, 2005.

[180] Thomas Laurell, Filip Petersson, and Andreas Nilsson. Chip integrated strategies for acoustic separation and manipulation of cells and particles. *Chem. Soc. Rev.*, 36(3):492–506, 2007.

[181] Mikael Evander, Linda Johansson, Tobias Lilliehorn, Jure Piskur, Magnus Lindvall, Stefan Johansson, Monica Almqvist, Thomas Laurell, and Johan Nilsson. Noninvasive Acoustic Cell Trapping in a Microfluidic Perfusion System for Online Bioassays. *Analytical Chemistry*, 79(7):2984–2991, apr 2007.

[182] Priscilla Rogers and Adrian Neild. Selective particle trapping using an oscillating microbubble. *Lab Chip*, 11:3710–3715, 2011.

[183] Robert Walker, Ian Gralinski, Kok Keong Lay, Tuncay Alan, and Adrian Neild. Particle manipulation using an ultrasonic micro-gripper. *Applied Physics Letters*, 101(16):163504–4, 2012.

[184] Priscilla Rogers, Ian Gralinski, Cameron Galtry, and Adrian Neild. Selective particle and cell clustering at air-liquid interfaces within ultrasonic microfluidic systems. *Microfluidics and Nanofluidics*, 14(3-4):469–477, 2013.

[185] Citsabehsan Devendran, Ian Gralinski, and Adrian Neild. Separation of particles using acoustic streaming and radiation forces in an open microfluidic channel. *Microfluidics and Nanofluidics*, 17:879–890, 2014.

[186] P. Glynne-Jones, C. E. M. Demore, Congwei Ye, Yongqiang Qiu, S. Cochran, and M. Hill. Array-controlled ultrasonic manipulation of particles in planar acoustic resonator. *IEEE Transactions on Ultrasonics Ferroelectrics and Frequency Control*, 59(6):1258–1266, jun 2012.

[187] Citsabehsan Devendran, Duncan R. Billson, David A. Hutchins, and Adrian Neild. Optimisation of an acoustic resonator for particle manipulation in air. *Sensors and Actuators B: Chemical*, 224:529–538, mar 2016.

[188] M Duvshani-Eshet, L Baruch, E Kesselman, E Shimoni, and M Machluf. Therapeutic ultrasound-mediated dna to cell and nucleus: bioeffects revealed by confocal and atomic force microscopy. *Gene Therapy*, 13(2):163–172, 2006.

[189] Goksen G. Yaralioglu, Ira O. Wygant, Theodore C. Marentis, and Butrus T. Khuri-Yakub. Ultrasonic Mixing in Microfluidic Channels Using Integrated Transducers. *Analytical Chemistry*, 76(13):3694–3698, jul 2004.

[190] Po-Hsun Huang, Yuliang Xie, Daniel Ahmed, Joseph Rufo, Nitesh Nama, Yuchao Chen, Chung Yu Chan, and Tony Jun Huang. An acoustofluidic micromixer based on oscillating sidewall sharp-edges. *Lab Chip*, 13(19):3847, 2013.

[191] Michael Hadjiargyrou, Kenneth McLeod, John P Ryaby, and Clinton Rubin. Enhancement of fracture healing by low intensity ultrasound. *Clinical Orthopaedics and Related Research*, 355:S216–S229, 1998.

[192] Jinjie Shi, Xiaole Mao, Daniel Ahmed, Ashley Colletti, and Tony Jun Huang. Focusing microparticles in a microfluidic channel with standing surface acoustic waves (SSAW). *Lab Chip*, 8:221–223, 2008.

[193] Per Augustsson, Jonas Persson, Simon Ekstrom, Mats Ohlin, and Thomas Laurell. Decomplexing biofluids using microchip based acoustophoresis. *Lab Chip*, 9:810–818, 2009.

[194] Jinjie Shi, Hua Huang, Zak Stratton, Yiping Huang, and Tony Jun Huang. Continuous particle separation in a microfluidic channel via standing surface acoustic waves (SSAW). *Lab Chip*, 9:3354–3359, 2009.

[195] Jeonghun Nam, Yongjin Lee, and Sehyun Shin. Size-dependent microparticles separation through standing surface acoustic waves. *Microfluidics and Nanofluidics*, 11(3):317–326, 2011.

[196] Xiaoyun Ding, Sz-Chin Steven Lin, Brian Kiraly, Hongjun Yue, Sixing Li, I-Kao Chiang, Jinjie Shi, Stephen J. Benkovic, and Tony Jun Huang. On-chip manipulation of single microparticles, cells, and organisms using surface acoustic waves. *Proceedings of the National Academy of Sciences*, 109(28):11105–11109, 2012.

[197] Ghulam Destgeer, Kyung Heon Lee, Jin Ho Jung, Anas Alazzam, and Hyung Jin Sung. Continuous separation of particles in a pdms microfluidic channel via travelling surface acoustic waves (TSAW). *Lab Chip*, 13:4210–4216, 2013.

[198] C. D. Wood, S. D. Evans, J. E. Cunningham, R. ORorke, C. Walti, and A. G. Davies. Alignment of particles in microfluidic systems using standing surface acoustic waves. *Applied Physics Letters*, 92(4):044104, 2008.

[199] Xiaoyun Ding, Sz-Chin Steven Lin, Michael Ian Lapsley, Sixing Li, Xiang Guo, Chung Yu Chan, I-Kao Chiang, Lin Wang, J. Philip McCoy, and Tony Jun Huang. Standing surface acoustic wave (SSAW) based multichannel cell sorting. *Lab Chip*, 12:4228–4231, 2012.

[200] David J. Collins, Tuncay Alan, and Adrian Neild. Particle separation using virtual deterministic lateral displacement (vDLD). *Lab Chip*, 14:1595–1603, 2014.

[201] David J. Collins, Belinda Morahan, Jose Garcia-Bustos, Christian Doerig, Magdalena Plebanski, and Adrian Neild. Two-dimensional single-cell patterning with one cell per well driven by surface acoustic waves. *Nature Communications*, 6:8686, nov 2015.

[202] Citsabehsan Devendran, Nipuna R Gunasekara, David J Collins, and Adrian Neild. Batch process particle separation using surface acoustic waves (SAW): integration of travelling and standing SAW. *RSC Advances*, 6(7):5856–5864, 2016.

[203] T. Franke, S. Braunmuller, L. Schmid, A. Wixforth, and D. A. Weitz. Surface acoustic wave actuated cell sorting (SAWACS). *Lab Chip*, 10:789–794, 2010.

[204] Feng Guo, Peng Li, Jarrod B. French, Zhangming Mao, Hong Zhao, Sixing Li, Nitesh Nama, James R. Fick, Stephen J. Benkovic, and Tony Jun Huang. Controlling cell-cell interactions using surface acoustic waves. *Proceedings of the National Academy of Sciences*, 112(1):43–48, 2015.

[205] Marco Cecchini, Salvatore Girardo, Dario Pisignano, Roberto Cingolani, and Fabio Beltram. Acoustic-counterflow microfluidics by surface acoustic waves. *Applied Physics Letters*, 92(10):104103, 2008.

[206] R. M. White and F. W. Voltmer. Direct piezoelectric coupling to surface elastic waves. *Applied Physics Letters*, 7(12):314–316, 1965.

[207] Lord Rayleigh. On waves propagated along the plane surface of an elastic solid. *Proceedings of the London Mathematical Society*, s1-17(1):4–11, 1885.

[208] Jinjie Shi, Shahrzad Yazdi, Sz-Chin Steven Lin, Xiaoyun Ding, I-Kao Chiang, Kendra Sharp, and Tony Jun Huang. Three-dimensional continuous particle focusing in a microfluidic channelvia standing surface acoustic waves (SSAW). *Lab Chip*, 11:2319–2324, 2011.

[209] Lord Rayleigh. On the circulation of air observed in kundt's tubes, and on some allied acoustical problems. *Philosophical Transactions of the Royal Society of London*, pages 1–21, 1884.

[210] Carl Eckart. Vortices and streams caused by sound waves. *Physical Review*, 73(1):68, 1948.

[211] WL Nyborg. Acoustic streaming. *Physical Acoustics*, 2(Pt B):265, 1965.

[212] James Lighthill. Acoustic streaming. *Journal of Sound and Vibration*, 61(3):391–418, 1978.

[213] Louis V. King. On the acoustic radiation pressure on spheres. *Proceedings of the Royal Society of London. Series A, Mathematical and Physical Sciences*, 147(861):212–240, 1934.

[214] K Yosioka and Y Kawasima. Acoustic radiation pressure on a compressible sphere. *Acta Acustica united with Acustica*, 5(3):167–173, 1955.

[215] L. P. Gor'kov. On the forces acting on a small particle in an acoustical field in an ideal fluid. *Soviet Physics Doklady*, 6(9):773–775, 1962.

[216] Larisa A Kuznetsova and W Terence Coakley. Microparticle concentration in short path length ultrasonic resonators: Roles of radiation pressure and acoustic streaming. *The Journal of the Acoustical Society of America*, 116(4):1956–1966, 2004.

[217] Paul Tho, Richard Manasseh, and Andrew Ooi. Cavitation microstreaming patterns in single and multiple bubble systems. *Journal of Fluid Mechanics*, 576:191–233, 2007.

[218] Christoph J Strobl, Zeno Von Guttenberg, and Achim Wixforth. Nano-and pico-dispensing of fluids on planar substrates using SAW. *Ultrasonics, Ferroelectrics, and Frequency Control, IEEE Transactions on*, 51(11):1432–1436, 2004.

[219] Martin Wiklund, Roy Green, and Mathias Ohlin. Acoustofluidics 14: Applications of acoustic streaming in microfluidic devices. *Lab Chip*, 12(14):2438–2451, 2012.

[220] Z v Guttenberg, A Rathgeber, S Keller, JO Rädler, A Wixforth, M Kostur, M Schindler, and P Talkner. Flow profiling of a surface-acoustic-wave nanopump. *Physical Review E*, 70(5):056311, 2004.

[221] WL Nyborg. Acoustic streaming. *Physical Acoustics*, 2(Pt B):265, 2012.

[222] Achim Wixforth. Acoustically driven programmable microfluidics for biological and chemical applications. *Journal of the Association for Laboratory Automation*, 11(6):399–405, 2006.

[223] Aisha Qi, Leslie Y. Yeo, and James R. Friend. Interfacial destabilization and atomization driven by surface acoustic waves. *Physics of Fluids (1994-present)*, 20(7):074103–14, 2008.

[224] James A Rooney and Wesley L Nyborg. Acoustic radiation pressure in a traveling plane wave. *American Journal of Physics*, 40(12):1825–1830, 1972.

[225] Robert T Beyer. Radiation pressure-the history of a mislabeled tensor. *The Journal of the Acoustical Society of America*, 63(4):1025–1030, 1978.

[226] F. E. Borgnis. Acoustic radiation pressure of plane compressional waves. *Rev. Mod. Phys.*, 25:653–664, Jul 1953.

[227] Boa-Teh Chu and Robert E Apfel. Acoustic radiation pressure produced by a beam of sound. *The Journal of the Acoustical Society of America*, 72(6):1673–1687, 1982.

[228] Henrik Bruus. Acoustofluidics 7: The acoustic radiation force on small particles. *Lab Chip*, 12(6):1014–1021, 2012.

[229] Mikkel Settnes and Henrik Bruus. Forces acting on a small particle in an acoustical field in a viscous fluid. *Physical Review E*, 85(1):016327, 2012.

[230] Ketav Kulkarni, James Friend, Leslie Yeo, and Patrick Perlmutter. Surface acoustic waves as an energy source for drop scale synthetic chemistry. *Lab on a Chip*, 9(6):754–755, 2009.

[231] Jun Kondoh, Norifumi Shimizu, Yoshikazu Matsui, Mitsunori Sugimoto, and Showko Shiokawa. Development of temperature-control system for liquid droplet using surface acoustic wave devices. *Sensors and Actuators A: Physical*, 149(2):292–297, 2009.

[232] Thibaut Roux-Marchand, Denis Beyssen, Frederic Sarry, and Omar Elmazria. Rayleigh surface acoustic wave as an efficient heating system for biological reactions: investigation of microdroplet temperature uniformity. *IEEE transactions on ultrasonics, ferroelectrics, and frequency control*, 62(4):729–735, 2015.

[233] Richie J Shilton, Virgilio Mattoli, Marco Travagliati, Matteo Agostini, Andrea Desii, Fabio Beltram, and Marco Cecchini. Rapid and controllable digital microfluidic heating by surface acoustic waves. *Advanced Functional Materials*, 25(37):5895–5901, 2015.

[234] Byung Hang Ha, Kang Soo Lee, Ghulam Destgeer, Jinsoo Park, Jin Seung Choung, Jin Ho Jung, Jennifer Hyunjong Shin, and Hyung Jin Sung. Acoustothermal heating of polydimethylsiloxane microfluidic system. *Scientific reports*, 5, 2015.

[235] Jinsoo Park, Byung Hang Ha, Ghulam Destgeer, Jin Ho Jung, and Hyung Jin Sung. Spatiotemporally controllable acoustothermal heating and its application to disposable thermochromic displays. *RSC Advances*, 6(40):33937–33944, 2016.

[236] JK Luo, Yong Qing Fu, and WI Milne. Acoustic wave based microfluidics and lab-on-a-chip. *Modeling and Measurement Methods for Acoustic Waves and for Acoustic Microdevices*, 2013.

[237] Wei-Kuo Tseng, Jr-Lung Lin, Wang-Chou Sung, Shu-Hui Chen, and Gwo-Bin Lee. Active micro-mixers using surface acoustic waves on y-cut 128 linbo3. *Journal of Micromechanics and Microengineering*, 16(3):539, 2006.

[238] Frank Kreith, Raj M Manglik, and Mark S Bohn. *Principles of heat transfer*. Cengage learning, 2012.

[239] RJ Goldstein and Kei-Shun Lau. Laminar natural convection from a horizontal plate and the influence of plate-edge extensions. *Journal of Fluid Mechanics*, 129:55–75, 1983.

[240] K Nassau, HJ Levinstein, and GM Loiacono. Ferroelectric lithium niobate. 2. preparation of single domain crystals. *Journal of Physics and Chemistry of Solids*, 27(6):989–996, 1966.

[241] David Issadore, Katherine J Humphry, Keith A Brown, Lori Sandberg, David A Weitz, and Robert M Westervelt. Microwave dielectric heating of drops in microfluidic devices. *Lab on a Chip*, 9(12):1701–1706, 2009.

[242] Nils E Bengtsson and Thomas Ohlsson. Microwave heating in the food industry. *Proceedings of the IEEE*, 62(1):44–55, 1974.

[243] Muhammed S Boybay, Austin Jiao, Tomasz Glawdel, and Carolyn L Ren. Microwave sensing and heating of individual droplets in microfluidic devices. *Lab on a Chip*, 13(19):3840–3846, 2013.

[244] Muhammed Said Boybay and Carolyn L Ren. Microwave in microfluidics. *Encyclopedia of Microfluidics and Nanofluidics*, pages 2241–2250, 2015.

[245] David Wong, Gurkan Yesiloz, Muhammed S Boybay, and Carolyn L Ren. Microwave temperature measurement in microfluidic devices. *Lab on a Chip*, 16(12):2192–2197, 2016.

[246] TA Litovitz and CM Davis. Structural and shear relaxation in liquids. *Physical acoustics*, 2(Part A):281–349, 1965.